



FRIEDRICH-SCHILLER-  
UNIVERSITÄT  
JENA



# DISSERTATION

for the attainment of the academic degree

doctor medicine (Dr.med.)

---

## Ischemia-reperfusion injury in a rat model of normothermic oxygenated machine perfusion and liver transplantation

---

Submitted to the Council of the Medical Faculty  
of the Friedrich-Schiller-Universität Jena by  
Xinpei Chen

Jena, 30.04.2024

## **Reviewer**

### **1. Prof. Dr. med. Uta Dahmen**

Department of General, Visceral and Vascular Surgery, Experimental  
Transplantation Surgery  
Jena University Hospital

### **2. PD. Dr. med. Olaf Dirsch**

Institute of Pathology  
BG Klinikum Unfallkrankenhaus Berlin

### **3. Prof. Dr. med. Daniel Seehofer**

Department of Visceral, Transplantation, Thoracic and Vascular Surgery  
University Hospital Leipzig

**Date of the public disputation: 03.09.2024**

# TABLE OF CONTENTS

LIST OF ABBREVIATIONS .....	iii
SUMMARY .....	v
ZUSAMMENFASSUNG .....	vii
1 INTRODUCTION.....	1
1.1 Global liver transplantation activity .....	1
1.2 Hepatic ischemia-reperfusion injury in liver transplantation .....	2
1.3 Predictive value and visualization of liver microcirculation .....	5
1.4 Impact of donor properties on hepatic IRI.....	6
1.5 Promises of liver machine perfusion .....	7
1.6 Urgent issues to be addressed in NMP model .....	9
1.7 Role of autophagy in liver machine perfusion.....	9
2 AIM AND HYPOTHESIS.....	11
2.1 Aim.....	11
2.2 Hypotheses.....	11
3 STUDY DESIGN .....	12
4 METHODS .....	14
4.1 Animal experiments .....	14
4.1.1 Animals .....	14
4.1.2 Procurement of liver grafts from DCD .....	14
4.1.3 NMP setup.....	15
4.1.4 Technique of orthotopic rat liver transplantation .....	15
4.2 Experimental groups.....	17
4.2.1 Group distribution for NMP study (Part I).....	17
4.2.2 Group distribution for LTx study (Part II) .....	19
4.3 Sample collection .....	21
4.3.1 NMP perfusate collection and analysis.....	21
4.3.2 LTx blood sample collection and analysis .....	22
4.3.3 NMP bile collection and analysis .....	22
4.3.4 Liver samples collection .....	22
4.4 Histology.....	23
4.4.1 HE staining and analysis .....	23
4.4.2 Immunohistochemistry and analysis.....	24
4.5 Protein analysis .....	27
4.5.1 Protein extraction and sample preparation.....	27
4.5.2 SDS-PAGE and Western Blot.....	28
4.6 Hepatic hemodynamics, tissue perfusion, and microcirculation.....	28
4.6.1 Hepatic hemodynamics.....	28
4.6.2 Tissue perfusion.....	29
4.6.3 Hepatic microcirculation.....	30
4.6.4 Stiffness of the liver.....	31
4.7 Statistical Analysis .....	32
5 RESULTS .....	33
5.1 Part I: NMP study.....	33
5.1.1 Establishment of NMP model .....	33
5.1.2 Overall impact of NMP on liver damage and function.....	34
5.1.3 Impact of perfusion flow rate and medium change on the outcome of NMP .....	35
5.1.4 Impact of donor properties on the outcome of NMP .....	43
5.1.5 Impact of age on autophagy in livers subjected to NMP .....	52
5.2 Part II: LTx study .....	54

5.2.1	Establishment of rat LTx.....	54
5.2.2	Characterisation of early hepatic IRI .....	60
5.2.3	Correlation of hepatic microcirculation with alterations of liver function, liver damage, and blood count after reperfusion.....	69
6	DISCUSSION .....	70
6.1	Part I: NMP study.....	70
6.1.1	Advantage of CO2 inhalation to induce cardiac death in liver graft donors...70	
6.1.2	Balancing oxygen supply and waste removal resulting in optimal perfusion condition .....	72
6.1.3	Impact of donor properties on outcome of NMP.....	73
6.1.4	Impact of age on autophagy in native and machine perfusion livers .....	75
6.2	Part II: LTx study .....	76
6.2.1	Impact of pressure-controlled and volume-controlled flushing on the reperfusion in LTx model .....	76
6.2.2	Asynchronous alteration of liver enzyme release and morphological damage in transplantation .....	77
6.2.3	Impairment of liver microcirculation after reperfusion in LTX.....	77
6.3	Part III: Comparison of morphological changes in different models of hepatic IRI ...78	
6.3.1	Zonated morphological damage pronounced in NMP but not in LTx.....	78
6.3.2	Pericentral translocation of HMGB1 and reduced expression of CYP1A2 pronounced in NMP but not in LTx .....	81
6.4	Limitation .....	82
7	CONCLUSION .....	83
8	REFERENCE.....	84
9	APPENDIXES .....	I
9.1	Supplement materials .....	I
9.2	List of figures and tables .....	VI
9.3	Permission to use previously published figures from other publications.....	IX
9.4	Curriculum vitae.....	XVII
9.5	Acknowledgements .....	XIX
9.6	Ehrenwörtliche Erklärung.....	XXI

## LIST OF ABBREVIATIONS

ALP	Alkaline phosphatasecrea
ALT	Alanine aminotransferase
AST	Aminotransferase
ATP	Adenosine triphosphate
CBD	Common bile duct
CYP	Cytochrome P450
DBD	Donor after brain death
DCD	Donor after circulatory death
FCS	Fetal calf serum
GODT	Global observatory on donation and transplantation
HA	Hepatic artery
HCO <sub>3</sub> <sup>-</sup>	Bicarbonate
HCT	Hematocrit
HGB	Hemoglobin
HMGB1	High mobility group box 1
HMP	Hypothermic machine perfusion
HRP	Horseradish Peroxidase
I/R	Ischemia reperfusion
IHVC	Inferior hepatic vena cava
IL-1	Interleukin-1
IL-2	Interleukin-2
IL-6	Interleukin-6
LC3-II	Light chain 3
LDH	Lactate dehydrogenase
LSEC	liver sinusoidal endothelial cells
LTx	Liver transplantation
MAPK	Mitogen-activated protein kinases
MC	Medium change
MCH	Mean corpuscular hemoglobin
MCHC	Mean corpuscular hemoglobin concentration
MCV	Mean corpuscular volume
mTOR	Mammalian target of rapamycin
NMP	Normothermic machine perfusion
NO	Nitric oxide
PCD	Perfused capillary density
PLT	Platelet
pO <sub>2</sub>	Partial pressure of oxygen
PPC	Proportion of perfused capillary
PV	Portal vein
PVDF	Polyvinylidenfluorid
PVF	Portal vein flow
PVP	Portal vein pressure
RAV	Right adrenal vein
RBC	Red blood cell
ROS	Reactive oxygen species
RRV	Right renal vein

SCS	Static cold storage
SDS	Sodium dodecyl-sulfate
SHVC	Superior hepatic vena cava
sWIT	Short warm ischemia time
TBST	Tris Buffered Saline with Tween-20
TCD	Total capillary density
TNCD	Total non-capillary density
TNF-a	Tumor Necrosis Factor Alpha
TVD	Total vessel density
WBC	White blood cell
WHVP	Wedged hepatic venous pressure
WIT	Warm ischemia time
$\gamma$ -GGT	$\gamma$ -glutamyltransferase
<b>Units</b>	
L	Litre
mL	Millilitre
$\mu$ L	Microlitre
kg	Kilogram
g	Gram
mg	Milligram
$\mu$ g	Microgram
h	Hour
min	Minute
s	Seconds
ms	Milliseconds
mm	Millimeter
cm	Centimeter
$\mu$ m	Micrometer

## **SUMMARY**

**Background:** Liver transplantation (LTx) is the most effective treatment for various end-stage liver diseases. However, there is a growing demand for donor organs. This demand is addressed by the increasing use of marginal organs obtained from so-called extended criteria donors, e.g., donors with high age, comorbidities, or after cardiac death. Marginal organs are more susceptible to the inevitable ischemia-reperfusion injury (IRI). Normothermic machine perfusion (NMP) is considered to be the most promising strategy to reduce IRI compared to hypothermic or other types of machine perfusion. However, little is known about (1) the optimal conditions of experimental NMP and (2) donor characteristics impacting the outcome of NMP and the underlying pathophysiological mechanism.

IRI causes microcirculation impairment after LTx, one of the key factors initiating the inflammatory vicious cycle. Visualization and quantification of microcirculation impairment might help to better determine the severity of early IRI.

**Aim:** The study aimed to establish (a) NMP and (b) LTx models using rat livers and characterize both models in terms of liver damage, function, and microcirculation. NMP study aimed to assess optimal balance between sufficient supply (flow rate) and adequate waste removal (medium change) as well as the impact of donor characteristics. LTx study aimed to study the impact of perfusion impairment on hepatic damage early after LTx.

**Methods and results:** For determination of optimal NMP conditions, the impact of flow rate (1, 2 and 3 ml/min/gr liver) and medium changes (partial replacement of perfusate either after 3 h or after 2 and 4h) was explored. In terms of donor properties, the influence of gender (male vs female), age (3-6m vs 24m), and duration of warm ischemia time (WIT, 20min vs 30min) were investigated. Livers were subjected to 6h of NMP using Williams E medium without oxygen carriers. Portal pressure (PVP) was measured continuously. Wedge hepatic vein pressure, hepatic perfusion, bile volume (indicator of liver function) and liver enzymes from perfusate samples were determined in hourly intervals. Tissue samples were taken at 2h, 4h, and 6h of perfusion to assess hepatic morphology based on HE staining, ischemic damage based on HMGB1, and metabolic function based on CYP1A2. Optimal balance between supply and drainage in terms of damage and function was when hyperperfusing the liver by setting the flow rate to 3ml/min/gr liver and exchanging half of the medium after 3h of perfusion.

Investigation of donor conditions revealed that young male rat livers (control group) subjected to 30min WIT were perfused homogeneously, with stable PVP and oxygenation. Livers produced more than 120ul/gr liver bile in 6 hours with a maximum of about 35 ul/gr liver in the first hours. In parallel, signs of liver damage in terms of enzyme release increased over time, as

confirmed by histology. Hepatic lobules showed zoned damage patterns with signs of pressure-related damage in the periportal zone and ischemic damage in the pericentral zone. Further confirmation was reached by visualizing the pericentral translocation of HMGB1 and the expression pattern of CYP1A2. Livers from female and donors subjected to shorter WIT were protected to a higher degree, as indicated by higher bile production, less enzyme release, and less histological damage. In contrast, aged livers were less well preserved.

In the LTx study, livers from young male donors were observed for 1h and 24h after reperfusion. Liver hemodynamic (PVP, PVF (portal vein flow)), perfusion (tissue oxygenation, tissue blood flow), and microcirculation (perfused capillary density) were monitored in the native liver of the recipient before explantation as well as in the transplanted liver graft one hour after reperfusion. Blood samples and liver tissue samples were also obtained from the donor during organ procurement and from the recipient at the time of sacrifice to quantify enzyme release as an indicator of hepatic damage and to assess hepatic morphology, ischemic damage, and metabolic function.

We observed a pronounced cardiovascular depression at 1h after reperfusion as indicated by lower PVP and PVF, but also in reduced tissue oxygen saturation and tissue blood flow and in terms of the reduced perfused capillary density. At this point, we observed severe liver damage in terms of liver enzymes, which recovered partially within 24 h.

In contrast, morphological signs of damage became apparent later compared to the enzyme release, corresponding to the HMGB1 translocation and the reduced CYP1A2 expression. Impaired perfusion parameters were inversely correlated to enzyme release.

**Conclusion:** NMP using oxygenated Williams E medium without additional oxygen carriers can preserve rat liver morphology and function for at least 6h. Best preservation is achieved when balancing oxygen supply and waste removal. However, donor properties such as gender and age, as well as even a minimal extension of WIT, have a significant beneficial respectively detrimental effect on organ preservation. Further work is needed to understand the underlying pathophysiological mechanism between donor characteristics, NMP condition, and organ preservation.

Intraoperative assessment of liver hemodynamics, perfusion and microcirculation seems to reflect severity of early IRI. Further work is needed to identify the most relevant parameter to predict severity of IRI based on an “easy to determine” intra-operative measurement.

Taken together, addressing the complex topic of IRI from the side of NMP to prevent severe IRI and from a diagnostic point of view will contribute to better prevention of severe liver damage.



## **ZUSAMMENFASSUNG**

**Hintergrund:** Lebertransplantation (LTx) ist die effektivste Behandlung für verschiedene Endstadium-Lebererkrankungen. Es besteht jedoch ein zunehmender Bedarf nach Spenderorganen. Dieser Bedarf wird durch die zunehmende Verwendung marginaler Organe gedeckt, die von sogenannten „extended criteria donors“ stammen, z. B. Spendern mit hohem Alter, Begleiterkrankungen oder nach Herz-Kreislauf-Tod. Marginale Organe sind anfälliger für den unvermeidbaren Ischämie-Reperfusionsschaden (IRI). Eine Strategie zur möglichen Verbesserung der Organqualität durch Reduzierung der IRI ist der Einsatz der normothermen oxygenierten Maschinenperfusion vor Implantation. Es ist jedoch wenig bekannt über (1) die optimalen Balance von Sauerstoffzufuhr und Elimination der Abbauprodukte und (2) die Spendermerkmale, die das Ergebnis der NMP und den zugrunde liegenden Schädigungsmechanismus beeinflussen.

IRI verursacht nach LTx eine Beeinträchtigung der Mikrozirkulation, einem der Hauptfaktoren, die das entzündliche Geschehen beim IRI initiieren. Die Quantifizierung der Mikrozirkulationsstörung könnte helfen, die Schwere der frühen IRI besser zu bestimmen.

**Ziel:** Die Studie hatte zum Ziel, (a) NMP- und (b) LTx im Rattenmodell zu etablieren und beide Verfahren hinsichtlich Leberschädigung, -funktion und -mikrozirkulation zu charakterisieren. In der NMP-Studie sollte die bestmögliche Balance zwischen Sauerstoffzufuhr und Entfernung der Abfallprodukte erzielt und die Auswirkungen der Spendermerkmalen bestimmt werden. In der LTX-Studie sollte der Zusammenhang zwischen früherer Mikrozirkulationsstörung und früherer IRI nach LTx untersucht werden.

**Methoden und Ergebnisse:** (1) Zur Bestimmung optimaler NMP-Bedingungen wurde der Einfluss der leichten Hyperperfusion und des teilweisen Wechsels des Perfusates (einmalig nach 3h oder zweimalig nach 2h und 4h) untersucht. Hinsichtlich der Spendermerkmale wurde der Einfluss des Geschlechts, des Alters und der Dauer der warmen Ischämiezeit (WIT) untersucht. Die Organe wurden 6h unter Verwendung von Williams E-Medium ohne Sauerstoffträger bei kontinuierlicher Messung des Portalvenendruckes (PVP) perfundiert. Der „wedge hepatic vein pressure,“ die Galleproduktion, und Parameter der Leberschädigung aus dem Perfusat wurden stündlich bestimmt. Alle 2h wurde Gewebeprobe entnommen, um die morphologische Schädigung anhand von HE-Färbung, den Ischämieschaden anhand der HMGB1-Färbung und die Stoffwechselfunktion anhand einer CYP1A2-Färbung zu beurteilen. Die geringste Schädigung bei bester Funktion wurde erzielt, wenn die Organe mit 3ml/min/gr Leber leicht hyperperfundiert und das Medium einmal partiell ausgetauscht wurde. Unter diesen Bedingungen wurden bei Organen von jungen männlichen Ratten nach einer WIT von

30min (Kontrollgruppe) eine homogene Perfusion bei stabilem PVP erzielt. Die Lebern produzierten in 6 Stunden mehr als 120  $\mu\text{l/h/gr}$  Leber Gallenflüssigkeit mit einem Maximum von knapp 35 $\mu\text{l/h/gr}$  Leber in der ersten Stunde. Parallel zur Abnahme der Galleproduktion nahmen die Anzeichen der Leberschädigung (Leberenzyme) zu. Die Histologie zeigte periportal Zeichen der hyperperfusionsbedingten Schädigung (zB Vakuolisierung) und eine perizentrale ischämische Schädigung, die durch die Translokation des nukleären Proteins HMGB1 und die reduzierte CYP1A2-Expression weiter bestätigt wurde. Weibliche Lebern und junge Lebern mit kürzerer WIT waren in höherem Maße geschützt, wie durch die höhere Gallenproduktion, geringere Enzymfreisetzung und weniger histologische Schädigung angezeigt wurde. Im Gegensatz dazu waren gealterte Lebern weniger gut konserviert.

In der LTx-Studie wurden Lebern von jungen männlichen Spendern transplantiert und für 1h bzw 24h nach Reperfusion beobachtet. Alle Durchblutungsparameter (PVP, PVF; Gewebesauerstoffsättigung, Gewebeblutfluß, perfused capillary density) als auch die Routinelaborparameter (klinische Chemie, Blutbild) und die Histologie wurden vor LTx und im Empfänger nach LTx bestimmt, n=6 für 1h, n = 5 für 24h Beobachtung. Eine Stunde nach Reperfusion waren sämtliche Parameter der Leberdurchblutung deutlich erniedrigt, was als indirektes Zeichen einer noch persistierenden Herz-Kreislaufstörung nach der anhepatischen Phase gewertet werden kann. Zeitgleich sahen wir eine deutliche Erhöhung der Leberenzyme, die nach 24h bereits in Rückbildung begriffen war. Zu diesem Zeitpunkt zeigten sich histologische Schädigungszeichen, sowohl in der HE- als auch in der HMGB1- und CYP-Färbung. Die statistische Analyse ergab eine starke inverse Korrelation der zeitgleich erhobenen Durchblutungsparametern und Enzymwerten.

**Schlussfolgerung:** Die NMP unter Verwendung von oxygeniertem Williams E-Medium ohne zusätzliche Sauerstoffträger kann die Morphologie und Funktion der Rattenleber für mindestens 6 Stunden erhalten. Die Spendermerkmale wie Geschlecht und Alter sowie eine auch minimale Verlängerung der WIT haben einen signifikanten, jeweils günstigen bzw. nachteiligen Effekt auf die Organkonservierung. Hier sind weitere Untersuchungen zur Aufklärung des pathophysiologischen Schädigungsmechanismus erforderlich.

Die intra-operative Bestimmung von Leber hämodynamik, -perfusion und -mikrozirkulation scheint den frühen IRI gut abzubilden. Hier sind weitere Studien erforderlich um den Parameter zu identifizieren, der intraoperativ einfach zu bestimmen und Vorhersagen zum Schweregrad der IRI ermöglicht. Die Behandlung des komplexen Themas der IRI von der Seite der NMP, um schwere IRI zu verhindern, und aus diagnostischer Sicht wird dazu beitragen, schwere Leberschäden besser zu verhindern.

# 1 INTRODUCTION

## 1.1 Global liver transplantation activity

**The number of liver transplantations is increasing constantly. However, the number of donor organs cannot match the need.** In 2022, 37,436 liver transplants (LTx) were performed globally (**Figure 1**), an increase of 8% from 2021 and a 49% increase from 2015 (including living and deceased donors)(GODT, 2023). In the United States, 9,527 transplants were performed in 2022, representing a 52% increase over the past decade. However, in this year, twice as many adult candidates (24,186 patients) remained on the liver transplant waiting list.

**Therefore, organs from living donors and so-called marginal grafts are used in increasing frequency to expand the donor pool.** In Asian countries, 2,260 liver grafts are obtained from living donors in 2022. In contrast, more than 90% of LTx are performed with livers from deceased donors in the Western world (Kwong et al., 2024). In the US alone, 603 grafts (6.3%) were obtained from living donors, whereas 8,924 (93.7%) were from deceased donors in 2022.

**This includes grafts from aged donors, grafts with morphological impairment such as steatosis or grafts subjected to warm ischemia as in donation after circulatory death (DCD).** The number of donations from older age groups has significantly increased by over 30% from 2012 to 2022. The sex composition of donors remained relatively unchanged in 2022: 62.4% male, 37.6% female. In addition, the proportion of adults receiving DCD livers doubled in the 10-year period from 2012 to 2022 and increased from less than 5% (4.6%) in 2012 to more than 10% (11.3%) in 2022 (Kwong et al., 2024).

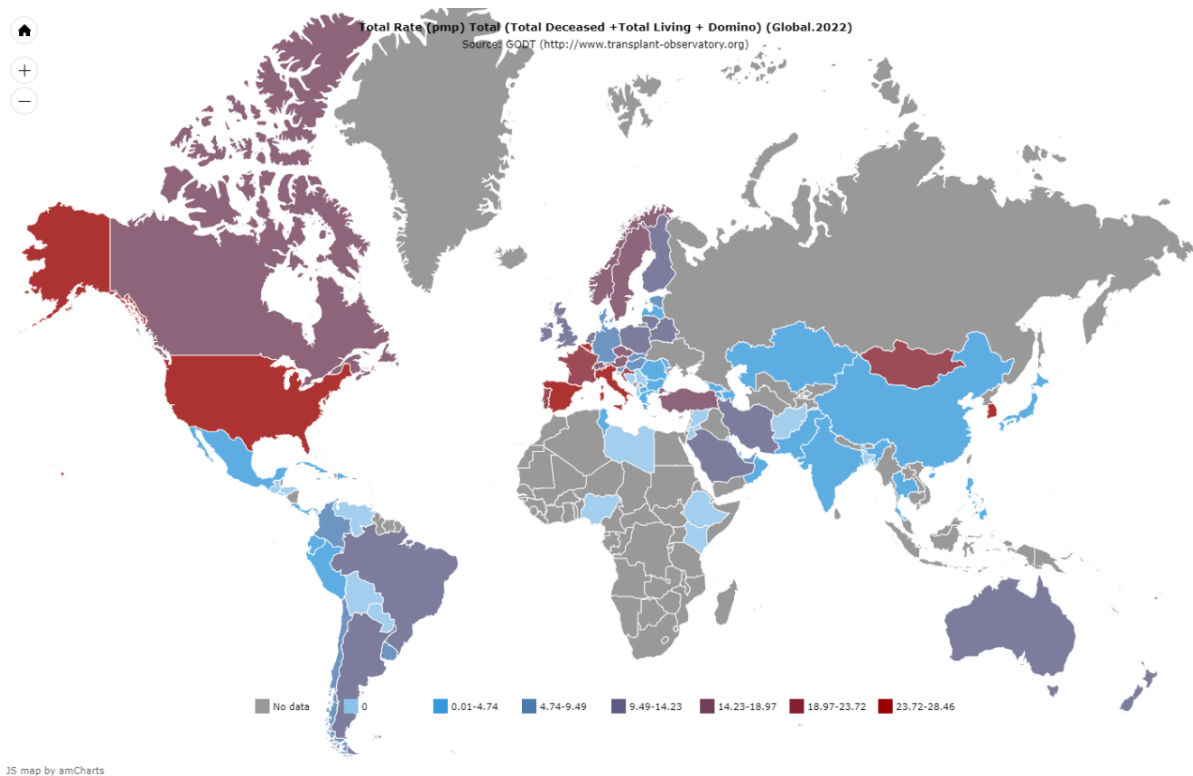


**Figure 1. Global liver transplant activity in 2022 per million population.** Overall 37, 436 liver transplants were performed, with 24% using living donors. The highest number of transplants per million population is seen in Korea, the United States, and several countries in Western Europe. Numbers provided by the Global Observatory on Donation and Transplantation (GODT), produced by the WHO-ONT. Accessed March 9, 2024 (GODT, 2023).

## 1.2 Hepatic ischemia-reperfusion injury in liver transplantation

**LTx is the most effective treatment for various end-stage liver diseases** (Sinha et al., 2024). However, LTx holds the immanent risks of ischemia-reperfusion injury (IRI). Ischemia starts with the interruption of blood supply during organ procurement and ends with reperfusion upon re-installing the blood flow, resulting in both cold and warm ischemia. The term IRI refers to tissue damage caused by interrupting and then reestablishing blood supply to the organ. Liver IRI has substantial effects on liver function and causes systemic injury. The extent of IRI is dependent on the length of warm and cold ischemia during organ procurement, transport, and implantation and on the individual recipient's susceptibility. Furthermore, susceptibility is dependent on donor characteristics such as age, gender, and comorbidity of the organ and or the recipient.

**The mechanism involved in IRI is complex (Figure 2).** Ischemic conditions disrupt cellular respiration, affecting the production of ATP due to the lack of oxygen and nutrients. Initially, there is a reduction in ATP production, prompting the initiation of anaerobic respiration and lactate accumulation. As a result, energy (ATP) is lost and succinate and dihydronicotinamide adenine dinucleotide (NADH) accumulates (Blacker & Duchon, 2016). Additionally, ischemia

prompts xanthine hydrogenase conversion into xanthine oxidase. This enzyme catalyzes hypoxanthine degradation under aerobic conditions (Jimenez-Castro et al., 2019). However, the generation of NADH and xanthine oxidase increases the production of reactive oxygen species (ROS), highly toxic molecules which can oxidize organic molecules and damage cell membranes through lipid peroxidation (Chullo et al., 2024).

The primary mechanism underlying damage during cold storage involves injury to liver sinusoidal endothelial cells (LSECs). These cells are pivotal in maintaining vascular homeostasis and immune function, making them a central target of cold ischemia, whereas warm ischemia predominantly affects hepatocytes. During cold ischemia, there is a significant accumulation of NADH in damaged hepatic sinusoidal endothelial cells, contributing to the inability of injured LSEC to produce nitric oxide (NO). Depletion of NO stores and uninhibited activity of vasoconstrictors such as thromboxane A<sub>2</sub> result in increased vascular tone and decreased blood flow to hepatocytes (Peralta et al., 2013). Furthermore, the Na<sup>+</sup>/K<sup>+</sup>-ATPase function is nearly shut down due to insufficient ATP supply. Failure of the Na<sup>+</sup>/K<sup>+</sup>-ATPase pump results in the intra- and extracellular sodium-potassium imbalance, resulting in swelling, bulging sacs, and fragmentation of cells (Tara et al., 2021).

**Blood reperfusion, rather than promptly restoring normal conditions, exacerbates the situation due to the excessive generation of ROS** (Cursio & Gugenheim, 2012). During this period, ROS overproduction activates Kupffer cells, thereby initiating a cascade of inflammatory events, including the release of proinflammatory cytokines such as Tumor Necrosis Factor Alpha (TNF- $\alpha$ ), Interleukin-2 (IL-2), Interleukin-6 (IL-6), Interleukin-1 (IL-1), and high mobility group box 1 (HMGB1) protein (Cursio et al., 2015). HMGB1 acts as an alarmin, an alarm protein signal that initiates the inflammatory response resulting from liver I/R injury (Gaskell et al., 2018). During reperfusion, HMGB1 translates the damage into the subsequent inflammatory reaction. HMGB1 translocates from the nucleus to the cytoplasm and further to the extracellular space. HMGB1 levels in serum increase during liver IRI as early as 1 h after reperfusion and increase further in a time-dependent manner up to 24 h (Liu et al., 2011; H. Yang et al., 2020). In addition, during reperfusion, ROS generated during reperfusion can degrade proteoglycans, posing a threat to the glycocalyx of the cell membrane. As a result of glycocalyx disruption, the LSEC surface is exposed and activated and, in turn, promote platelets and leukocytes adherence into the liver sinusoids, negatively affecting microcirculation (van Golen et al., 2012).

**In addition, autophagy plays a vital role during liver IRI.** Autophagy is an intracellular self-digestion pathway initiated to remove damaged organelles and proteins, which maintains

cell survival, differentiation, and homeostasis (Mizushima, 2007). There is some contradictory data regarding the effects of autophagy in liver IRI. Ischemia-reperfusion injury in warm ischemia leads to rapid depletion of ATP. Mitochondria in hepatocytes are overloaded with ROS (Kim et al., 2003). Loss of substrates for oxidative phosphorylation leads to increased mitochondrial permeability, especially in the reperfusion phase. Autophagy is protective in this setting as it leads to the shuttling of damaged mitochondria into the autophagosome, limiting the production of ROS. Cursio et al. observed that overexpression of Beclin 1 or induction of autophagy through mammalian target of rapamycin (mTOR) inhibitors such as rapamycin reduces IRI-induced hepatocyte death (Cursio et al., 2015). Similarly, previous reports indicated that treating LSECs subjected to static cold storage with simvastatin induced expression of the vasoprotective transcription factor Kruppel-like factor 2. Further, HMGB1 released during IRI is a competitive binder of Beclin which in return induces autophagy. The protective effects of reducing HMGB1 secretion after IRI may be related to decreased autophagy when lower levels of HMGB1 are present (Shen et al., 2013). In contrast, several previous studies observed downregulating autophagy can attenuate liver IRI. Kang et al. revealed that melatonin downregulated autophagy via activation of mTOR signal which resulted in improvement of liver IRI (Kang et al., 2014). Besides, Fang et al. observed chloroquine inhibited autophagy and induced apoptosis aggravating liver IRI (Fang et al., 2013).

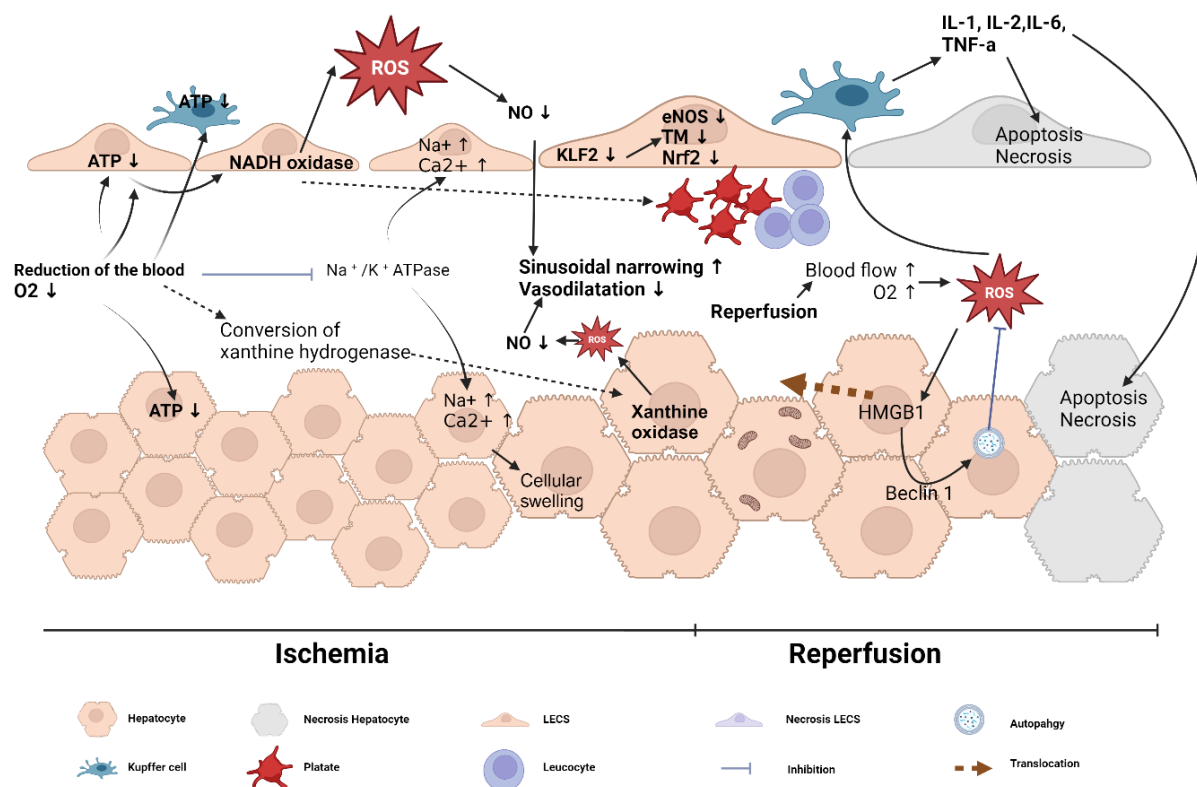


**Figure 2. Mechanisms involved in liver IRI.** The process of liver I/R injury involves a series of complex events, such as energy depletion of mitochondria (ATP depletion), metabolic acidosis, Kupffer cell activation, calcium overload, oxidative stress, and the upregulation of pro-inflammatory cytokine, resulting in cellular swelling, apoptosis, and necrosis. ATP: adenosine triphosphate; LSEC: liver sinusoidal endothelial cell; IL-1: interleukin-1; IL-2: interleukin-2; IL-6: interleukin-6; NO: nitric oxide; ROS: reactive oxygen species; TNF: tumor necrosis factor- $\alpha$ ; eNOS: endothelial nitric oxide synthase; TM: thrombomodulin; Nrf2: nuclear factor erythroid 2-related factor 2. Figure generated using BioRender.

### 1.3 Predictive value and visualization of liver microcirculation

**Reperfusion after prolonged ischemia is affecting hepatic perfusion.** As explained above, reoxygenation during reperfusion is impairing microcirculation due to the narrowing of the sinusoidal bed. Endothelial cell swelling and dysfunction, sludge formation with microthrombi, and leukocyte stagnation, may even lead to sinusoidal perfusion failure, a major determinant of IRI of the liver (Vollmar & Menger, 2009).

Previous studies in rats demonstrated the pivotal role of the first few minutes after revascularization in developing hepatic reperfusion injury (Lu et al., 2014; Siniscalchi et al., 2016). Therefore, severity of initial microvascular dysfunction might serve as a predictive parameter for the early graft function during the clinical course following liver transplantation (Marambio et al., 2018; Puhl et al., 2005). Marambio et al. revealed that portal flow of more than 123 mL/min per 100 g liver is indicative of a better survival after liver transplant (Marambio et al., 2018). Moreover, another previous study demonstrated the value of intraoperative microcirculation assessment for prediction of postoperative graft function by monitoring hepatic microcirculation 5min and 30min after reperfusion (Puhl et al., 2005).

Intravenous fluorescence microscopy is one of the standard methods for investigating liver hemodynamics in experimental settings. Due to its high technical complexity and the requirement of potentially toxic fluorescent dyes for contrast enhancement, intravital fluorescence microscopy can not be applied in the clinic. As a result, some other techniques have been used clinically, including thermodiffusion and laser Doppler flowmetry (Aykut et al., 2015; Ince, 2005; Puhl et al., 2005). Both methods demonstrated the value of assessing liver microcirculation and tissue perfusion in the clinic. Nevertheless, the hepatic sinusoidal network cannot be visualized directly in vivo using these techniques.

In contrast, orthogonal polarized spectral and sidestream dark field imaging video microscope devices are developed to visualize the alteration of microcirculation. However, due to technical limitations and poor image quality, these technique devices remained rather research tools for visual assessment of microcirculation, but did not make it into clinical routine. Recently, Cytocam, a novel handheld microscope based on incident dark field illumination

(IDF) technique, has been introduced. Improved contrast and image quality, as well as ease of use, render this handheld device a promising tool also for clinical application. CytoCam has been shown to be valuable and promising for intraoperative assessment of hepatic perfusion and microcirculatory alterations in hepatobiliary surgery, including liver resections (Uz et al., 2021) and portal vein embolization (Shen et al., 2020; Uz et al., 2022).

#### **1.4 Impact of donor properties on hepatic IRI**

**The severity of liver ischemia-reperfusion injury in LTx is affected by donor characteristics such as donor gender, age, and comorbidity, but also mode of death (Figure 3).** Understanding the impact of donor properties, therefore, is critical to success in LTx.

**Female liver grafts perform better than male grafts.** The liver, as a primary target for estrogen, relies on hepatic estrogen signaling to attenuate hepatic IRI and expedite recovery (Han et al., 2023). Based on previous rodent research, females are less susceptible to IRI, a protective mechanism initiated by estrogen. The protective effect of estrogen may involve its direct effect on the vascular endothelium by increasing the production of endothelial cell-derived NO (Harada et al., 2001). It has been suggested that estrogen could act as a ‘survival factor’ for hepatic endothelial cells. Thus, male mice pre-treated with estrogen exhibit improved outcomes following IRI and, conversely, ovariectomised mice or female mice pre-treated with an estrogen receptor antagonist observed poorer outcomes (de Vries et al., 2013). In parallel, a 20-year follow-up study of 313 liver graft recipients revealed that gender significantly affected post-transplant survival. Graft survival rate in female was significantly higher than in males. (females 61.4% vs male: 47.9%,  $P = 0.017$ , (Nephew et al., 2021)).

**Aged livers are more sensitive to IRI** due to age-related impaired hepatic microcirculation, morphological changes, and hepatocyte dysfunction (Durand et al., 2019). At the cellular level, older donors have fewer and less functional mitochondria, rendering aged liver grafts susceptible to ATP depletion during static cold storage (SCS) and warm reperfusion (Dar et al., 2019). Clinical data indicate that age of donor is a significant determinant of survival after transplantation. Schwartz et al. revealed that the 5-year post-transplant survival rate of liver grafts obtained from donors over 70 years reached to 55%, compared to 73% in the age of less than 70 years (Schwartz et al., 2012). One of the reasons contributing to the higher susceptibility for IRI is the age-related development of either hepatic fibrosis leading to increased stiffness of the organ but also the accumulation of fat in the liver, the age-related development of hepatic steatosis. Fibrosis and steatosis both impair the microcirculation of the liver due to the



compression of sinusoids either by deposition of a surplus of extracellular matrix or the intracellular accumulation of lipid droplets enlarging the hepatocytes.

**The mode of death of the organ donor is also affecting the outcome after transplantation.**

In contrast to grafts obtained from donors after brain death (DBD), organ obtained from DCDs experience warm ischemia due to the interruption of vascular perfusion prior to cold preservation. During this phase, hepatocytes suffer from oxygen and nutrient deprivation, resulting in decreased intracellular energy and increased oxidative stress, which aggravates liver injury (Petrovic et al., 2022). Furthermore, clinical studies demonstrated that the use of livers from DCD was historically characterized by increased rates of biliary complications and inferior short-term graft survival compared to grafts obtained from donor after brain death allografts.

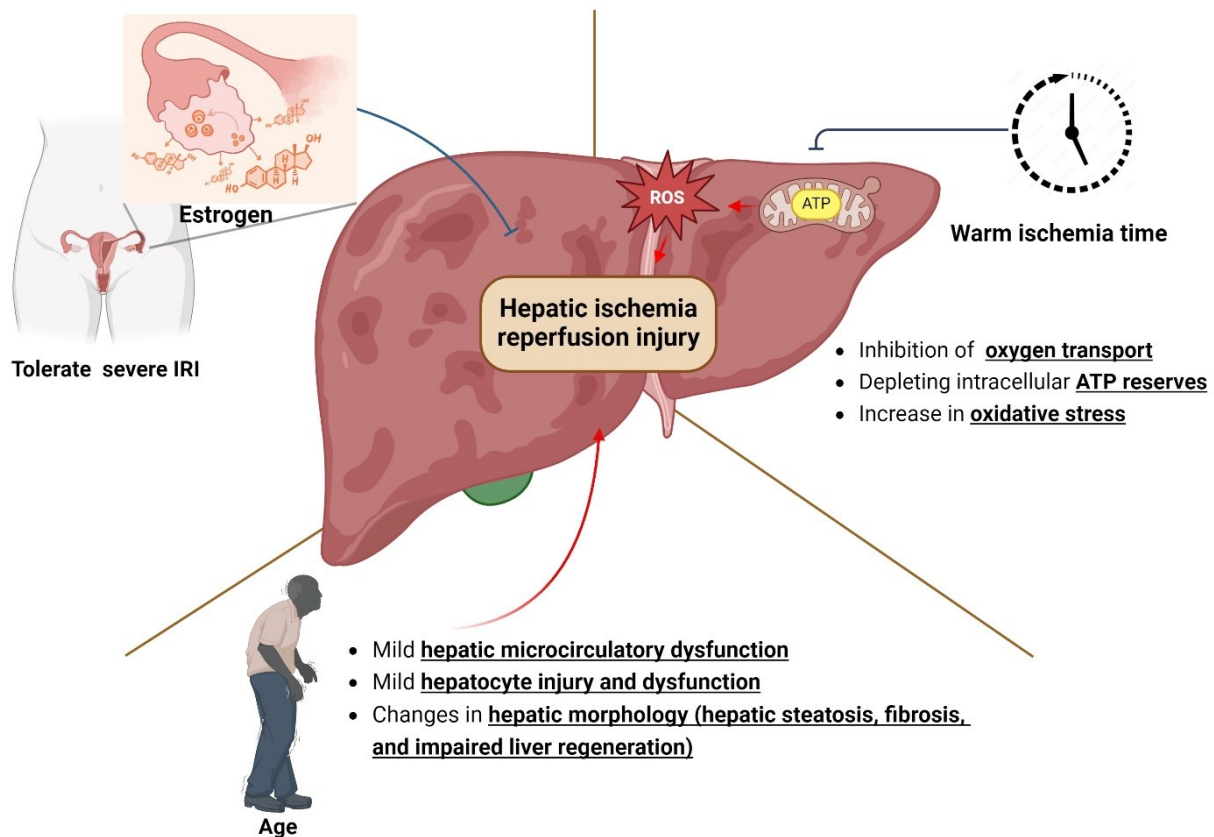


**Figure 3. Impact of donor properties on hepatic IRI.** Aged and grafts obtained donors after cardiac death are more susceptible to liver I/R injury. In contrast, female grafts are less susceptible to IRI due to the protective role of estrogen. (Figure generated using BioRender).

### 1.5 Promises of liver machine perfusion

**In the context of the increasing demand for donor use of marginal organs, the potential benefits of machine perfusion (MP) need to be explored in detail.** Given its simplicity and cost-effectiveness, SCS has become the standard-of-care preservation method in liver

transplantation. Nevertheless, its efficacy is limited when preserving livers from marginal donors due to higher susceptibility to IRI because of structural abnormalities and easier depletion of energy stores, and loss of cellular function (Bruinsma et al., 2013).

Normothermic machine perfusion (NMP) provides perfusion conditions close to the physiological situation. The liver graft is subjected to perfusion at 37°C using an oxygen-rich perfusate supplemented with essential nutrients to maintain metabolic functions *ex vivo*, see **Figure 4** (Manzia et al., 2019). This technique stands out for its potential to preserve grafts from marginal donors, primarily attributed to reduced cold ischemic time and maintenance of cellular metabolic functions. Unlike SCS and hypothermic machine perfusion (HMP), which prioritizes metabolic reduction to extend graft viability, NMP maintains the liver at a state close to its physiological, metabolic rate, and synthetic function (Laing et al., 2017).

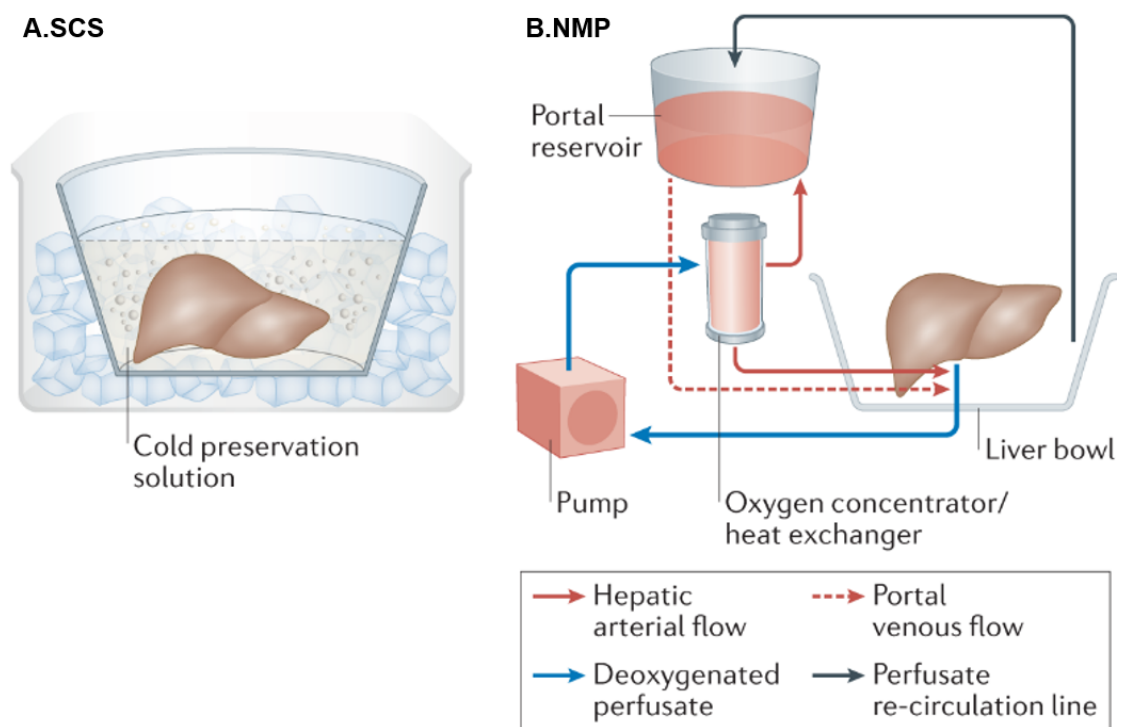


**Figure 4. Schematic representation of SCS and NMP systems.** (A). For SCS, the liver is placed in a preservation solution within an ice box to maintain a temperature of 4 °C. (B). For NMP, a special device suitable only for normothermic liver perfusion is needed. In this fully cannulated circuit, perfusate flows from the inferior vena cava to a centrifugal pump before passing to an oxygen concentrator/heat exchanger. Blood then flows into the liver directly via the hepatic artery or to the portal reservoir. (The figure obtained from Ceresa et al. (Ceresa et al., 2022) with friendly permission of publisher Springer Nature. Permission number: 5764720851339)

**MP improved the outcomes of allografts procured from DCD experiencing long-term WIT.** Regardless of temperature, MP could resuscitate liver grafts that had been exposed to WIT for at least 60 minutes (Muth et al., 2023). MP significantly improved survival rates and prevented liver damage (Perk et al., 2011; Tolboom et al., 2008; Uygun et al., 2010). Based on

these results, it is evident that SCS is limited when applied to DCD grafts. Compared to SCS and hypothermic perfusion, liver grafts show higher metabolic activity during subnormothermic machine perfusion and NMP. Under these conditions, bile production, lactate clearance, and urea production can be used to measure metabolic activity. Prior to transplantation, liver graft viability can be assessed using these parameters.

Several studies have shown that NMP attenuates preservation-related damages in livers obtained from DCD (De Stefano et al., 2021; Tolboom et al., 2008). Moreover, the clinical data support this finding. One phase III RCT reported that organs subjected to NMP were less likely to be discarded and presented with lower peak enzyme release than those that underwent SCS (Nasralla et al., 2018). Despite similar graft survival in the NMP and SCS groups, NMP showed 54% longer preservation and 20% greater organ utilization without compromising graft survival.

In addition, NMP may even serve as a novel avenue for ex situ treatment of donor livers to further optimize them for transplantation. Nagrath et al. described a medium containing a combination of defatting agents (Nagrath et al., 2009). This combination decreased the intracellular lipid content of cultured hepatocytes by 35% over 24 hours, and of perfused livers by 50% over 3 hours.

### **1.6 Urgent issues to be addressed in NMP model**

**The optimal perfusion settings are not yet fully defined.** Due to the use of different perfusates, perfusion circuits, and devices, as well as perfusion routes, flows, and pressures, it is difficult to determine a specific machine perfusion setting best suited for ex vivo liver MP of certain types of grafts (Muth et al., 2023). Most studies emphasize that integrating a dialysis unit into the perfusion circuit might result in higher survival rates because harmful metabolic products produced during MP can be eliminated. Additionally, most publications indicated that oxygen carriers such as blood (Shonaka et al., 2019) and artificial oxygen carriers (Bodewes et al., 2020), already successfully used in the past, should be considered as options for the experimental design. However, Haque et al. observed NMP system can preserve rat grafts for 24 hours without oxygen carriers (Haque et al., 2020).

In addition, there have been no or only partial answers to clinically so far, no publications focus on the impact of donor properties on the outcome of NMP.

### **1.7 Role of autophagy in liver machine perfusion**

**The role of autophagy during the IRI is discussed controversially. It seems that autophagy exerts a beneficial effect on IRI in liver machine perfusion.** A previous study indicated that hepatic protection during HMP was associated with mitophagy activation through

enhanced Parkin mitochondrial translocation and cell anti-apoptosis. In addition, Ohman et al. observed in a recent NMP study functional livers demonstrated more changes in the expression of genes associated with autophagy than did nonfunctional livers (Ohman et al., 2022). Active autophagy in functional livers was evidenced by higher expression of LC3-II protein after 6 h of perfusion. In contrast to non-functional livers, persistent activation of ribosomal protein S6 kinase likely repressed autophagy during NMP, hindering the response of liver to injury and stress. Moreover, NMP protects against biliary injury in DCD rat liver via inhibiting autophagy. (Bai et al., 2023). Therefore, modifying autophagy during machine perfusion may be an attractive therapeutic strategy to improve donor liver organ function prior to transplantation.

Taken together, IRI remains a major problem in liver transplantation, which is addressed in this study from two complementary points of view:

- 1 Use of machine perfusion to reduce IRI of marginal livers
- 2 Assessment of hepatic microcirculation early after LTx to predict severity of hepatic IRI

## **2 AIM AND HYPOTHESIS**

### **2.1 Aim**

In this study, we set four aims for NMP:

1. Establish a stable NMP model for rat livers obtained from DCD.
2. Investigate the optimal balance between sufficient supply and adequate waste removal in machine perfusion conditions for livers obtained from DCD by detecting liver damage.
3. Explore the impact of donor properties such as age, gender, and duration of warm ischemia on the outcome of NMP by detecting liver damage, liver function, and liver microcirculation.
4. Understand the impact of age on the liver subjected to NMP by investigating autophagy as one key mechanism.

Similarly, we set three aims for LTx:

1. Establish a stable rat orthotopic LTx model.
2. Explore the impact of early I/R injury in rat LTx model on liver damage, liver function, and liver microcirculation.
3. Investigate the correlation of liver microcirculation impairment with liver damage and liver function after LTx.

### **2.2 Hypotheses**

1. Regarding the optimal balance of supply and waste removal in NMP, we hypothesized that slight hyperperfusion is needed to compensate for the limited oxygen supply when using oxygenated medium as perfusate and that partial medium change is improving graft integrity and function due to waste removal.
2. Regarding the impact of donor properties on NMP, we hypothesized that (a) female and sWIT DCD livers were protected to a higher degree, as indicated by higher bile production, lower enzyme release, lower liver microcirculation damage, and lower histological damage, and that (b) aged DCD livers were less well preserved possibly due to structural impairment;
3. Regarding the role of autophagy in aged livers subjected to NMP, we hypothesized that (a) autophagy was impaired in the aged liver, and that (b) NMP activates autophagy;
4. Regarding the early I/R injury in rat LTx, we hypothesized that (a) hepatic morphology, liver function, and liver microcirculation are impaired to varying degrees early after liver transplantation and that (b) liver microcirculation is correlated to liver damage, blood components, and liver function.

### **3 STUDY DESIGN**

To achieve these goals, we designed a study with two parts.

#### **Part I: The NMP study consisted of 4 steps**

1. To establish the NMP model, the optimal sequence of surgical steps, the choice of perfusate (perfusion medium, perfusion time), and the flushing condition (solution, volume, speed, and heparin doses) were evaluated.
2. To identify the optimal perfusion conditions representing the best balance between supply and waste removal, the impact of flow rate and medium change was tested. In the first step, young male livers obtained from DCD were subjected to NMP after a WIT of 30 minutes using a flow rate of either 1, 2, or 3 ml/min/g liver. In the second step, the impact of medium changes during the 6 hours perfusion period was evaluated. Half of the perfusate was either not exchanged or replaced once after 3 hours of perfusion, or twice after 2 and 4 hours of perfusion, respectively (n=3/group). The resulting optimal conditions were used in the following experiments.
3. To explore the impact of donor properties on the outcome of NMP, 4 groups were designed based on gender, age and WIT. Livers from young male rats aged between 10 and 20 weeks were subjected to NMP after a WIT of about 30min, using a perfusion rate of 3ml/min/gr liver with one medium change after 3h were used as control. Livers from female donors of a similarly wide age range were used to explore the impact of donor gender, livers from male donors of 24 months were used to explore the impact of age, and livers from young male donors experiencing a WIT of 20 min were used to assess the impact of ischemia time.
4. To investigate the role of autophagy in the aged liver, 2 groups were designed based on the donor age. Livers obtained from young and old male rats subjected to liver explantation were used as control group. Livers from young and old male rats subjected to 6 hours of NMP were used as the experimental group.

#### **Part II: The LTx study consisted of 3 steps**

1. To establish stable allogeneic rat LTx model, male Wistar rats were subjected to orthotopic LTx using the Two-Cuff technique. Stability of the surgical procedure was assumed when 3 rats tolerated the LTX-procedure for at least 24h without obvious complications.
2. To explore the impact of early IRI on liver damage and liver function, young male recipient rats were subjected to orthotopic liver transplantation. Donors livers were subjected to 1 hour of cold storage. Recipients were sacrificed 1h and 24h after LTx (n=5 in 24h, n=6 in 1h) to obtain blood and liver samples. For control purposes, blood and liver samples were

also obtained from the donors.

3. To investigate hepatic microcirculation early after liver transplantation and to explore the correlation between liver microcirculation and liver damage and function, the donors and recipients were subjected to the same procedure as described above. The portal vein pressure, portal vein flow rate, liver stiffness, perfused capillary density in the liver and the proportion of perfused capillaries were detected in the donors prior to harvesting the liver and in the recipients 1h after LTx, respectively.

## **4 METHODS**

### **4.1 Animal experiments**

#### **4.1.1 Animals**

Female and male Wistar young rats aged 10-30 weeks (300-450g weight) and old rats aged 120-125 weeks (550-650g) were obtained from Janvier (France) and Charles River (Germany). Rats were randomly housed in groups and had free access to food and water. The cages were kept under constant environmental conditions with a twelve-hour light/dark cycle in a conventional animal facility, constant room temperature ( $21 \pm 2$  °C), and 45–65% relative humidity. Animal experiments were performed according to the current German regulations and guidelines for animal welfare and documented according to the ARRIVE Guidelines for Reporting Animal Research. The animal experiment protocol was approved by the Internal animal protection officer/Thüringer Landesamt für Verbraucherschutz, Thuringia, Germany (Approval-Number: TWZ-02-2022, TWZ-04-2024, UKJ-23-004, UKJ-22-036, and UKJ-17-106). All possible measures were taken to minimize animal suffering and decrease the number of animals used.

#### **4.1.2 Procurement of liver grafts from DCD**

The rats were euthanized through CO<sub>2</sub> inhalation. Assurance of complete cessation of both cardiac heart and respiratory movements as tested by palpation marked the initiation of the warm ischemia time (WIT). WIT was defined as the period between the cessation of cardiac activity and the connection with the perfusion apparatus. All livers were subjected to in situ warm ischemia for durations of either 20 or 30 minutes. After a transverse laparotomy, the intestine was retracted to the lower right to fully expose the liver. The common bile duct (CBD) was cannulated with a Fr 2 polyurethane cannula (Table S1). After ligating and transecting the hepatic artery, the portal vein (PV) was cannulated with an 18G steel cannula (Table S1). The liver was flushed via the PV cannula (10ml/min) with 100 mL of Ringer-lactate solution containing 500U heparin (Table S2), maintained at room temperature with a flow rate of 10ml/min. The inferior hepatic vena cava (IHVC) and the thoracic segment of the superior hepatic vena cava (SHVC) were transected to serve as outflow tracts during the flushing. Subsequently, a Fr 1 polyurethane cannula (Table S1) was inserted through the SHVC to the left hepatic vein. After flushing, the liver was removed by transecting the ligaments and CBD. The excised liver was then weighed, placed in a petri dish, and transferred to the machine perfusion system.



### 4.1.3 NMP setup

The NMP circuit (**Figure 5**) included a perfusion chamber, one peristaltic pump, a hollow fiber membrane oxygenator, a bubble trap, and a reservoir. The system temperature was set at 37°C. The liver was continuously perfused for 6 hours. Portal vein pressure and wedge hepatic pressure were measured hourly, see chapter 4.6.1. The perfusion solution (Table S4) consisted of 400ml phenol red-free Williams E Medium, supplemented with 100ml fetal bovine serum, 100 U/mL penicillin, 100 mg/ml streptomycin, 0,292 g/l L-glutamine, 1U/L insulin, and 10 mg/L hydrocortisone. Carbogen (95% O<sub>2</sub> + 5% CO<sub>2</sub>) was used for oxygenation. The inflow pO<sub>2</sub> was continuously maintained at >300 mmHg (flow rate: 4L/min).

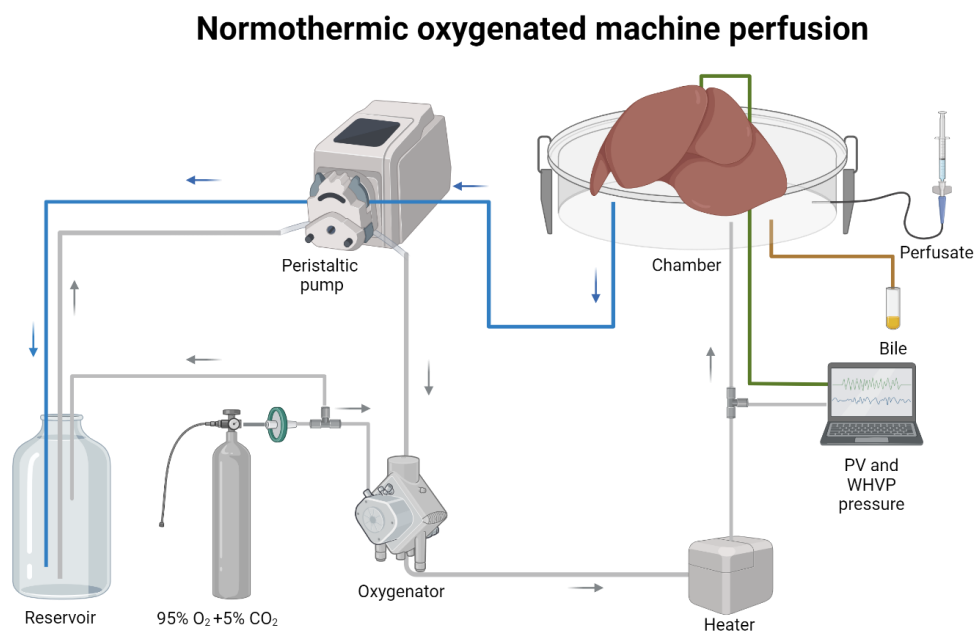


**Figure 5. Setup of the NMP system.** (Figure generated using BioRender)

### 4.1.4 Technique of orthotopic rat liver transplantation

#### *Donor procedure*

The donor rats received a subcutaneous injection with 0.05 mg/g body-weight buprenorphine subcutaneously 30min before surgery followed by induction and maintenance of anesthesia with 4% and 2.5% isoflurane inhalation, respectively. After confirming the absence of reflexes, the rats underwent hepatectomy. The rat was placed in a supine position on its back. Following transverse laparotomy, about 1cm below the rib cage, the intestine was placed to the lower left side of the abdominal cavity to expose the liver and covered with wet gauze. The falciform ligament, left diaphragmatic vein, and hepato-esophageal artery were divided and transected sequentially. After opening the retroperitoneum to access the inferior hepatic vena cava (IHVC),

the right renal vein (RRV) and the right adrenal vein (RAV) were ligated and dissected. The hepatic artery (HA), splenic, and duodenal-pancreatic veins were ligated using 6-0 silk and dissected. A 22G, 5 mm stent with a rough surface was inserted into the common bile duct (CBD), and secured in position with a 6-0 ligature. As a next step, 1 IU/gr body weight of heparin was injected through the dorsal vein of the penis. After cannulating the portal vein (PV) with an 18G needle, the liver was flushed with 0.2ml/gr body weight of cold ringer lactate with 1 IU/gr body weight of heparin using a pressure of 20cm water column. At the same time, the IHVC was opened below the left renal vein to allow an adequate outflow, and the diaphragm was opened to transect the SHVC above the diaphragm in the thorax. Flushing took about 10 minutes to 15 minutes, corresponding to a physiological flow rate of 1-2ml/min/gr liver. The diaphragm was dissected completely, and the liver was placed into a Petri dish with ice-cold saline solution.

#### *Back-table procedure*

After transferring the graft to a cell culture dish containing 0-4°C ice-cold saline solution and placing the dish on ice, the cuff was inserted into the PV, followed by everting the vessel around the edge to expose the intima. A ligation was placed to secure the vessel in this position. The same procedure was performed in the IHVC. After that, the SHCV was freed, and all remaining tissue of the diaphragm was removed and trimmed to a length of about 5mm. Two 8-0 single-armed prolene stay sutures were placed at the opposite lateral edges of the SHVC, from outside to inside. After that, the graft was stored in the refrigerator at 0-4 °C.

#### *Recipient procedure*

The recipient rats were subjected to the same anesthesia and laparotomy procedures as the donors. The left diaphragmatic vein, hepato-esophageal artery, and RAV were ligated and dissected. Systemic heparinization was performed as in the donor after ligating and dissecting proximal and distal CBD and HA. The SHVC was blocked with a Satinsky clamp which was placed on the right side. Consequently, IHVC and PV were blocked using microvascular clamps, thereby starting the anhepatic phase. During the anhepatic phase, the isoflurane concentration was decreased to 0.6%. The donor liver was transferred into the recipient's abdomen. After fixing two stay sutures at the two corners of the SHVC, the posterior and anterior walls were sutured from right to left and from left to right, respectively. For PV anastomosis, stay sutures (7-0 prolene) were placed on both sides of the PV and held in place with mosquito clamps for retraction. Then, the cuff was inserted and secured with 6-0 silk suture. After removing the

portal and Satinsky clamps, the isoflurane concentration was adjusted to 1%. The same procedure was performed for the IHVC anastomosis. For the BD anastomosis, the remaining BD in the recipient was partially opened to insert the BD stent. Then the BD stent was secured with 2 silk sutures. The intestine was placed back into the abdominal cavity, and the muscle and skin layer were sutured separately with a running suture using prolene 4-0. After closing the abdomen, 0.5% glucose solution in a dose of 0.01ml/g/gr body weight was injected subcutaneously.

## 4.2 Experimental groups

### 4.2.1 Group distribution for NMP study (Part I)

The NMP study (Part I) was performed in 4 steps (Figure 6): **Step I:** Setting up the surgical model. **Step II:** Identification of optimal perfusion conditions representing the best balance between oxygen supply and waste removal, see Figure 7. **Step III:** Exploration of donor properties potentially affecting the outcome of NMP, see Figure 8. **Step IV:** Investigation of the relationship between age and autophagy, see Figure 9.

In the **Step I**, we explored the sequence of surgical steps as well as the solution for flushing and perfusions to get a stable NMP model. In **Step II**, we investigated the impact of flow rate and medium change. Firstly, young male livers obtained from DCD were subjected to NMP after a WIT of 30 minutes using a flow rate of either 1, 2, or 3 ml/min/g liver. Secondly, we evaluated the impact of medium changes during the 6h perfusion period. Half of the perfusate was either not exchanged or replaced once after 3 hours of perfusion, respectively twice after 2 and 4 hours of perfusion. As shown in Figure 7, the resulting optimal conditions were used in the following experiments.

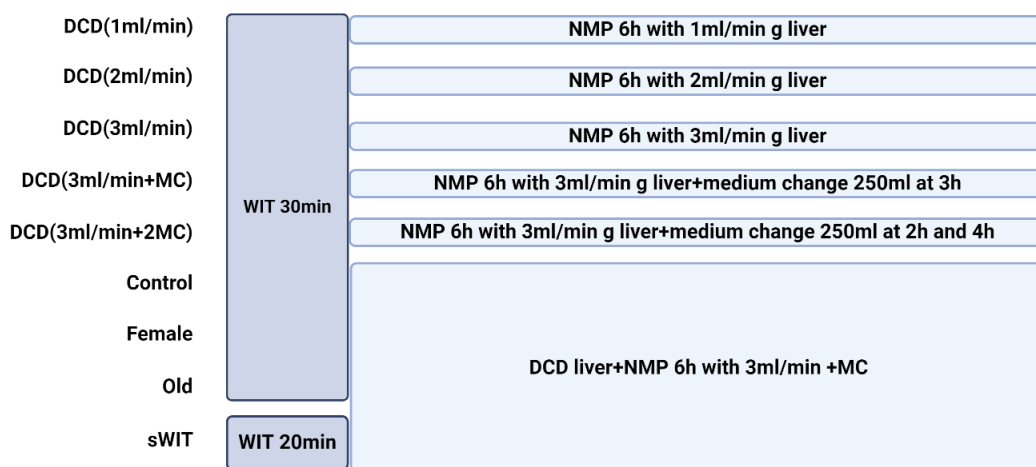
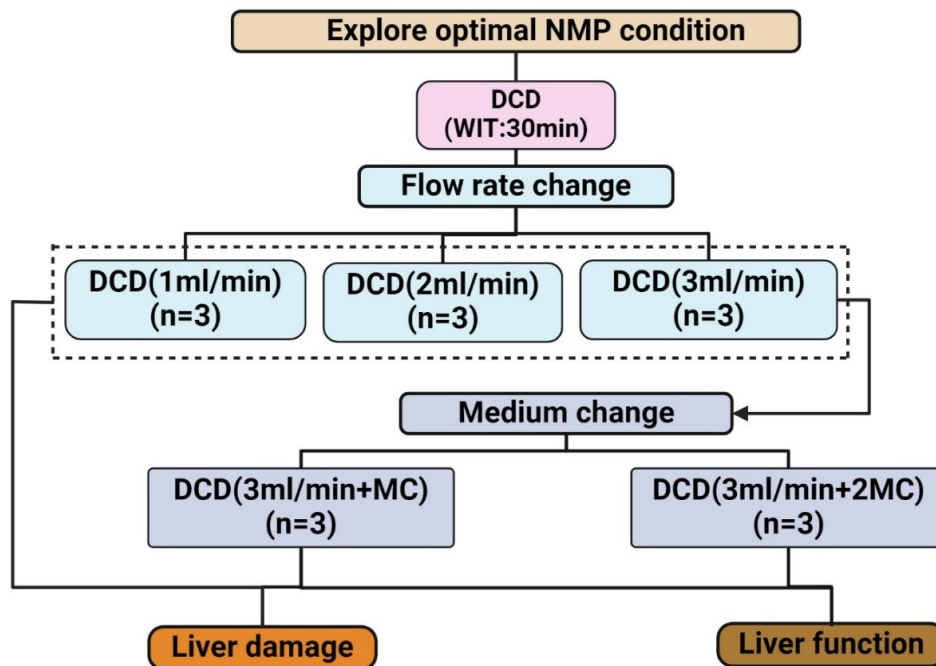
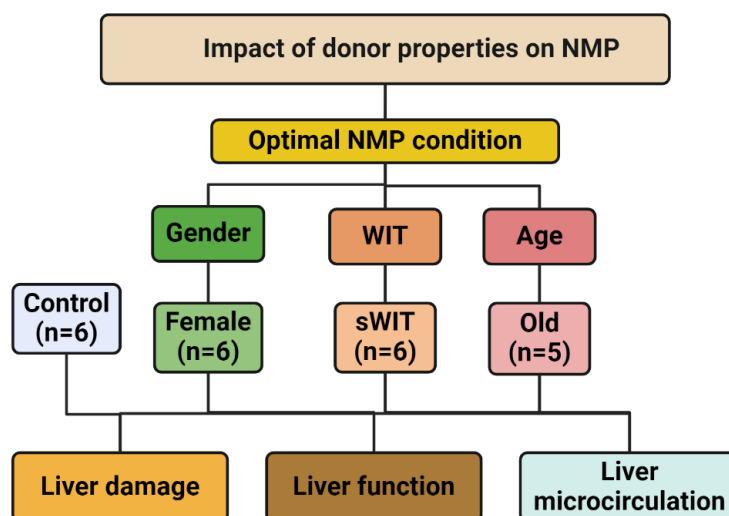


Figure 6. Experimental design of NMP experiment. (Figure generated using BioRender)



**Figure 7. Experimental design for identification of optimal perfusion conditions representing the best balance between oxygen supply and waste removal.** (Figure generated using BioRender)

To explore the impact of donor properties on the outcome of NMP (**Step III, Figure 8**), 4 groups were designed based on gender, WIT, and age of the rat. Livers from young male rats aged between 10 and 20 weeks subjected to NMP after a WIT of 30min, using a perfusion rate of 3ml/min/gr liver with one medium change after 3h, were used as control. Livers from female donors of the same age were used to explore the impact of donor gender, livers from male donors over 24 months were used to explore the impact of age, and livers from young male donors subjected to a shorter WIT of 20 min were used to assess the impact of ischemia time.



**Figure 8. Experimental design for exploration of donor properties potentially affecting the outcome of NMP.** (Figure generated using BioRender)

To investigate the relationship between age and autophagy and explore the impact of NMP on autophagy (**Step IV, Figure 9**), two groups were designed based on age. Liver explanted from young and old male rats serving as recipients of liver grafts were used as control. Livers from young and old male rats subjected to 6 hours of NMP were used as experimental groups. Liver samples were obtained after 2h, 4h and 6h of machine perfusion. Protein expression level of the autophagy markers p62 and LC3b was detected by western blot.

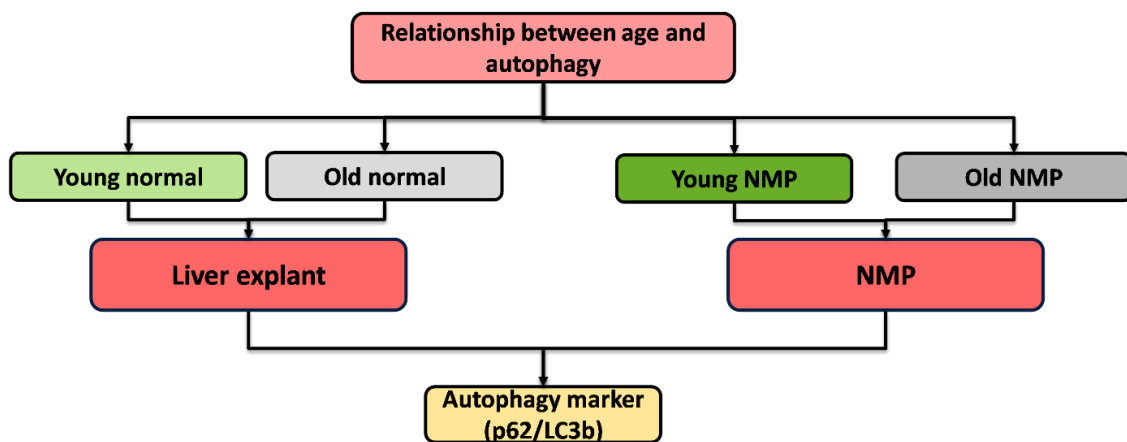


**Figure 9.** Experimental design for investigating the relationship between age and autophagy. Native explanted livers were used as controls and livers subjected to 6h of NMP were as experimental groups.

#### 4.2.2 Group distribution for LTx study (Part II)

The LTx study (Part II) consists of three steps (**Figure 10**): **Step I:** Establishment of rat LTx in respect to learning the sequence of surgical steps separately, reducing the anhepatic time to less than 25 min, improving the intra-operative management to achieve homogenous reperfusion reproducibly, **Step II:** Exploration of early ischemia-reperfusion injury in rat liver transplantation using an observation time of either 1 or 24h, and **Step III:** Investigation of liver microcirculation and correlation of liver microcirculation, damage and function after rat liver transplantation.

First, to establish rat liver transplantation (**Step I, Figure 10**), the training was divided into 3 phases. **Phase A:** “dry exercise” using surrogate materials; **Phase B:** cadaver training, including **Phase B1:** anastomosis training using cadaveric vessels, and **Phase B2:** LTx full procedure training using cadavers; **Phase C:** living animal training, including **Phase C1:** Technical training of full LTx procedure using living animals without postop observation, **Phase C2:** Training of full LTx using living animals to determine postoperative 24h survival rate, **Phase C3:** Training of full LTx-procedure with planned short term observation of 1h to ensure reproducible results, and **Phase C4:** Evaluation of optimized flushing conditions. Phase A consisted of practicing microsurgical handling using surgical gauze and practicing

anastomosis using silicone tubes. Phase B1 consisted of practicing anastomosis on vessels (SHVC) from rat cadavers to improve tissue handling. Phase B2 consisted of training the full procedure on rat cadavers to practice all relevant steps of LTx. Phase C consisted of full procedure technical training using living rats. In Phase C1, animals were sacrificed immediately after completing the procedure. In Phase C2, animals were observed to record the survival time of maximally 24h. Phase C3 consisted of performing the full transplantation procedure training to achieve planned short term observation. Phase C4 consisted of training the full transplantation procedure and optimizing the flushing condition to achieve homogenous reperfusion. Here, animals were euthanized at the end of reperfusion.

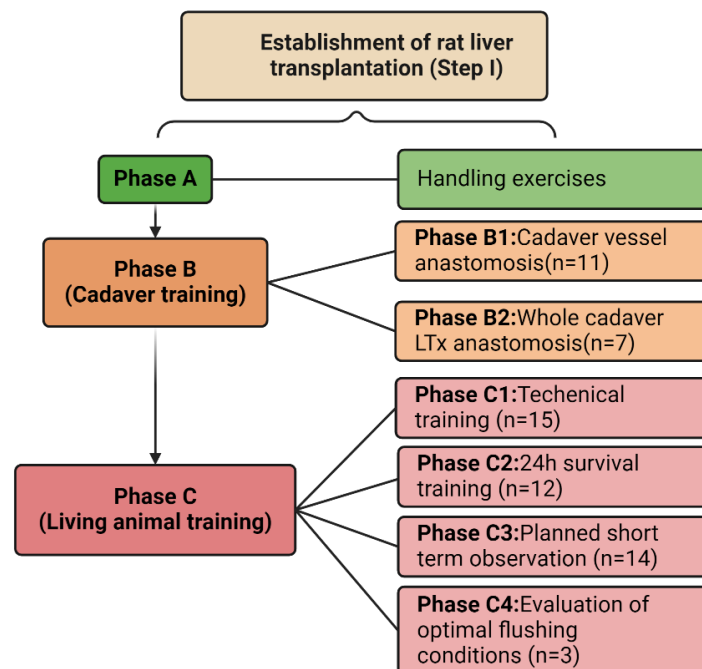


**Figure 10. Experimental design for establishment of rat LTx model.** (Figure generated using BioRender)

Second, to explore the extent and severity of early I/R injury (**Step II, Figure 11**) in terms of hepatic function and hepatic damage, young male recipient rats were subjected to orthotopic liver transplantation. The liver grafts were subjected to 1 hour of cold storage. The recipients were sacrificed 1h respectively 24h after transplantation (**Figure 12**).

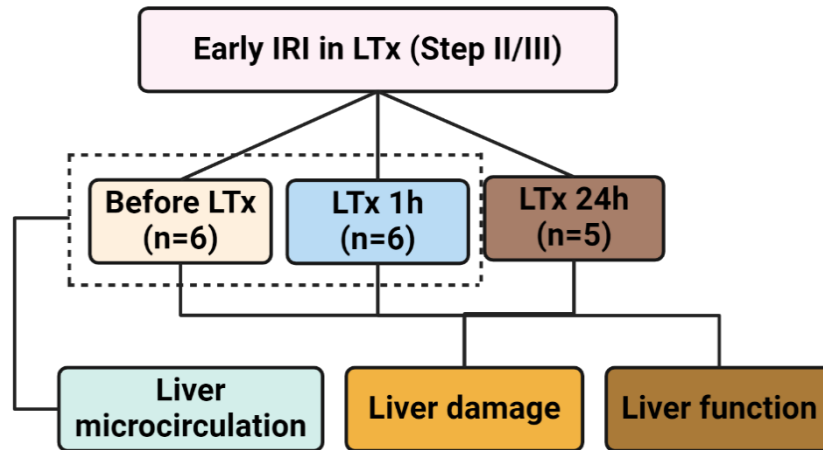


**Figure 11. Experimental design for investigation of early ischemia-reperfusion injury and liver microcirculation.** (Figure generated using BioRender)

Lastly, we investigated hepatic microcirculation and perfusion impairment after early liver transplantation and explored the correlation between liver microcirculation and liver function and damage parameters (**Step III, Figure 11**). The donors and recipients were subjected to the same procedure as in Step II. In addition, hepatic hemodynamics in terms of (portal vein pressure (PVP), portal vein flowrate (PVF)), hepatic microcirculation, in terms of liver perfused capillary density, and proportion of perfused capillaries and liver stiffness, were assessed in the donors prior to explantation and in recipients 1h after transplantation, respectively. Severity of early IRI 1h after reperfusion in terms of liver function and damage parameters was compared to the results obtained after 24h.

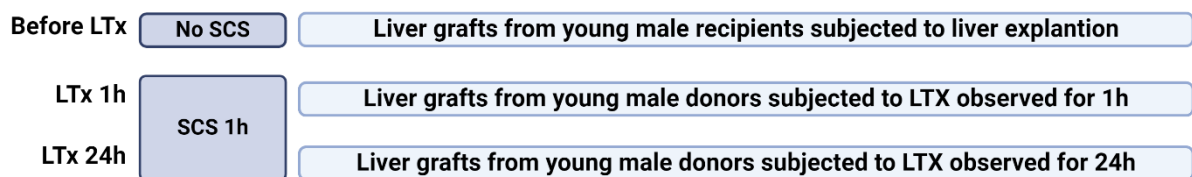


**Figure 12. Group distribution for investigating early IRI and liver microcirculation after reperfusion.** (Figure generated using BioRender)

## 4.3 Sample collection

### 4.3.1 NMP perfusate collection and analysis

Blood gas analysis was performed at 0h, 1h, 3h, and 5h during perfusion on inflow and outflow perfusate samples, testing partial pressure of oxygen ( $pO_2$ ), partial pressure of carbon dioxide ( $pCO_2$ ), bicarbonate ( $HCO_3^-$ ), potassium, and PH. The oxygen consumption rates during NMP were calculated using the following equation: Oxygen consumption ( $\mu\text{mol}$

$O_2/\text{min/g liver} = (C_{\text{in}} - C_{\text{out}})/\text{portal flow (ml/min/g liver)}$  where  $C_{\text{in}}$  and  $C_{\text{out}}$  are the oxygen concentrations in the inflow and outflow, respectively. Oxygen solubility in water = oxygen concentration ( $\mu\text{mol O}_2/\text{ml}$ ) /  $pO_2$  (kPa). Oxygen solubility in water at  $37^\circ\text{C} = 0.01056 \mu\text{mol O}_2/\text{ml/kPa}$  (Han et al., 2023).

$$\text{Oxygen consumption} = \frac{(pO_2^{\text{in}} - pO_2^{\text{out}}) \times 0.01056}{\text{Portal flow}}$$

In addition, outflow perfusate (2 mL) was collected hourly and centrifuged at 4,000 rpm for 10 minutes to obtain the supernatant. The aminotransferase (AST), alanine aminotransferase (ALT), glucose, and lactate dehydrogenase (LDH) levels were measured in the supernatant using an automated Bioanalyzer (Cobas 800, Roche).

#### 4.3.2 LTx blood sample collection and analysis

The recipient rats received a subcutaneous injection with 0.05 mg/g body-weight buprenorphine subcutaneously 30min before surgery followed by sacrifice at 1h and 24h post-transplant via overdose of isoflurane. To detect the release of liver enzymes and renal function, blood (2 mL) was collected via IHVC and centrifuged at 4,000 rpm for 10 minutes to obtain the plasma. AST, ALT, albumin, alkaline phosphatase (ALP), amylase, bilirubin, cholinesterase, cholesterol,  $\gamma$ -glutamyltransferase ( $\gamma$ -GTT), glucose, urea, creatinine, triglycerides, total protein, and LDH levels were measured in the plasma using the automatic biochemical analyzer (Cobas 8000, Roche).

In addition, 1ml EDTA blood was collected for a blood count. The white blood cells (WBC), red blood cells (RBC), hemoglobin (HGB), hematocrit (HCT), mean corpuscular volume (MCV), mean corpuscular hemoglobin (MCH), mean corpuscular hemoglobin concentration (MCHC), and platelet (PLT) were measured by VetScil ABC Hematology analyzer.

#### 4.3.3 NMP bile collection and analysis

As described by others (Liu et al., 2021; Op den Dries et al., 2016), bile production per hour per gram liver (ml/h/gr liver) is considered to be an easy-to-determine but very valuable indicator of hepatic function during machine perfusion. The bile was collected and weighed in hourly intervals.

#### 4.3.4 Liver samples collection

For the NMP study, liver tissue samples were harvested after 2nd (inferior caudate lobe), 4th (superior caudate lobe), and 6th (the remaining liver lobes) hour of machine perfusion. Samples



from native livers were obtained from the explanted liver of recipients. Samples from the transplanted livers were harvested at 1h post-transplant and 24h post-transplant, respectively. All liver samples were fixed in a 5% Formaldehyde solution (Table S2) and stored at 4°C for at least 24h; samples from the remaining liver (one samples from each liver lobe) was snap-frozen in liquid nitrogen. Tissue samples were stored at -80°C until use.

#### **4.4 Histology**

Liver tissue samples were fixed with 4% formaldehyde followed by paraffin-embedding. Then, 3µm tissue sections were prepared and mounted on positively charged slides (Eprelia, Netherlands). Sections were subjected to Hematoxylin–Eosin (HE) staining to assess morphology and evaluate liver injury. Other sections were used for immunohistochemistry to determine the spatial distribution and zonal expression of CYP1A2 and visualize and quantify HMGB1 translocation.

##### **4.4.1 HE staining and analysis**

HE staining involved deparaffinizing and rehydrating the 3µm sections with ascending grades of alcohol, followed by staining with hematoxylin and eosin solutions. The sections were then dehydrated using ascending alcohol concentrations. Finally, the slides were digitized using a full slide scanner from Hamamatsu, Japan, equipped with the NDP.view2Plus image viewing software, Version U12388-02, at a magnification level of 40x.

Liver damage was assessed using a modified Suzuki score for samples obtained from liver after NMP (Chen et al., 2023) and a conventional Suzuki score, respectively. In addition to the conventional Suzuki Score for the samples obtained from transplanted animals (Suzuki et al., 1993) assessing vacuolization, necrosis, and congestion, the following parameters were considered: pyknosis, erythrocytes in vessels and sinusoids, hepatocyte detachment, and vessel detachment. The illustration of cellular features of the modified Suzuki score is shown in **Figure 13**. Each corresponding histological change is scored from 0 to 3 depending on the extent. The scoring rules are as follows (**Table 1**): Score 0: No specific histological change in the fixed magnification; Score 1: Specific histological change in the fixed magnification in less than 30% of the tissue; Score 2: Specific histological change in the fixed view greater than 30% but less than 60% of the tissue in the fixed magnification; Score 3: Specific histological change in the fixed magnification in more than 60% of the liver section. Two independent reviewers (CHT, XPC) scored three representative regions of interest (ROI) in the periportal and pericentral zones, respectively. Any differences were resolved via discussion with a third reviewer (dah and/or ODI) one being a board certified hepatopathologist.

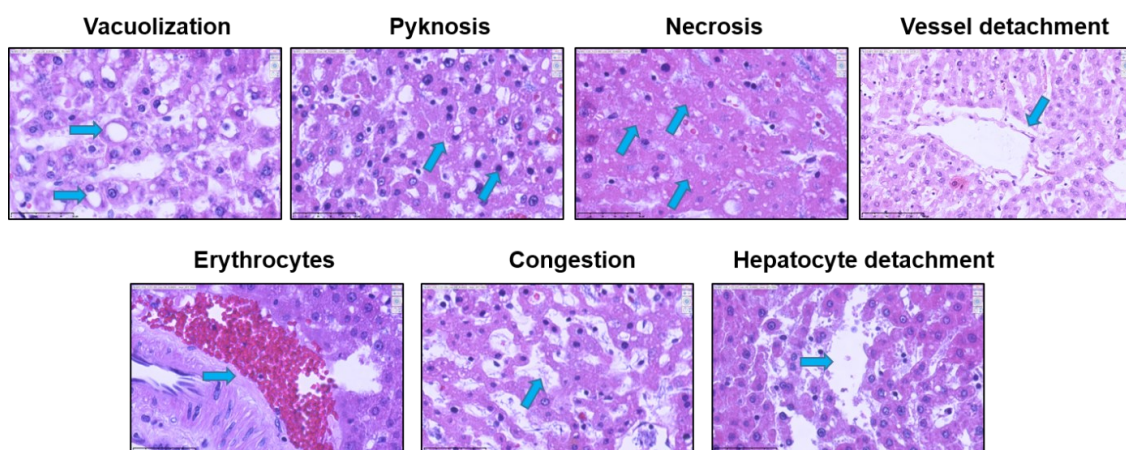


**Figure 13.** The illustration of cellular features for modified SUZUKI score (X80). In addition to the conventional Suzuki Score for assessing vacuolization, necrosis, and congestion, the following parameters were considered in modified Suzuki score: pyknosis, erythrocytes in vessels and sinusoids, hepatocyte detachment, and vessel detachment.

**Table 1. Criteria for the modified Suzuki score**

Histological changes	Score				Magnification
	0	1	2	3	
<b>Vacuolization</b>	None	<30%	30%-60%	>60%	40x
<b>Necrosis</b>	None	<30%	31%-60%	>60%	40x
<b>Congestion/ Sinusoidal dilatation</b>	None	<30%	31%-60%	>60%	40x
<b>Erythrocytes in vessels and sinusoids</b>	None	<30%	31%-60%	>60%	40x
<b>Hepatocyte detachment</b>	None	<30%	31%-60%	>60%	40x
<b>Vessel detachment</b>	None	<30%	31%-60%	>60%	40x
<b>Pyknosis</b>	None	<30%	31%-60%	>60%	40x

#### 4.4.2 Immunohistochemistry and analysis

Immunohistochemistry was performed using 3  $\mu\text{m}$ -thick formalin-fixed paraffin-embedded liver tissue sections. Two different stainings were performed using antibodies against CYP1A2 and HMGB1. CYP1A2 as a drug metabolizing enzymes which was used as indirect marker of hepatic function. HMGB1 was used as marker of ischemic damage, since ischemia is causing translocation from the nucleus into the cytoplasm (Table S6). Liver tissue sections were deparaffinized and rehydrated with ethanol in descending grades. In the next step, the antigens were retrieved by placing the section in Trisodium citrate buffer (PH 6.1) followed by heating to 100°C for 30 minutes using a steamer (Braun, Germany). Tissue sections were subjected to peroxidase blocking to inhibit the endogenous peroxidase activity. Afterwards, endogenous avidin and biotin activity was inhibited using an Avidin/Biotin Blocking Kit (Table S1).

Thereafter, endogenous IgG was blocked using a commercially available ready-to-use protein block (Table S1).

For CYP1A2-staining, sections were incubated overnight with the primary mouse monoclonal antibody (1/3000) (Table S6) at a temperature of 4°C. Subsequently, sections were incubated with the goat anti-mouse IgG H&L (biotin) secondary antibody (1/2000) (Table S6) for 60 minutes at room temperature.

For HMGB1, sections were incubated with the primary rabbit polyclonal antibody (1/2000) (Table S6) for one hour at room temperature. Subsequently, sections were incubated with goat anti-rabbit IgG H&L (biotin) (1/5000) secondary antibody (Table S6) for 30 minutes at room temperature.

All sections were subjected to Streptavidin HRP (Table S1) for 10 minutes at room temperature. The reaction was visualized using DAB-chromogen for 3 to 5 minutes while maintaining the ambient temperature. Counterstaining was performed using Mayer's hematoxylin for 15 minutes. A negative reagent-control slide was included for each run, using the same protocols but without applying the primary antibody. Used a section known to contain the antigen to be detected as a positive control for each run. In addition, one positive control was included in each run, using a section with a known expression of the given antigen. The stained slides were scanned and digitized as described above.

For quantitation of the extent of necrosis in LTx samples respectively of CYP1A2-expression in NMP and LTx samples, we used the generic 128 algorithms of the Histokat Software (Table S3) to determine the relative surface covered by a patterns (necrosis) or signal CYP1A2 staining. The Histokat software is based on a machine-learning algorithm developed by Fraunhofer MEVIS. The whole slide scans are divided into square tiles of a given size by the algorithm. A pattern recognition algorithm was trained using a minimum of 30 tiles from each liver lobes and four representative images of the series. First, we uploaded the whole slide scan to this program (**Figures 14 A-B**). Then, the foreground classification was performed and the corresponding tissue was marketed in pink (**Figures 14 C-D**). We used pattern recognition to identify areas with necrotic or viable respectively positive or negative signals which were marked in red and blue. Finally, Histokat automatically calculated the relative surface covered by the red overlay color in percent of the total surface of the section, indicating the relative areas with the targeted pattern (**Figures 14 E-F**).

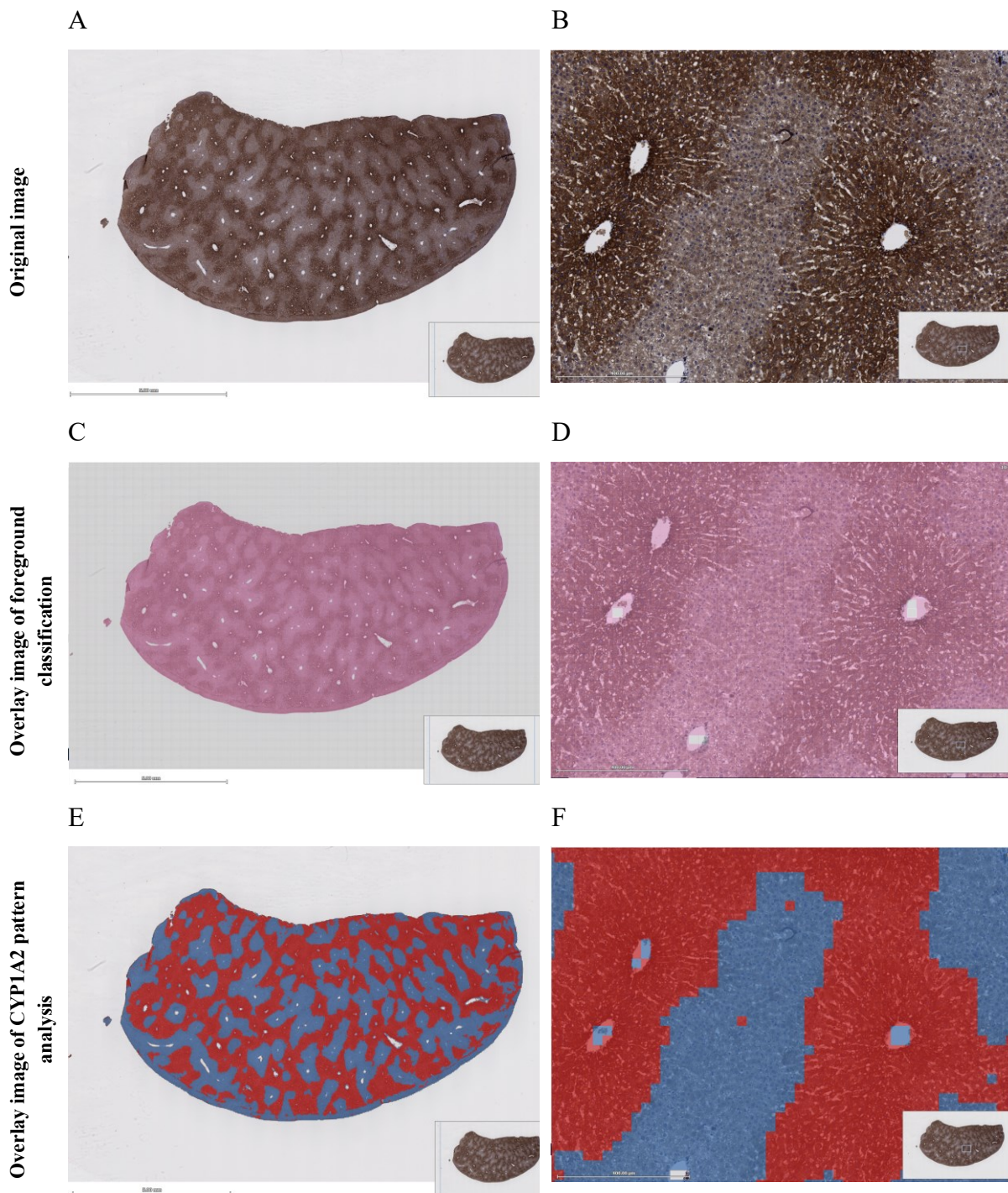


**Figure 14. Image analysis of whole slide scan with sections from liver lobes using Histokat pattern recognition algorithm.** A-B. The original image after CYP1A2 staining. C-D: Overlay image of liver after color coding the foreground classification with pink. E-F: Overlay image of liver after color coding the immunohistochemical visualization of CYP1A2 expression. Square tiles classified into two color classes (blue for the CYP negative or mildly stained hepatocytes and red for strong to moderate CYP stained hepatocytes).

Image J (Table S3) was used to determine the area fraction of the HMGB1 signal in the periportal and pericentral regions separately, a feature which is not possible using Histokat, respectively. The steps are shown in **Figure 15**. The 40X images in uncompressed tiff-format

of representatively selected periportal and pericentral areas were uploaded into Image J. Then, the images omitting the negative signal were obtained using the color split channels tool. As a next step, the threshold was adjusted to include all the positive signals. After that, the hepatocytes were chosen based on the diameter of the nucleus. Finally, the percent of hepatocyte nuclei expressing the HMGB1 signal was calculated automatically.

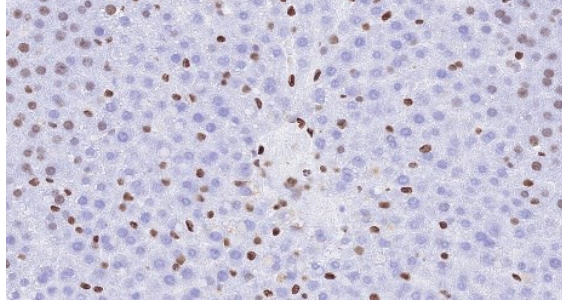
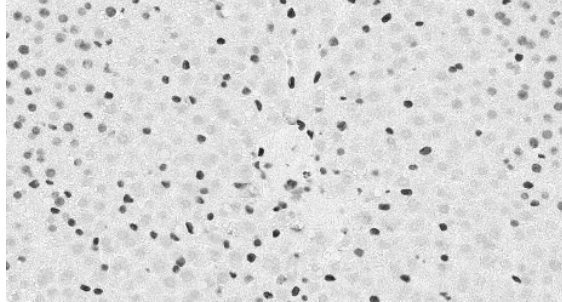
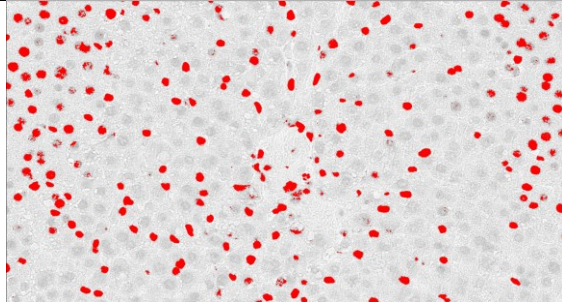
Steps	Imgaes
Upload images representing the regions of interest into image J.	
Using the color split channels tools to split the image into 3 single images, omitting the blue, red, and green colors. The blue channel image was used to identify the positive nucleus, omitting the blue.	
Adjust the threshold of the selected blue channel image to cover all the positive signals with red. Automatically measure the percent of the red relative surface.	

Figure 15. Image analysis of HMGB1 using Image J.

## 4.5 Protein analysis

### 4.5.1 Protein extraction and sample preparation

Snap-frozen liver tissue was lysed in 1× protein lysis buffer (Table S7), followed by homogenization using a SpeedMill Plus with lysis tube A. Tissue lysates were then centrifuged for 10 minutes at 14,000 × rpm in a 4 °C pre-cooled micro-centrifuge. The lysate was transferred to a new Eppendorf tube on ice. The protein concentration of each lysate was determined by the BCA protein assay kit following the manufacturer’s instructions. Concentration of all the

samples was adjusted to 2 $\mu$ g/ $\mu$ l. Samples containing an equal amount of total protein were denatured in a loading buffer (Table S7) by heating for 5 minutes in a thermomixer (Eppendorf Centrifuge 5420, Germany) at 95 °C and then cooled down to room temperature prior to electrophoresis.

#### **4.5.2 SDS-PAGE and Western Blot**

10  $\mu$ L of each sample and a molecular weight marker (Table S2) were loaded into SDS-PAGE gel (Table S8) to determine adequate separation of the targeted protein at the respective protein size. Stacking and separate gel concentrations were set 5% and 12%, respectively. The SDS-PAGE was run in a mini gel tank filled with 1 $\times$  running buffer (Table S7) at 80V for 30 minutes, followed by 100V for approximately 2 hours. Meanwhile, polyvinylidene difluoride (PVDF) membranes (Table S1) were activated in methanol for 1 minute and then soaked in 1 $\times$  transfer buffer (Table S7). Filter papers (Table S1) and sponges were also soaked in 1 $\times$  transfer buffer for 10 minutes prior to assembly of the transfer “sandwich”. After electrophoresis, the gels were removed from the electrophoresis apparatus and equilibrated by soaking in 1 $\times$  transfer buffer for 10 minutes. Transfer sandwiches were assembled and placed in a mini transfer tank. To transfer separated proteins from the gels onto PVDF membranes, the wet transfer was performed at 200mA for 2 hours. After transfer, membranes were blocked in 5 % milk in TBST (Table S7) at room temperature for 1 hour with constant rocking. Membranes were then incubated in primary antibodies (Table S9) diluted in a blocking solution overnight at 4 °C with gentle rocking. After incubation, membranes were washed with 1 $\times$  TBST thrice for 10 minutes each with gentle rocking. Afterward, the membranes were incubated with the secondary antibody (Table S9) diluted in a blocking solution for 1 hour at room temperature with gentle rocking. Membranes were again washed with 1 $\times$  TBST three times for 10 minutes each with gentle shaking. As a next step, membranes were then incubated in freshly prepared chemiluminescent HRP substrate (Table S1), and chemiluminescence signals were captured using the Fusion FX7 (Table S3). Quantitative analysis of western blotting results in terms of signal intensity was performed using the software Image J.

### **4.6 Hepatic hemodynamics, tissue perfusion, and microcirculation**

#### **4.6.1 Hepatic hemodynamics**

Continuous monitoring of PV pressure in NMP was performed by using a reusable BP transducer provided by ADInstruments (Table S3). Hourly monitoring of wedge hepatic venous pressure (WHVP) was achieved by inserting a Fr 1 polyurethane cannula into the stem of the

left hepatic vein. The catheter was connected to the ADI system via a 3-way stopcock, which was closed for the hourly measurement.

Similarly, in LTx study, portal vein pressure and portal vein flow (PVF) were monitored in the donor liver before liver explantation and in recipient liver after 1h transplantation, respectively. For the PVP measurement, a Millar catheter was inserted via the splenic vein to the portal vein and connected to the ADI system. For PVF measurement, microvascular perivascular flow prob (Transonic) was placed around the portal vein and connected to the device.

#### 4.6.2 Tissue perfusion

Liver microvascular perfusion was assessed as an additional parameter to evaluate hepatic microcirculation after NMP and transplantation via the spectrometric device O2C (LEA Medizintechnik GmbH, Germany). The O2C-assessment was performed hourly in NMP, as well as before and after LTx 1h, respectively (**Figure 16**). A specially designed probe (LFX-53) for rat liver was used with laser separation 1.2 mm and white separation 1.2 mm. The sensor is embedded into a silicone membrane with a diameter of 15mm, which is placed on the surface of the liver and remains in place via capillary adhesion forces. The O2C device can provide the following three parameters of organ microcirculation: relative microvascular perfused blood flow (Flow) [AU] which indicates the volume flow in relative units; tissue oxygen saturation (SO<sub>2</sub>) [%], and relative tissue hemoglobin concentration (rHb) [AU] which represents the hemoglobin content in measured tissue. The sensor was placed on three ROI on the left lateral liver lobe to record the signal for 10s, as suggested by Li et al.(C. H. Li et al., 2017).

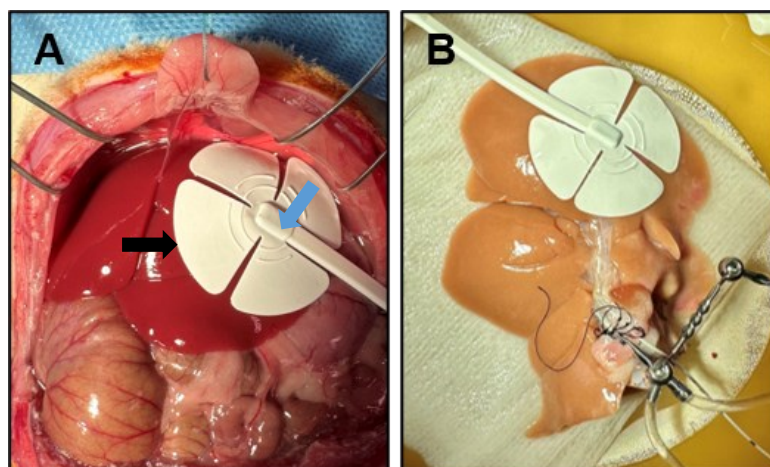


**Figure 16. Image illustrating the monitoring of liver microvascular perfusion via O2C in the liver. (A) O2C sensor of left lateral liver lobe in situ in living animals. (B) O2C sensor on left lateral lobe ex-situ on liver subjected to NMP. Please note the shamrock shape of the silicone membrane (black arrow) and the small square sensor (blue arrow)**

### 4.6.3 Hepatic microcirculation

Liver microcirculation was assessed (1) in the normal liver tissue either in the native liver of the donor or in the recipient liver prior to explantation and (2) in transplanted recipient liver grafts after 1h after LTx to assess impact of early IRI on hepatic microcirculation in real time. Assessments were performed via Cytocam (Braedius, Netherlands) using an incident dark field imaging technique. Using Cytocam-IDF imaging, microcirculation on organ surfaces can be visualized with IDF illumination and optical and technical features. It uses incident dark field illumination with high-brightness LEDs with a very short illumination pulse time of 2 ms. It is computer-controlled and electronically synchronized to the illumination pulses in order to acquire and analyze images. This feature, in combination with a specialized set of lenses, projects images onto a computer-controlled image sensor and results in high penetration and sharp contour visualization of the microcirculation, showing flowing red and white blood cells. The device is constructed of aluminum and titanium, resulting in a lightweight (120 g) and pen-like instrument (length 220 mm, diameter 23 mm). The camera is fully digital, with a high-resolution sensor used in binning mode, resulting in a 3.5-megapixel frame size. The combination of an optical magnification factor of 4 and the large image area of the sensor provides a field of view of  $1.55 \times 1.16$  mm, about three times larger than the field of view of previous devices (**Figure 17**).

Image sequences were captured at 25 frames/s. Image sequences generated by Cytocam were captured using CCTools V2 (Table S3) and stored on a laptop. Three consecutive video sequences of 4 s were captured before and one hour after LTx on the left lateral lobe surface to minimize heterogeneity in the selected region of interest.

CCTools V2 was used to analyze the captured images. Both capillaries and non-capillary vessels were captured and analyzed. The analysis of the microvascular density was restricted to vessels with a diameter  $<16 \mu\text{m}$ . In addition, the number of vessel segments, vessel density, and total length of vessels in capillary respectively non-capillary vessels were analyzed. Furthermore, the density and proportion of perfused capillary vessels were analyzed. As shown in **Table 2**, a total vessel density (TVD), including both total capillary density (TCD) and total non-capillary density (TNCD), was determined to measure the total vessel area per surface area reflecting diffusive capacity. Perfused capillary density (PCD) estimates the functional capillary density, which accounts for both convective and diffusive properties of the visualized microcirculatory bed. The proportion of perfused capillary (PPC) represents the percentage of the total microcirculatory vessel length with flow grades that met the accepted threshold (sluggish or continuous) (Uz et al., 2021).



**Table 2. The definition and characteristics of key parameters in CytoCam**

Microcirculation parameters	Definition and characteristics
Total capillary density (TCD, mm/mm <sup>2</sup> )	Measurement of total capillary area per surface area. Determinant of capillary distance to tissue (diffusive capacity).
Proportion of perfused capillary (PPC, %)	Percentage of the total microvascular length with flow grades that met the accepted threshold (sluggish or continuous).
Perfused capillary density (PCD, mm/mm <sup>2</sup> )	$PPC \times TVD$ . Estimates the functional capillary density, which accounts for both convective and diffusive properties of the visualized microcirculatory bed.

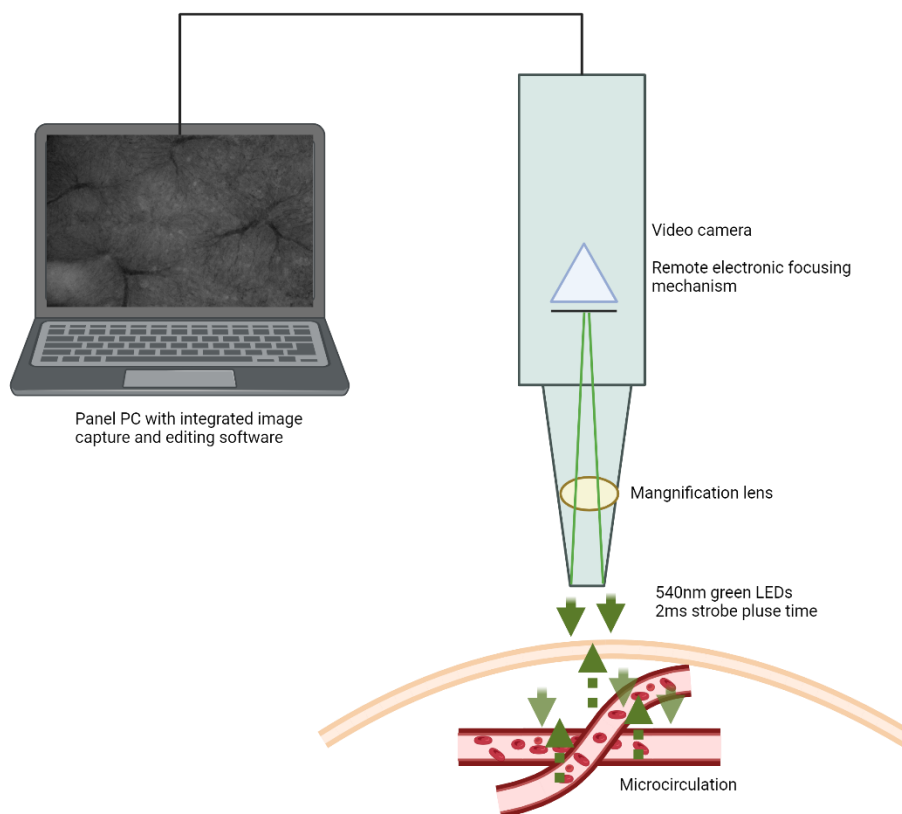


**Figure 17. Cytocam IDF video microscope.** As hemoglobin absorbs light at 540 nm, the tip of the Cytocam probe emits green light at that wavelength, resulting in dark appearance on the screen.

#### 4.6.4 Stiffness of the liver

Liver stiffness was assessed after terminating the 6h NMP to relate any changes in perfusion pressure to eventually preexisting differences in mechanical properties of the organs between

the groups. For the LTx, to investigate the differences in mechanical properties after reperfusion, the measurement of liver stiffness was performed in explanted native livers (1) obtained from recipients prior to implantation and subjected to 1h of SCS and (2) livers grafts explanted 1h after LTx. For the measurement, the liver was placed on 3 layers of gauze, followed by placing the sensor of the device (HPE III Basic (Table S2) gently on the surface of the left lateral lobe. Measuring parameters including measuring method (Shore 000), measuring distance (2.5mm) and display range (0-100). The measuring value of the device is unit free. According to the suggestion of the manufacturer, a lobe must have a flat face with a diameter of more than 3.5 cm. The measurement was repeated 3 times, selecting different regions of interest in the same left lateral lobe.

#### **4.7 Statistical Analysis**

All data are expressed as mean  $\pm$  SD (standard deviation) and analyzed using GraphPad Prism 9.5 software (Table S3). Normal distribution was determined first. Differences between the two groups were analyzed using a two-tailed Student's t-test. For more than two groups, differences were analyzed using one-way ANOVA, followed by Tukey's post hoc test. The liver pressure measurements in NMP explants were analyzed by a general linear model for repeated measurements using SPSS Statistics 26.0 (Table S3), followed by LSD post hoc test when comparisons included more than two groups. The correlation analysis was evaluated using the Pearson Product Moment Correlation. The heat map was performed with Origin (Table S3). The statistically significant differences were expressed at \*P < 0.05, \*\*P < 0.01, \*\*\*P < 0.001, and ns = not significant. The number of biological replicates (n) is specified in the results section and figure legends. The graphical representations of results were achieved using GraphPad Prism 9.5 software.

## 5 RESULTS

### 5.1 Part I: NMP study

#### 5.1.1 Establishment of NMP model

To establish the stable NMP model, we designed three steps (**Figure 18**). Firstly, three rat cadavers were used to get familiar with the NMP procedure, including the steps of cannulation, flushing, transection IHVC, mobilization, transfer, and connection to the perfusion device. At this point, the whole procedure took about  $70 \pm 15$  min. Secondly, we improved the flushing by modifying the flushing solution, flushing rate, flushing volume, heparin concentration, and the sequence of surgical steps. For this step, nine animals were used to improve surgical conditions. The additional training resulted in a reduction of the warm ischemia time to  $50.1 \pm 8.9$  min. We observed that flushing the liver with 100 ml of Ringer-Lactate solution containing 500 IU of heparin at a flow rate of 10 ml/min rate can result in a relatively homogeneous appearance of the liver. Lastly, we used 4 animals for final optimization, we exchanged perfusion solution (from DMEM to William E without phenol red). We replaced the perfusion cannula (from an intravenous plastic catheter (26G) by a metal perfusion cannula with a basket at the tip), and prolonged the perfusion time (from 1, 2, 3 to 6 hours). The additional training allowed a further reduction of warm ischemia time to  $37.5 \pm 2.1$  min (**Figure 19**).

As a result, we flushed the liver with 100 ml of Ringer-Lactate solution containing 500 IU of heparin and using a flow rate of 10 ml/min and perfused the liver using complete William E medium without phenol red for the 6 hours normothermic oxygenated machine perfusion.

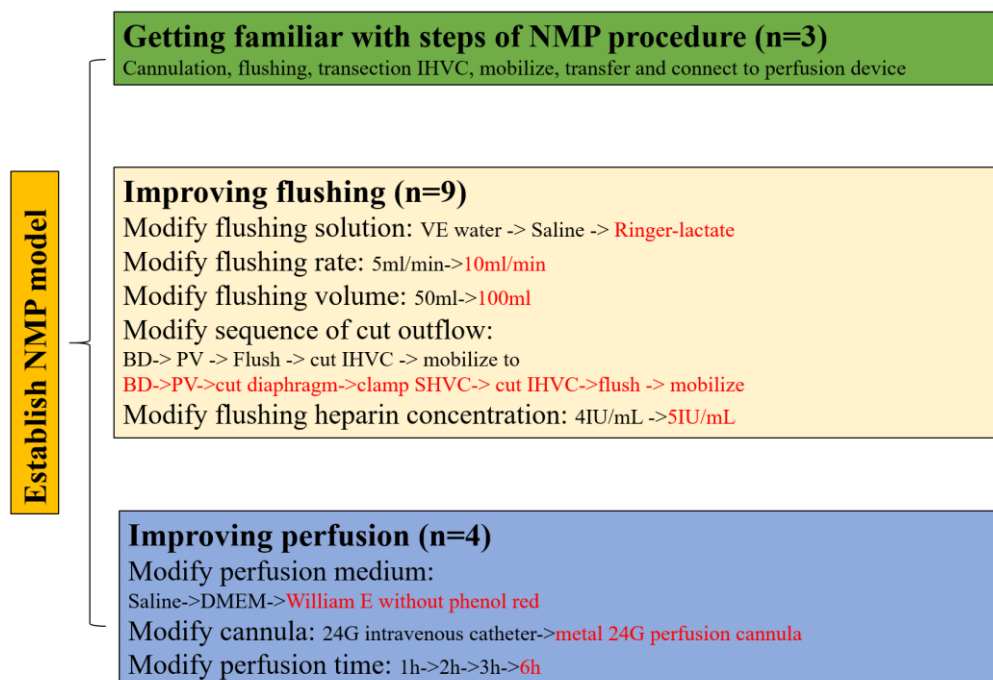


**Figure 18. Illustration of the three steps for establishing NMP: getting familiar with the steps of the procedure, improving flushing, improving perfusion.** Black font: starting condition, red font: final. IHVC: infrahepatic vena cava, suprahepatic vena cava, BD: bile duct

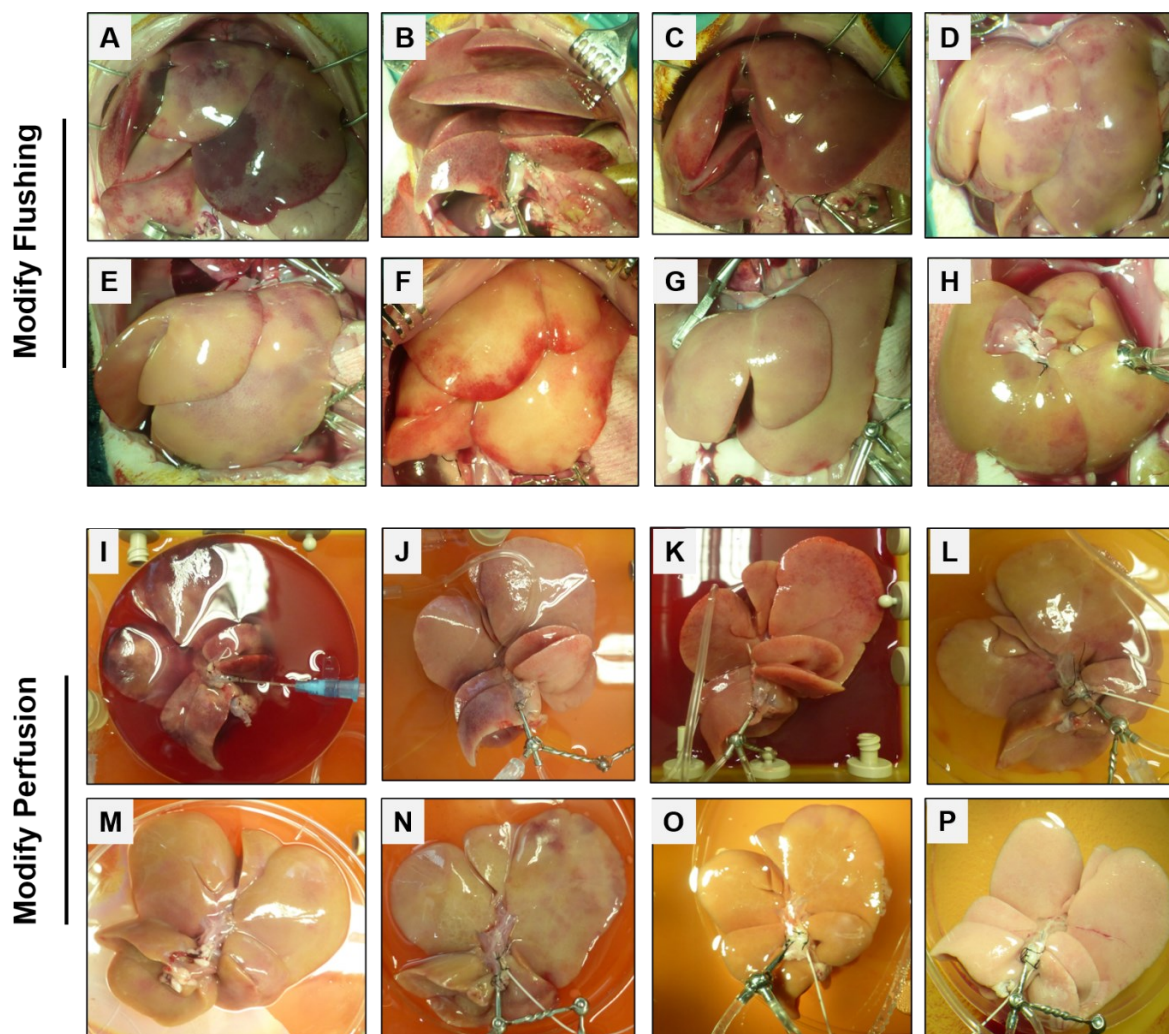


**Figure 19. Sequence of images illustrating the improvement of flushing and perfusion.** (A-C) Modification of flushing medium. (D-F) Modification of flushing rate and volume, and surgical steps. (G-H) Modification of heparin concentration in flushing medium. (I) Modification of perfusion cannula. (J-L) Selection of perfusion medium. (M-P) Prolongation of perfusion time with 1h (M), 2 h (N), 3h (O), and 6h (P).

### 5.1.2 Overall impact of NMP on liver damage and function

Subjecting rat livers from donors after cardiac death to NMP using oxygenated cell culture medium (Williams E w/o phenol red) caused an injury to the liver. This injury was associated with an inevitable loss of function in terms of bile production over the 6h of perfusion. However, the injury developed gradually and was highly dependent on NMP conditions and donor properties, as shown in detail below.

As described by others (Liu et al., 2021; Op den Dries et al., 2016), bile production per hour per gram liver (ml/h/gr liver) is considered be an easy-to-determine but very valuable indicator of hepatic function during machine perfusion. The highest volume of bile was consistently

observed in the first hour and decreased thereafter, indicating that the liver was viable throughout the perfusion but nevertheless did experience a loss of function under the given NMP conditions. This finding was paralleled by an increase in liver enzymes in the perfusate, indicating continuous hepatocyte injury. Hepatocyte injury occurred mainly in the pericentral region in the form of nuclear pyknosis and vacuolization resulting in a higher modified Suzuki score compared to the periportal region.

In contrast, perfusion parameters such as perfusion pressure remained relatively stable throughout the 6h observation, indicative of the absence of major vascular obstruction.

### **5.1.3 Impact of perfusion flow rate and medium change on the outcome of NMP**

#### **5.1.3.1 Best prevention of liver damage and preservation of liver function by slight hyperperfusion of the liver**

To explore the optimal NMP condition, a total of 9 animals were subjected to the NMP. We examined the influence of different perfusion flow rates on the preservation of the liver graft. As shown in **Figure 20**, all livers were rather homogeneously perfused with a stable PV pressure during 6 hours NMP, but with slight irregularities in the two groups subjected to a flow rate of 1 or 2 ml/min/gr liver. However, when applying the higher flow rate, all livers from all 3 groups with a flow rate of 3ml/min/gr liver were perfectly perfused irrespective of the eventual medium change.

When comparing total bile production in the 1ml/min, 2ml/min, and 3ml/min groups, the liver subjected to a flow rate of 3ml/min produced significantly more bile after the 6h NMP ( $97.1 \pm 10.4 \mu\text{L/g}$  liver compared to  $10.4 \pm 3.1$  in the 1ml/min group and  $36.4 \pm 8.6 \mu\text{L/g}$  liver in the 2ml/min group ( $p < 0.05$ ). An opposite trend occurred with perfusate enzymes: there was a two-fold increase in AST and a two-fold increase in ALT in the 2 ml/min group compared to the 3 ml/min group. However, the release of LDH did not differ in the 2 and 3ml/min groups but was substantially higher in the 1ml/min group (**Figure 21A-D**). Both results together

suggest that hepatic damage increased over time, whereas function decreased. The glucose levels remained relatively stable over time.

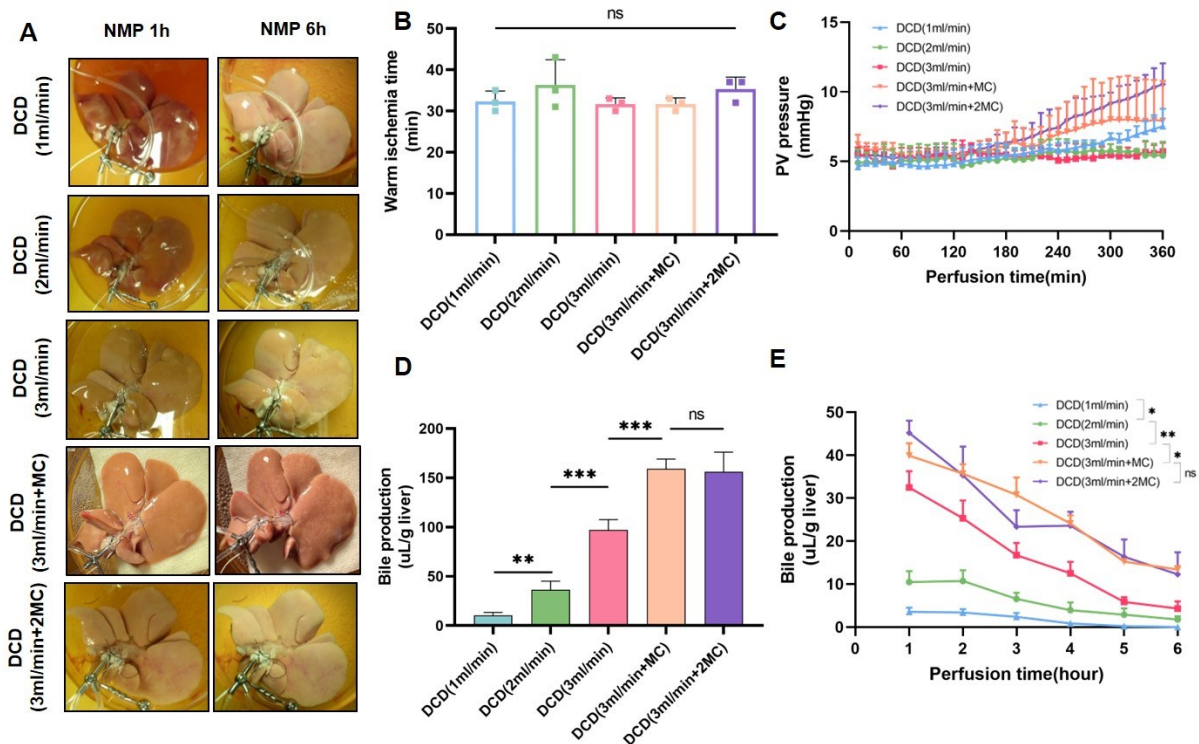


**Figure 20. Impact of NMP condition on liver function (n=3/group).** (A) Homogenous perfusion in livers subjected to different perfusion conditions at 1h and 6h of NMP demonstrating. (B) Stable warm ischemia time in livers to different perfusion condition groups. (C) Stable PV pressure over time in the liver subjected to different perfusion conditions. (D) Total bile production and bile production per hour (E) in livers subjected to different perfusion conditions. Data expressed as mean  $\pm$  SD, one-way ANOVA followed by Tukey's post-hoc test. \*P < 0.05, \*\*\*P < 0.001, \*\*\*\*P < 0.0001 and ns = not significant. n, number of animals.

Interestingly, blood gas analysis showed that none of the different flow rates affected acid-base homeostasis. As shown in **Figure 21E-H**, the levels of  $\text{HCO}_3^-$ ,  $\text{K}^+$ ,  $\text{PO}_2$ , and pH in the 1ml/min, 2ml/min, and 3ml/min groups remained relatively stable throughout 6h of perfusion. However, the  $\text{HCO}_3^-$  and  $\text{K}^+$  levels in the 3ml/min group were  $12.9 \pm 0.8$  mmol/L and  $7.6 \pm 0.2$  mmol/L, respectively, which were lower than those in the 2ml/min group, also suggesting better preservation when applying the higher flow rate. The pH was stable but slightly acidic throughout the 6h of perfusion and did not differ when applying different perfusion rates (1ml/min, 2ml/min, and 3ml/min groups  $6.93 \pm 0.1$  vs.  $6.98 \pm 0.1$  vs.  $7.02 \pm 0.1$ ).

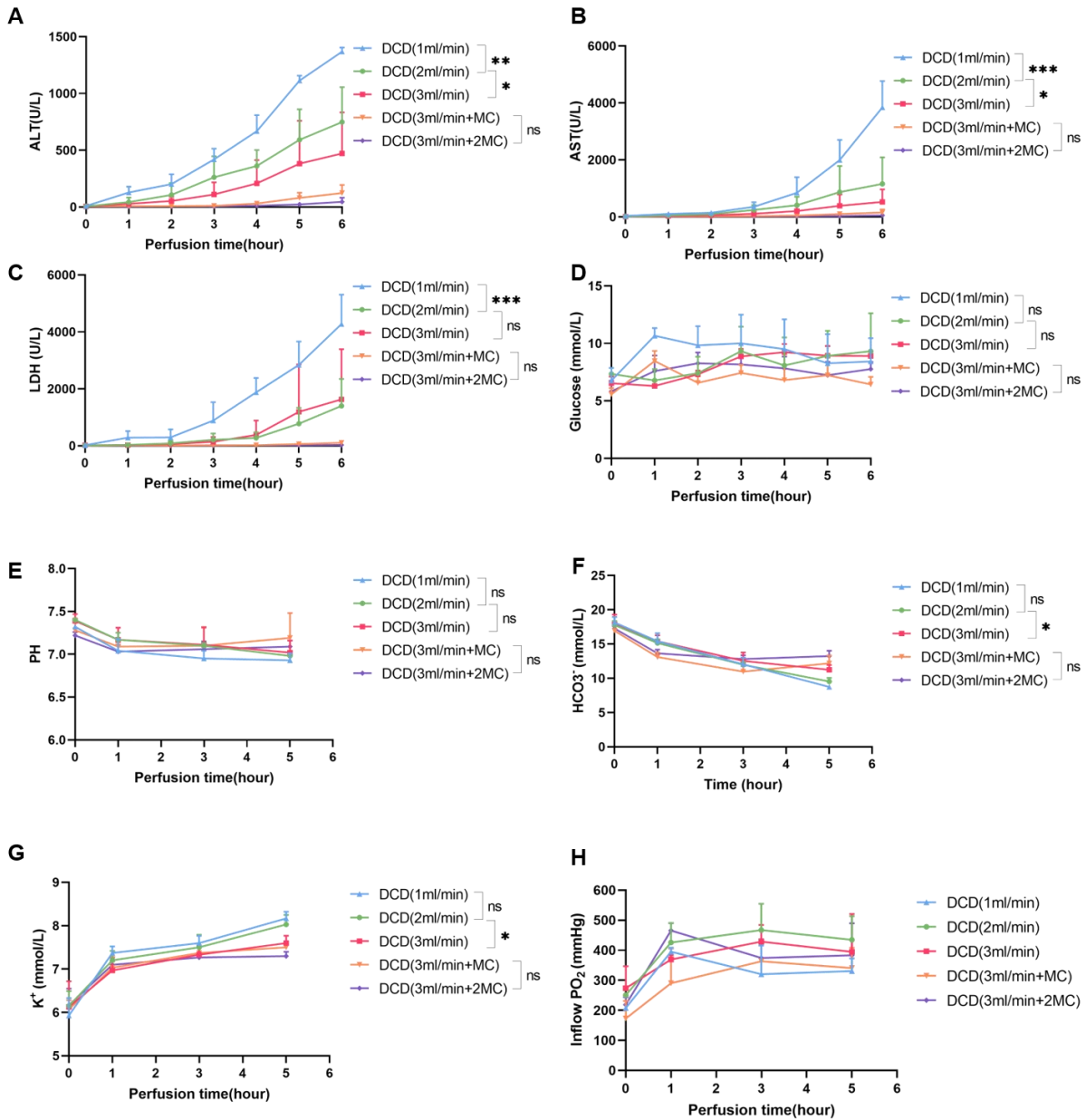


**Figure 21. Enzyme release and acid-base homeostasis in livers subjected to different perfusion conditions (n=3/group).** The lower release of liver enzymes and stable acid-base homeostasis when using a flowrate of 3ml/min/g liver and one partial exchange of medium. (A-D) The levels of ALT, AST, LDH, and glucose over NMP time (n=3). (E-H) The levels of PH, HCO<sub>3</sub><sup>-</sup>, K<sup>+</sup>, and PO<sub>2</sub> over NMP time (n=3). Data expressed as mean ± SD, one-way ANOVA followed by Tukey's post-hoc test. \*P < 0.05 and ns = not significant. n, number of animals in each group.

Upon histological analysis, we observed bacterial contamination in 5/9 livers in the samples obtained after 6h of NMP. We saw a few larger vessels and some sinusoids obstructed with bacterial clots. This additional finding did not interfere with other observations.

Liver morphology analysis revealed a typical damage pattern with signs of pressure related mild damage in the periportal area and signs of severe ischemic damage in the pericentral area

and a more viable appearing midzone. In the periportal area, we observed mainly vacuolization indicative a pressure related damage. In contrast, in the pericentral region we observed more severe damage in terms of vacuolization, pyknosis as well as hepatocytes detachment indicative of ischemic damage

When comparing the impact of the different perfusion conditions, we observed a similar impact of the flow rate as described for the enzyme release. Perfusion with 3ml/min/g liver resulted in less hepatic damage resulting in a lower modified Suzuki score compared to the other groups. As shown in **Figure 22**, the damage in the pericentral area was more severe than the periportal area. Interestingly, there was massive hepatic sinusoidal congestion in the periportal area in the 1 ml/min group. However, the pericentral damage in the 3ml/min group was milder than in the 1ml/min and 2ml/min groups.

HMGB1 translocates from the nucleus to the cytoplasm in response to ischemia. As described in the method section, we separately quantified the relative area covered by positively stained hepatocyte nuclei in the periportal and pericentral regions. In images from HMGB1 stained normal livers, about 20% of the periportal and pericentral surfaces are covered by nuclear signals. Over the course of 6h of NMP, we observed no loss of HMGB1 nuclear signals in the periportal region. In contrast, in the pericentral region, the relative surface covered by positively staining hepatocyte nuclei decreased from about 20% to less than 10%. In other words, HMGB1-translocation occurred in more than 50% of the hepatocytes in the pericentral region. This finding is indicative of ischemic damage in the pericentral area, which increased over the course of 6h of NMP.

The extent of this ischemic damage differed between the flow rate groups and was decreasing with the increase of the perfusion flow rate. Slightly hyperperfusing the liver (flow rate of 3ml/min/gr liver) was associated with reduced ischemic damage as indicated by a larger relative area covered with positively staining hepatocyte nuclei. This observation suggests a flow rate dependent oxygenation gradient along the hepatic sinusoid with more efficient oxygen and nutrient supply in the periportal region compared to the pericentral region.



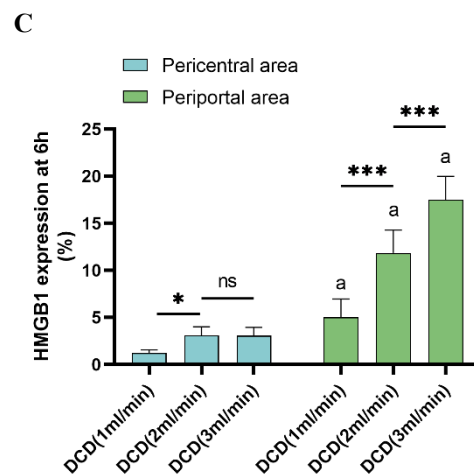
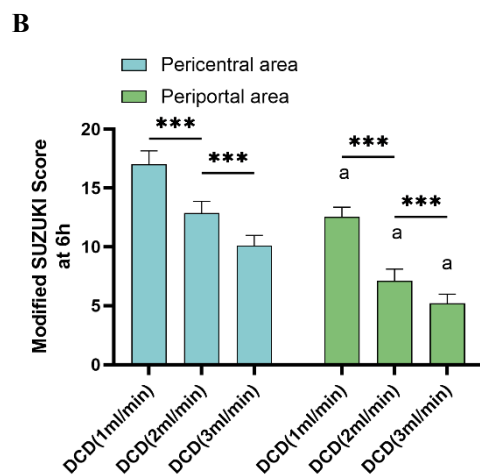
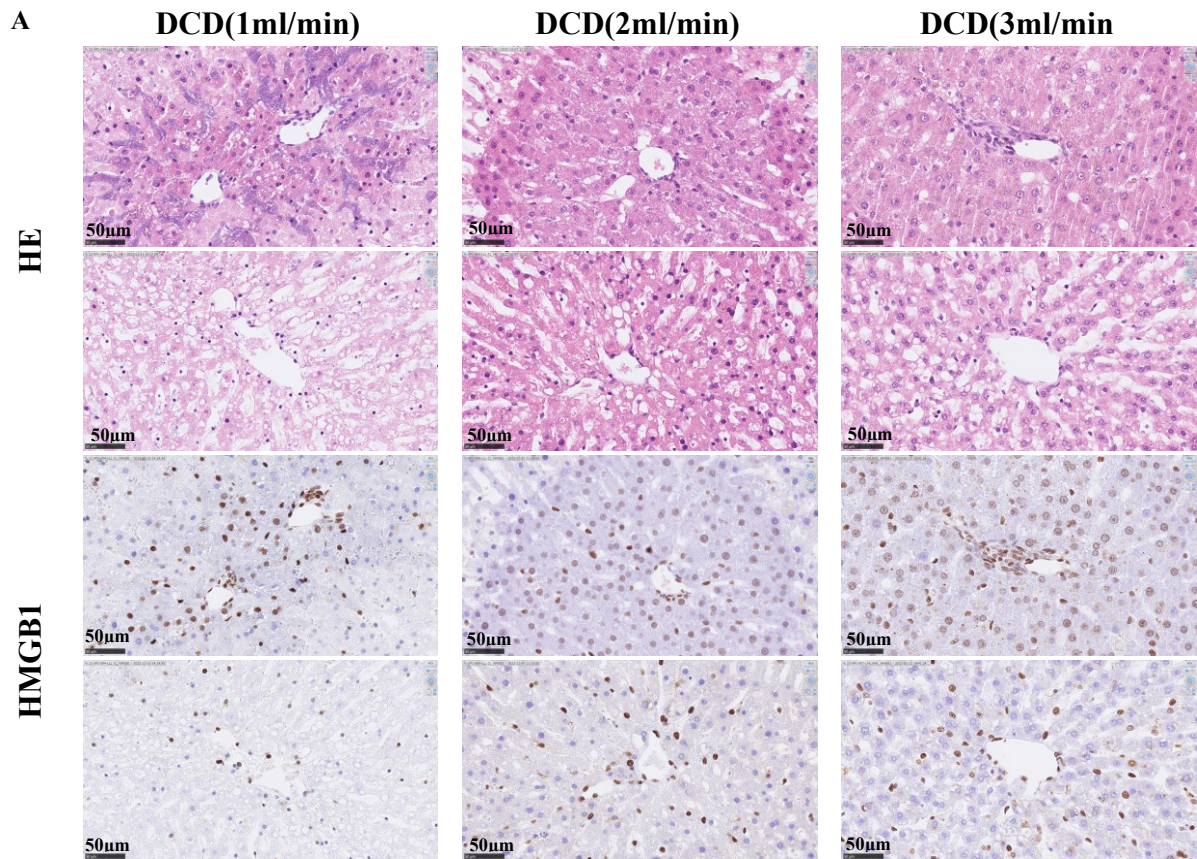


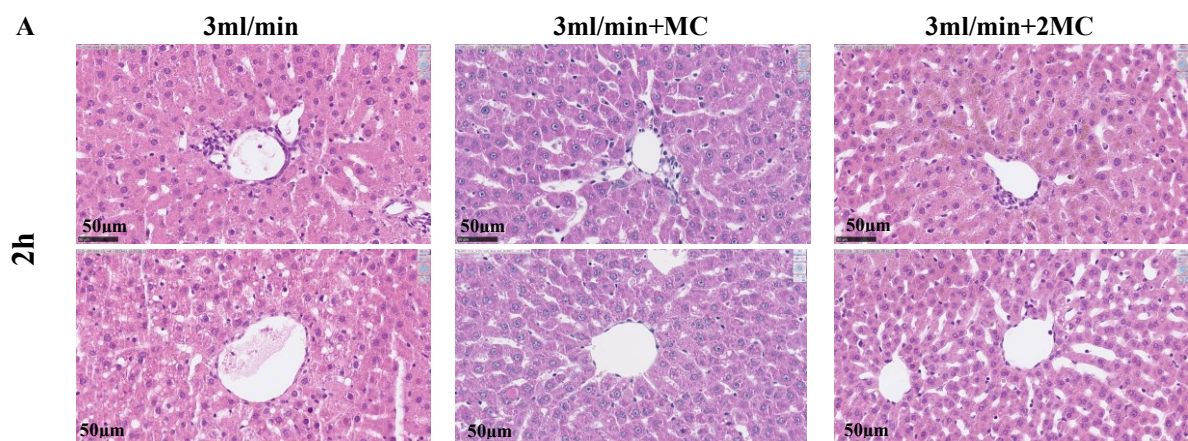
**Figure 22. Impact of perfusion flow rate on zoned hepatic morphological damage and HMGB1 translocation (n=3/group).** Best prevention of liver damage and preservation of liver function by slight overperfusion of the liver. (A) The results of H&E and HMGB1 staining in the periportal and pericentral area after 6h NMP. Semiquantitative analysis of the hepatic injury using modified Suzuki score, Scale bar 50 $\mu$ m. (B) and HMGB1 translocation (C) in the periportal and pericentral area over the course of 6h NMP. Data expressed as mean  $\pm$  SD, one-way ANOVA followed by Tukey's post-hoc test. \*P < 0.05, \*\*\*P < 0.001, and ns = not significant. a, there is a significant difference compared to the pericentral area (P < 0.05).

### 5.1.3.2 Best prevention of liver damage and preservation of liver function by medium change after 3h

After the identification of slight overperfusion as the optimal flow rate, we attempted to further improve the preservation of the liver by discarding the waste products from the perfusate. For this purpose, we exchanged half of the medium once or twice in the course of the 6h perfusion. We observed that exchanging half of the perfusate after 3h of perfusion was associated with significantly less damage, as indicated by the enzyme release, better preserved hepatic morphology and better function, as indicated by the higher bile production per hour. As shown in **Figure 20**, compared to the 3ml/min group without medium change, we observed a higher mean bile production of  $155.1 \pm 14.9 \mu\text{L/g liver}$  and  $156.1 \pm 20.1 \mu\text{L/g liver}$ , respectively in one-time and twice medium change. However, we did not observe a significant difference when changing the medium twice at 2h and 4 h compared to a single change after 3h.

Upon histological analysis, we also observed bacterial contamination in 1/6 livers in samples obtained after 6h of NMP. As stated above, this additional finding did not interfere with other observations. The additional medium change did not change the histological observation principally but gradually (**Figure 23**). Perfusion with 3ml/min+MC was associated with a better-preserved morphology, as indicated by the lower modified Suzuki score compared to the group without medium change. However, hepatic morphological damage aggravated in both periportal and pericentral areas over the time as expected.

Quantification of HMGB1 translocation confirmed that refreshing the medium was associated with less ischemic damage (**Figure 24**). Translocation was less pronounced in the pericentral region of livers subjected to a flow rate of 3ml/min/gr liver and one medium change, compared to the livers subjected to 3ml/min/gr liver without partial medium replacement. Based on the above results, we considered the 3ml/min+MC as the optimal NMP condition for exploring the impact of donor properties on NMP.



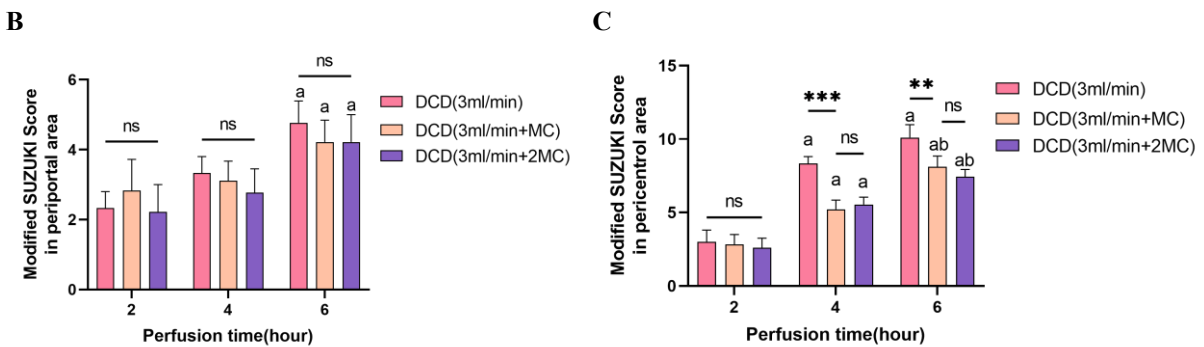
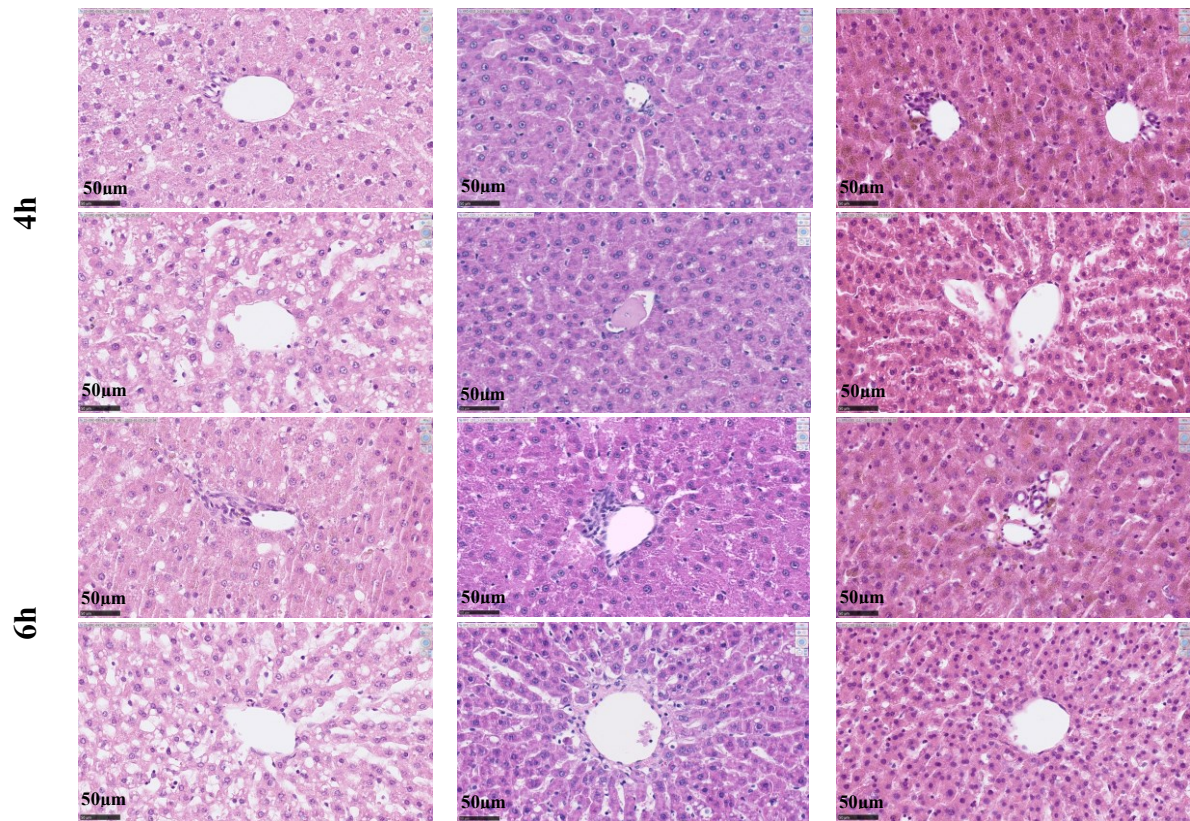


**Figure 23. Impact of medium change on zoned hepatic morphological damage (n=3/group).** Best prevention of liver damage and preservation of liver function by partial exchange of medium after 3h. (A) HE staining in the periportal and pericentral area over NMP time. Quantitative analysis of the hepatic injury using modified SUZUKI score in the periportal (B) and pericentral area (C) over NMP time. Data expressed as mean  $\pm$  SD, one-way ANOVA followed by Tukey's post-hoc test. \* $P < 0.05$ , \*\*\* $P < 0.001$ , and ns = not significant. a, there is a significant difference compared to 2h ( $P < 0.05$ ). b, there is a significant difference compared to 4h ( $P < 0.05$ ). n, number of animals in each group.

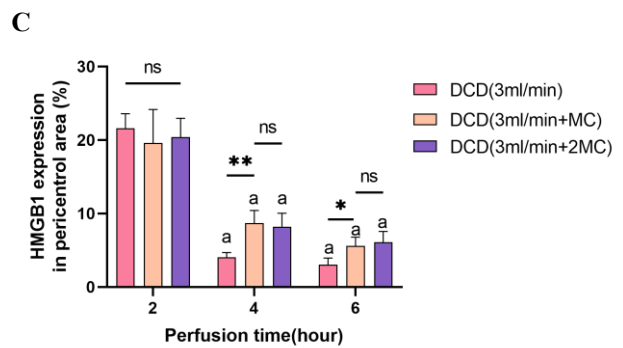
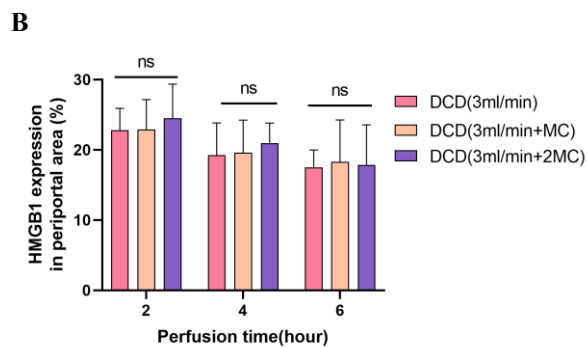
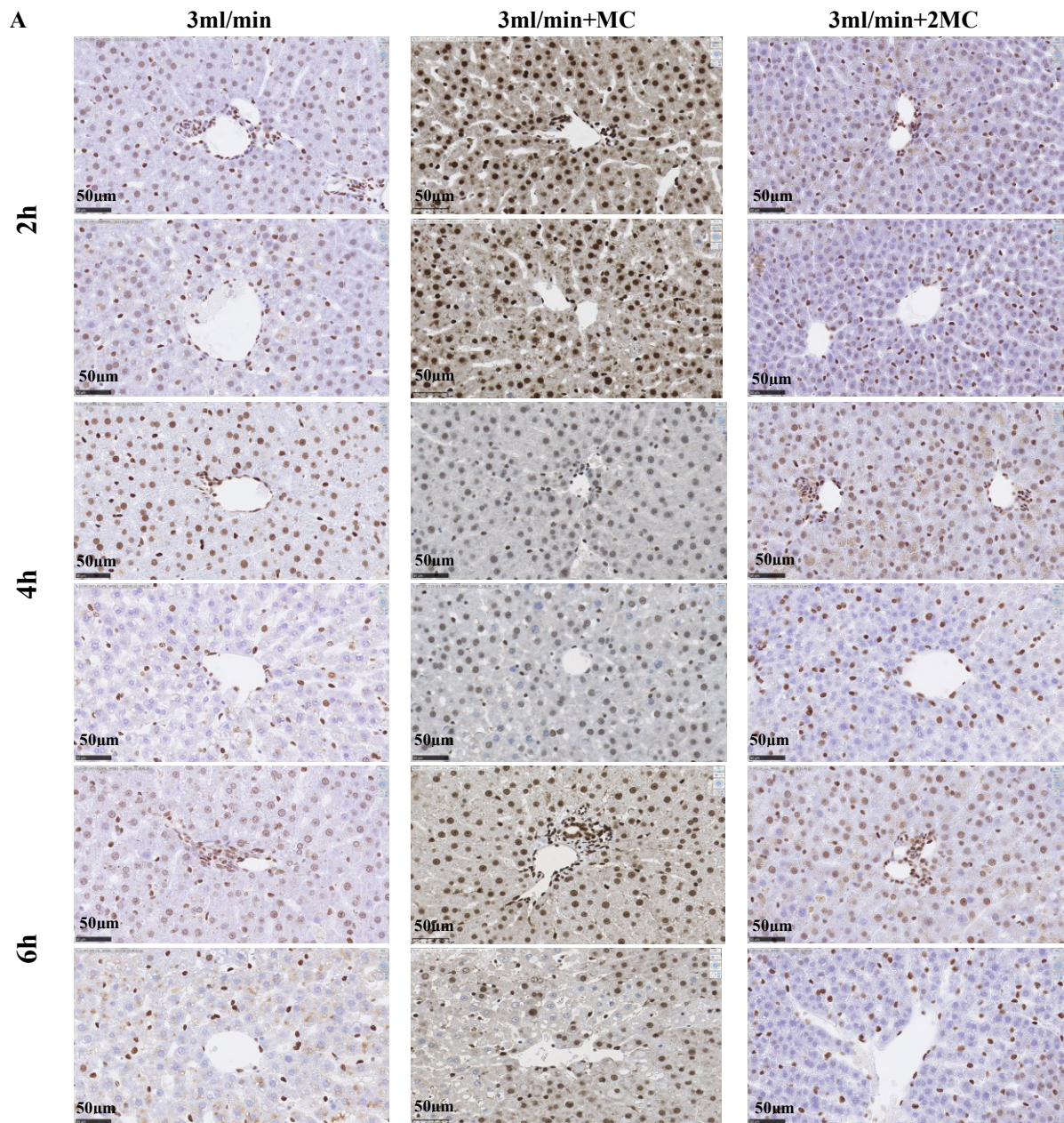


**Figure 24. Impact of medium change on zonated HMGB1 translocation (n=3/group). Less HMGB1 translocation by partial exchange of medium after 3h. (A) HMGB1 staining in the periportal and pericentral area over NMP time. Quantitative analysis of the HMGB1 translocation in the periportal (B) and pericentral area (C) over NMP time. Data expressed as mean  $\pm$  SD, one-way ANOVA followed by Tukey's post-hoc test. \*P < 0.05,**

\*\*P < 0.01, and ns = not significant. a, there is a significant difference compared to 2h (P < 0.05). a, there is a significant difference compared to 2h (P < 0.05). n, number of animals in each group.

#### **5.1.4 Impact of donor properties on the outcome of NMP**

A total of 23 rats were subjected to NMP to explore the donor properties on the outcome of NMP. We found that gender, age, and WIT are factors potentially influencing the outcome of NMP of livers from DCD. Female livers obtained from DCD and subjected to 30min of WIT had a similar outcome than male livers subjected to 20min of WIT. In contrast, male livers from senescent donors exhibited substantially more damage than young male livers.

##### **5.1.4.1 Impact of donor properties on bile production and liver stiffness**

All livers were homogenously perfused in the control, female, sWIT, and old group, as shown in **Figure 25A** for the 1st and the 6th hour of NMP. As expected, we did not observe a significant difference in WIT between the control group ( $31.5 \pm 0.9$  min), female group ( $32.7 \pm 3.1$  min), and old group ( $31.3 \pm 1.1$  min). This finding demonstrates that, indeed, the experiments were conducted under similar conditions. In contrast, the warm ischemia time in the sWIT group was significantly shorter, with  $20.2 \pm 3.5$  minutes (**Figure 25B**), as we had planned.

As expected, the stiffness of the livers from the male, female, 20min and 30min ischemia groups was similar. In contrast, the stiffness of the old livers was higher due to the expected age-related fibrotic changes (**Figure 25C**).

Control livers produced about  $121.9 \pm 16.4$   $\mu\text{L}$  bile/gr liver in 6 hours with a maximum of  $34.4 \pm 4.1$   $\mu\text{L}$  in the first hour. In comparison, the female and sWIT livers produced about  $162.8 \pm 11.5$   $\mu\text{L}$  bile/gr liver and  $149.2 \pm 14.4$   $\mu\text{L}$ /gr liver, respectively, in 6 hours. However, the old male livers produced significantly less bile, reaching only  $35.2 \pm 4.8$   $\mu\text{L}$ /gr liver which is less than 25% of the volume produced by young female livers (**Figure 25D-E**).

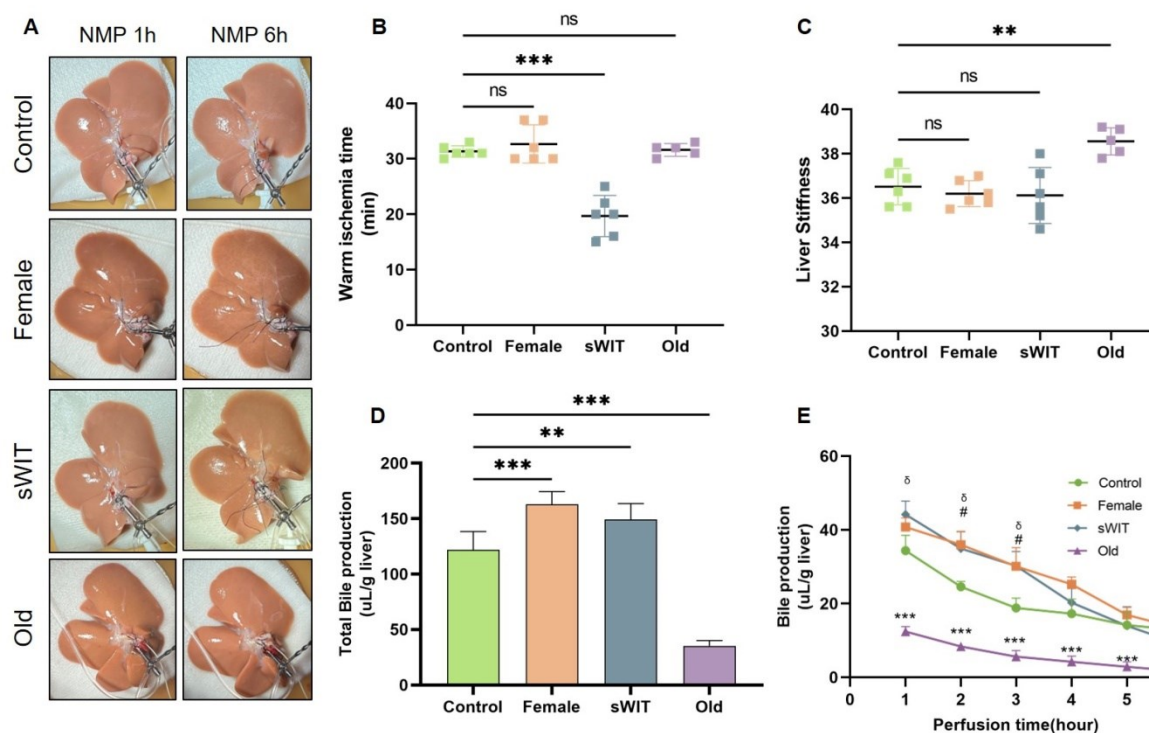


**Figure 25. Bile production and liver stiffness in respect to donor properties.** Higher bile production in female and short WIT, but lower in old age. (A) The appearance of livers in different donor properties groups at 1h and 6h NMP. (B) The warm ischemia time in different donor properties groups. (C) The liver stiffness after 6h NMP in different donor properties groups. (D) Total Bile production and bile production per hour (E) in different donor properties groups. Data expressed as mean  $\pm$  SD, one-way ANOVA followed by Tukey's post-hoc test. \*: Old vs Control  $P < 0.05$ . #: Female vs Control  $P < 0.05$ ,  $\delta$ : sWIT vs Control  $P < 0.05$ . \* $P < 0.05$ , \*\* $P < 0.01$ , \*\*\* $P < 0.001$ , and ns = not significant.

#### 5.1.4.2 Impact of donor properties on liver enzymes and acid-base homeostasis

Liver damage, as indicated by the release of ALT, AST, and LDH (**Figure 26A-D**) in the perfusate, increased with the duration of NMP reaching maximal levels of  $299.1 \pm 37.6$  U/L,  $477.3 \pm 117.5$  U/L, and  $1517.7 \pm 755.2$  U/L respectively at 6h. Compared to the control, the livers of the female and sWIT groups released less enzymes, indicating less damage to the liver. However, the release of liver enzymes in the old group was twice as high as that of the control group. In contrast, the glucose levels in all groups were relatively stable during NMP.

The perfusate blood gas analysis (**Figure 26E-G**) indicated that female gender and sWIT had no impact on acid-base homeostasis. In contrast, old age was associated with pronounced acidosis with significantly lower pH and  $\text{HCO}_3^-$  ( $\text{pH} = 6.78 \pm 0.1$ ,  $\text{HCO}_3^- = 8.3 \pm 1.3$  mmol/L). In addition, oxygen consumption as an indicator of hepatocytes functional active was used to detect the oxygen-carrying capacity of hepatocytes (**Figure 26H**). We found that oxygen consumption decreased during NMP in all groups, a finding compatible with the observed

decreasing bile production indicative of decreased function corresponding to the duration of NMP. Compared to the control liver, oxygen consumption of the old liver was lower but higher in the female and sWIT livers, in line with the other findings.

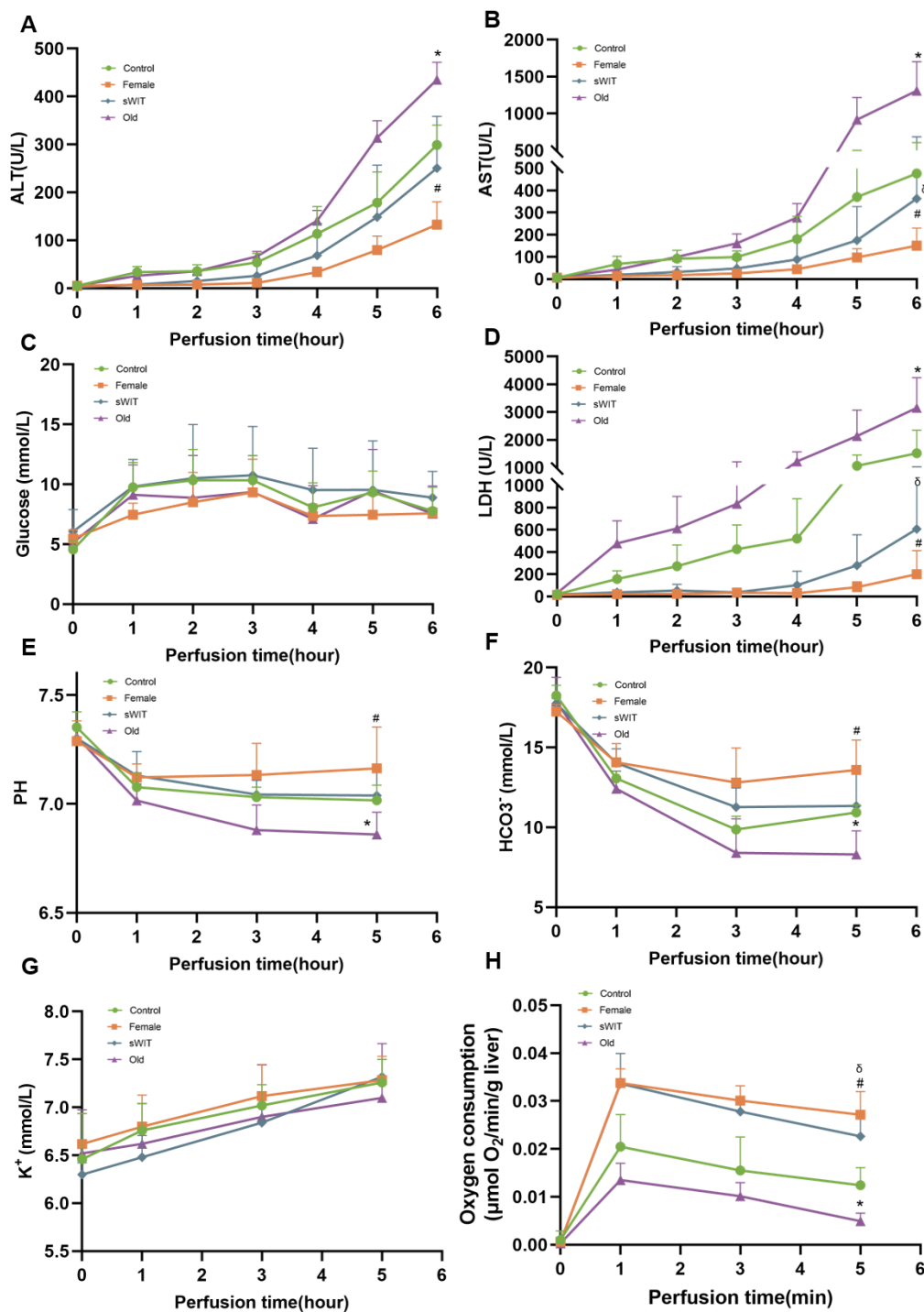
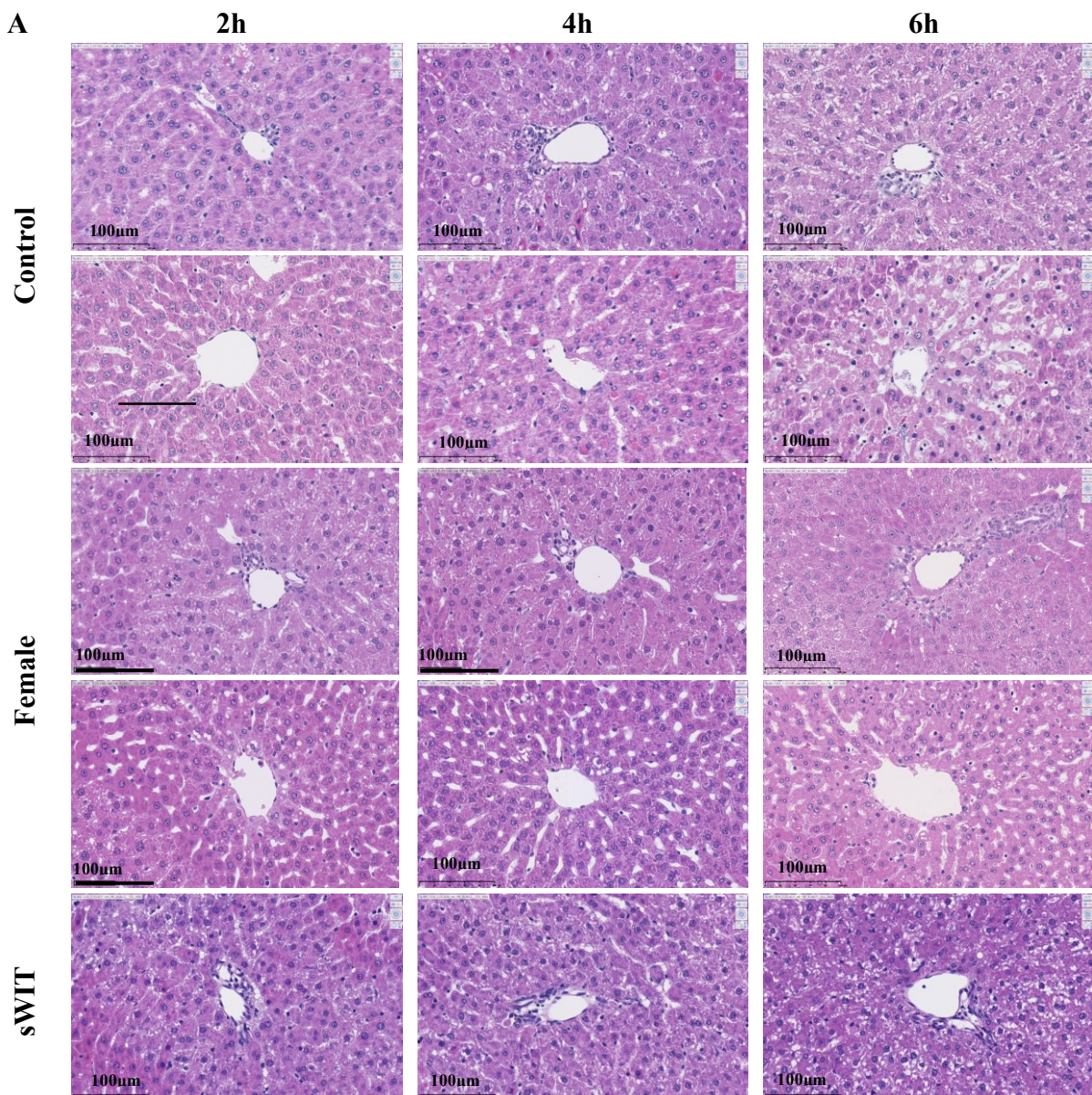


**Figure 26. Impact of donor properties on liver enzymes release and acid-base homeostasis.** Lower release of liver enzymes and stable acid-base homeostasis in female and short WIT, but the higher release of liver enzymes with pronounced acidosis in male old age group. (A-D) The levels of ALT, AST, LDH, and glucose over NMP time. (E-H) The levels of PH, HCO<sub>3</sub><sup>-</sup>, K<sup>+</sup>, and PO<sub>2</sub> over NMP time. Data expressed as mean ± SD, one-way ANOVA followed by Tukey's post-hoc test. \*: Old vs Control P<0.05. #: Female vs Control P<0.05, δ: sWIT vs Control P< 0.05, and ns = not significant.

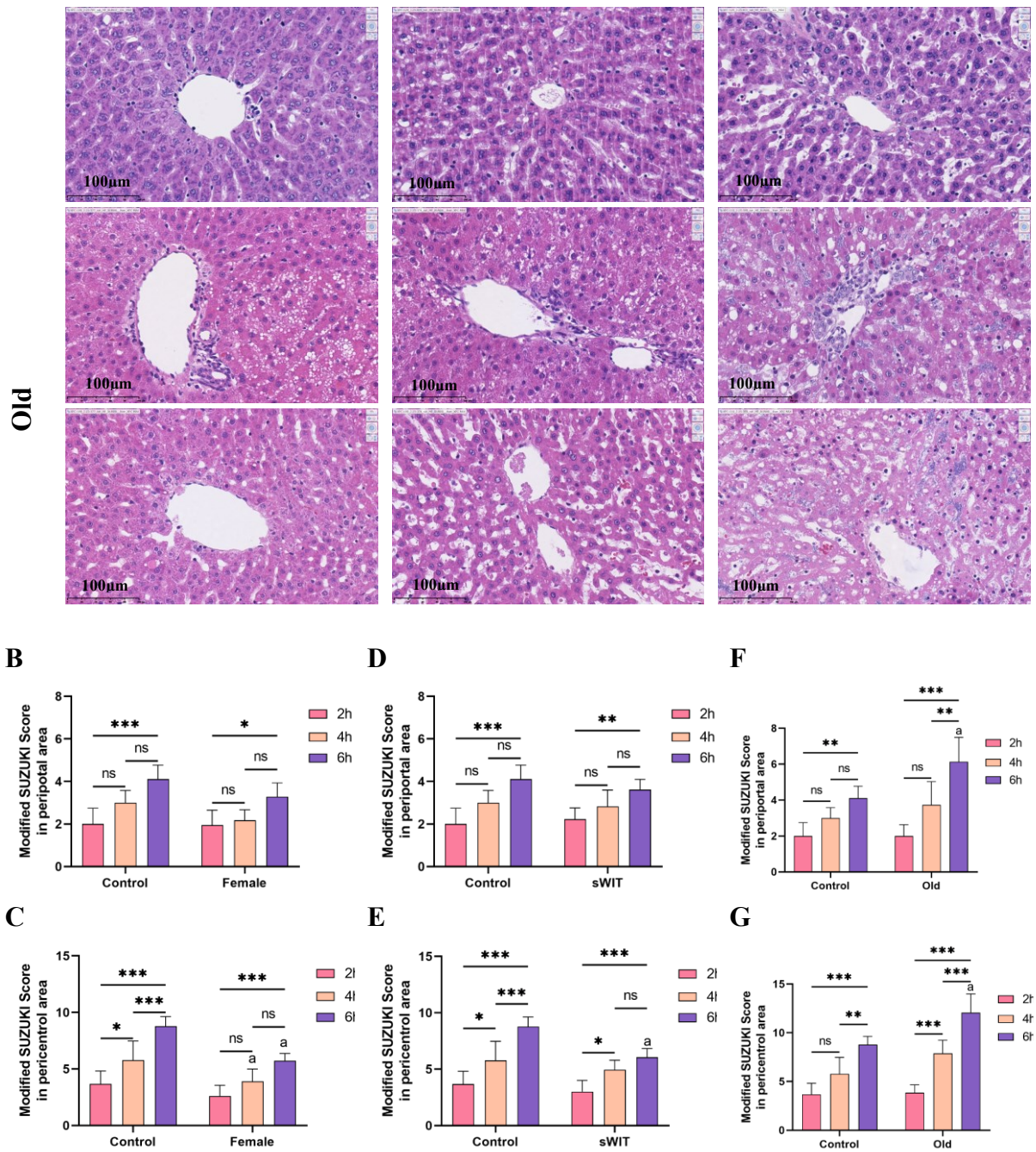
### 5.1.4.3 Impact of donor properties on liver morphology

In six of twenty three we also observed contamination after 6 hours of NMP, as confirmed by morphology.

To investigate the impact of donor properties on hepatocyte damage, liver morphology and HMGB1 translocation we analyzed the images from the respective stainings. As described before and shown in **Figure 27**, hepatocyte damage occurred mainly in the pericentral region in the form of nuclear pyknosis and vacuolization, resulting in a higher modified Suzuki score compared to the periportal region. As expected, the severity of damage was related to the duration of perfusion, meaning that hepatocyte injury worsened with the duration of NMP. Compared to the control, the female and sWIT livers showed less pericentral injury, reaching a score of  $5.7 \pm 0.7$  and  $6.1 \pm 0.8$ , whereas old livers showed substantially more signs of damage, reaching a score of  $6.2 \pm 1.4$  and  $12.1 \pm 1.9$  in periportal and pericentral areas, respectively.



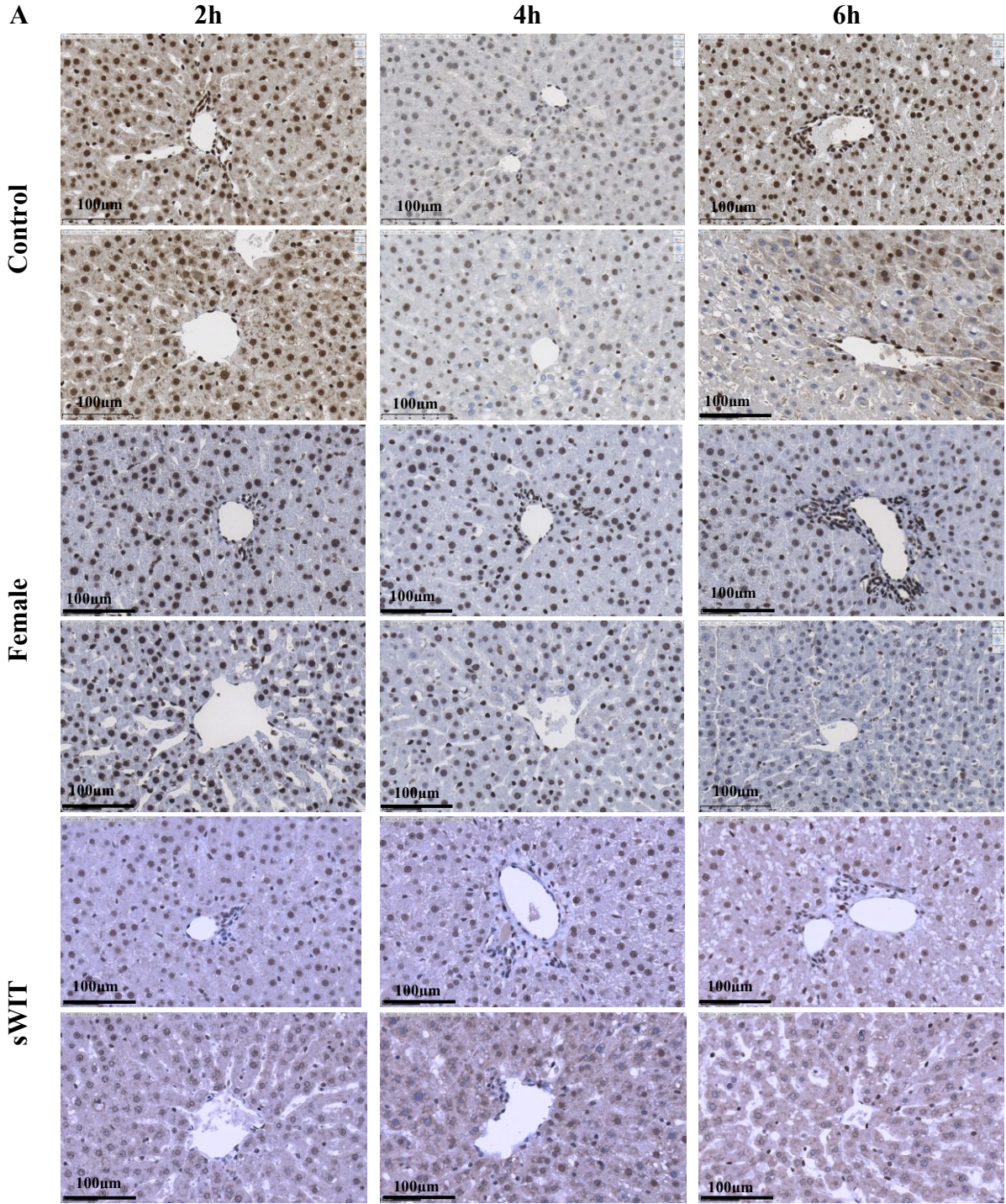




**Figure 27. Impact of donor condition on morphological damage.** (A) HE staining of the livers subjected to 6h NMP based on the donor properties. Quantitative analysis of the liver injury using modified SUZUKI score between control and the female in the periportal (B) and pericentral area (C) over NMP time. Quantitative analysis of the liver injury using modified SUZUKI score between control and sWIT in the periportal (D) and pericentral area (E) over NMP time. Quantitative analysis of the liver injury using modified SUZUKI score between control and old in the periportal (F) and pericentral area (G) over NMP time. Data expressed as mean  $\pm$  SD, one-way ANOVA followed by Tukey's post-hoc test. \* $P < 0.05$ , \*\* $P < 0.01$ , \*\*\* $P < 0.001$ , and ns = not significant. a, there is a significant difference compared to the control ( $P < 0.05$ ).

The HMGB1 translocation results supported this finding (Figure 28). The extent of pericentral translocation was more pronounced when the organs were subjected to 30 min WIT compared to 20 min and also more pronounced in old versus young livers. In other words,

HMGB1 translocation in the pericentral region followed the same pattern: lower in female and sWIT livers but higher in old livers with prolonged NMP and moderate in control livers. In contrast and as described above, the duration of NMP did not affect HMGB1 translocation in the periportal region.



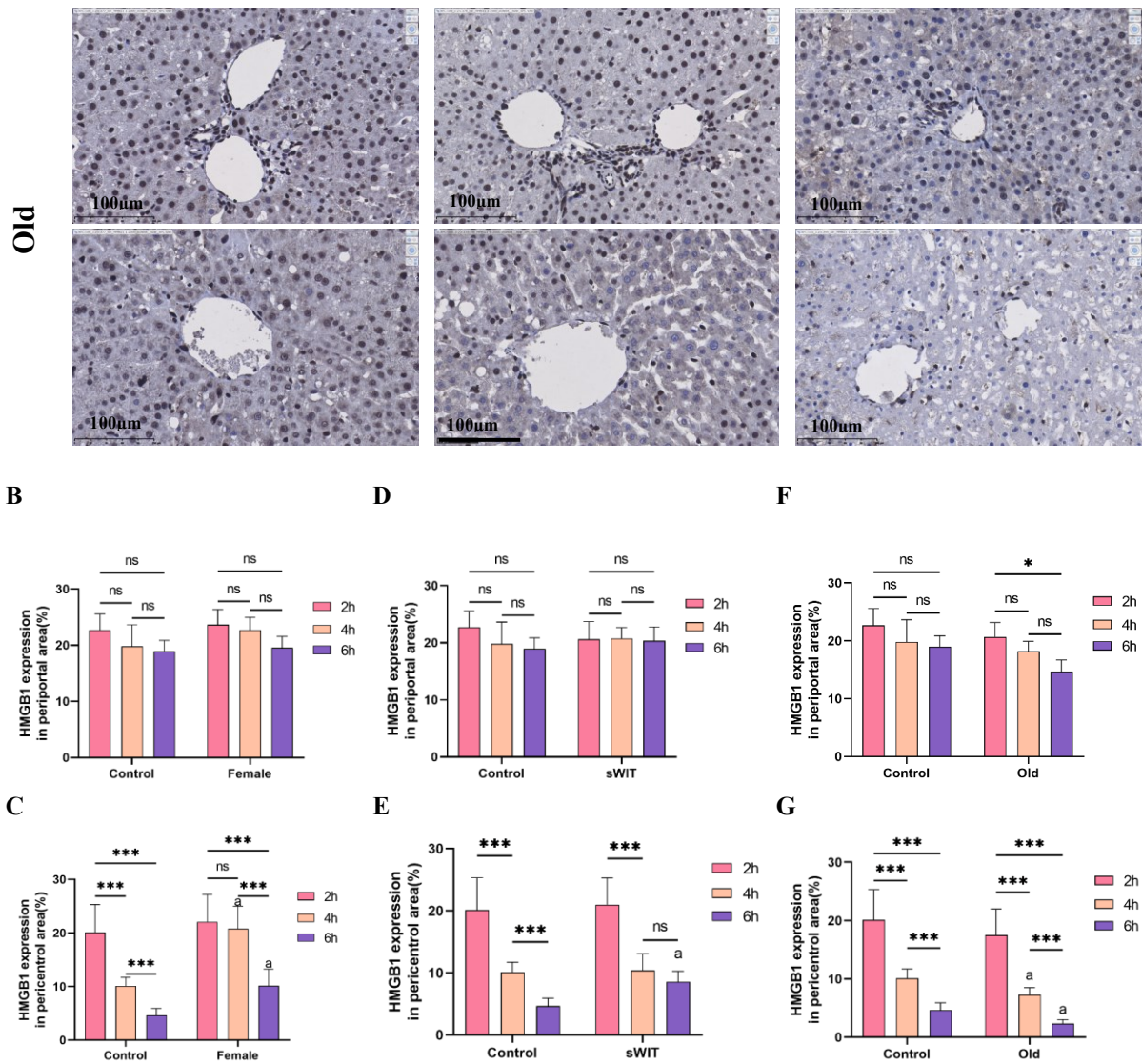


**Figure 28. Impact of donor condition on HMGB1 translocation.** Less HMGB1 translocation over NMP time in female gender and sWIT, but more in old age group. (A) HMGB1 staining of the livers subjected to 6h NMP based on the donor properties. Quantitative analysis of the HMGB1 translocation between control and female in the periportal (B) and pericentral area (C) over NMP time. Quantitative analysis of the HMGB1 translocation score between control and sWIT in the periportal (D) and pericentral area (E) over NMP time. Quantitative analysis of the HMGB1 translocation between control and old in the periportal (F) and pericentral area (G) over NMP time. Data expressed as mean  $\pm$  SD, one-way ANOVA followed by Tukey's post-hoc test. \*\*\* $P < 0.001$ , and ns = not significant. a, there is a significant difference compared to the control ( $P < 0.05$ ).

In addition, CYP1A2, used as an indirect marker of liver metabolism function was assessed at 2h, 4h, and 6h during NMP. As shown in **Figure 29**, we observed the expected zoned pericentral expression pattern of CYP1A2. However, the relative surface covered with the CYP1A2 signal decreased throughout the course of NMP. Compared to the control, the CYP1A2 expression in female was expressed more widely, corresponding to better liver function in terms of the bile production. In contrast, the relative extent of CYP1A2 expression

in terms of the area fraction in the old livers was significantly lower compared to all other groups, suggesting an impaired function as already observed for the relative bile production.

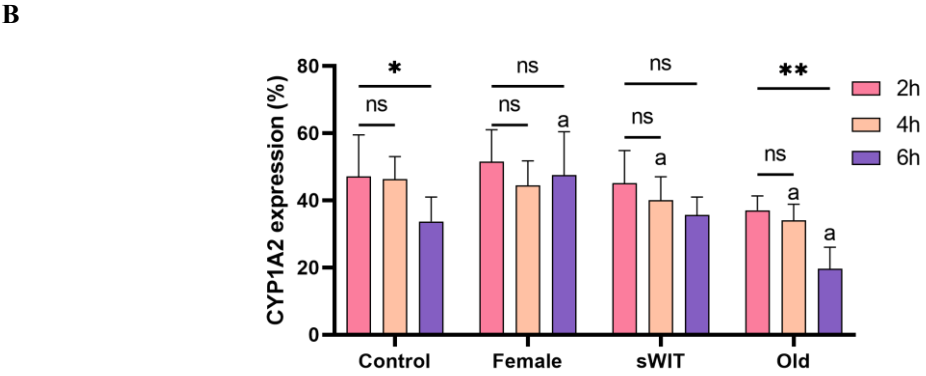
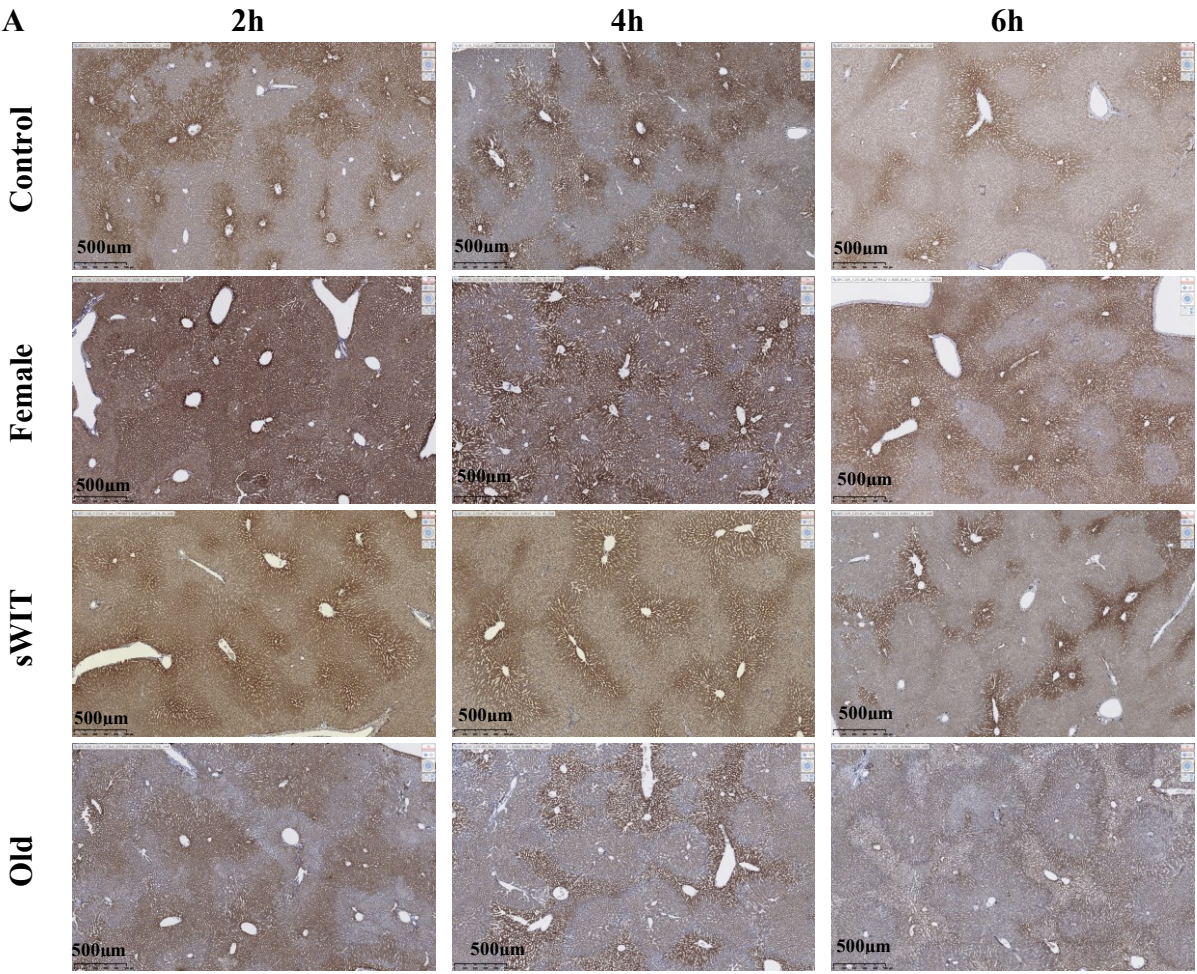


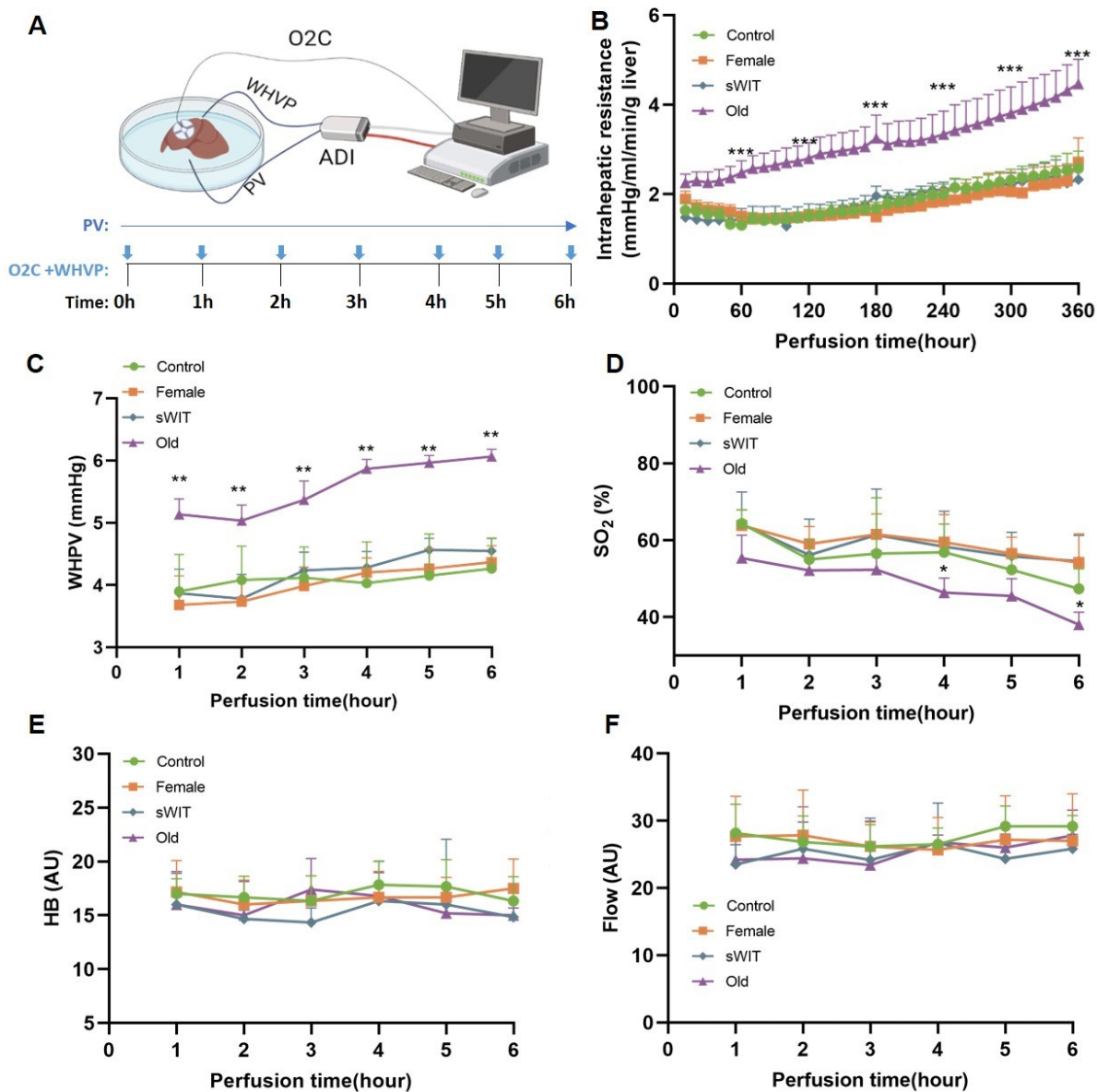
**Figure 29. Impact of donor condition on CYP1A2 expression.** Higher CYP1A2 expression during NMP in female gender and short WIT, but lower in old age. (A) CYP1A2 staining of the livers subjected to 6h NMP based on the donor properties. Quantitative analysis of the CYP1A2 expression in different donor properties groups. Data expressed as mean ± SD, one-way ANOVA followed by Tukey's post-hoc test. \*P < 0.05, \*\*P < 0.01, \*\*\*P < 0.001, and ns = not significant. a, there is a significant difference compared to the control (P < 0.05).

#### **5.1.4.4 Impact of donor properties on liver microcirculation**

Portal vein pressure and wedge hepatic vein pressure were constantly monitored as indirect indicators of intrahepatic resistance and liver sinusoidal pressure, as shown in **Figure 30**, respectively.

During NMP, PVP was relatively stable throughout the course of perfusion and in similar ranges (PV pressure: 4-10 mmHg). In parallel, the intrahepatic resistance and WHVP of the control group were also relatively stable, reaching  $2.5 \pm 0.7$  mmHg/min/gr liver and  $4.3 \pm 0.5$  mmHg at 6h NMP. However, intrahepatic resistance and WHVP pressures of the old liver were significantly higher compared to the other group and increased with the duration of perfusion (intrahepatic resistance:  $4.5 \pm 0.8$  mmHg/min/gr liver; WHVP:  $6.1 \pm 0.2$  mmHg after 6h NMP).

In addition, we used the O2C device for real-time monitoring of capillary-venous oxygen saturation, hemoglobin level, and microvessel perfusion flow. Normal values as determined in donor liver prior to explantation are in the range of  $49 \pm 4.3$  %,  $33.8 \pm 1.6$  AU, and  $208.7 \pm 11.9$  see also chapter 5.2.6. We observed that the tissue oxygen saturation decreased with the duration of NMP, from  $64.3 \pm 3.3$  % reaching  $50.8 \pm 3.4$  % after 6h NMP in control group. In comparison, the relative hemoglobin amount level and relative blood flow of microvessels perfusion were relatively stable, as expected, reaching  $13.3 \pm 2.1$  AU and  $29.2 \pm 1.5$  AU, respectively. Furthermore, donor age significantly impacted the oxygen saturation during NMP. As compared to the control, the SO<sub>2</sub> in the old reached  $38 \pm 3$  % after 6h NMP, indicating the damage of the oxygen-uptake capacity of hepatocytes. However, oxygen saturation in the sWIT and female group was relatively stable after 6h NMP, reaching  $54.5 \pm 6.13$  % and  $54.2 \pm 6.8$  %, respectively.



### 5.1.5 Impact of age on autophagy in livers subjected to NMP

To assess age dependent differences in autophagy, we checked the protein levels of 2 widely used autophagy namely LC3b-II and p62 via western blot in normal young and old livers. As shown in **Figure 31**, we observed that the expression of p62 was lower whereas the expression of LC3b-II was higher in aged livers, indicating that autophagy was impaired in the aged livers.

Furthermore, the levels of both autophagy markers were detected in livers subjected to 6h NMP. Similarly, we observed that the expression of p62 was even lower in aged livers subjected to 6h of NMP, whereas the expression of LC3b-II was higher in aged livers. In both groups, this effect was even more pronounced in aged livers.

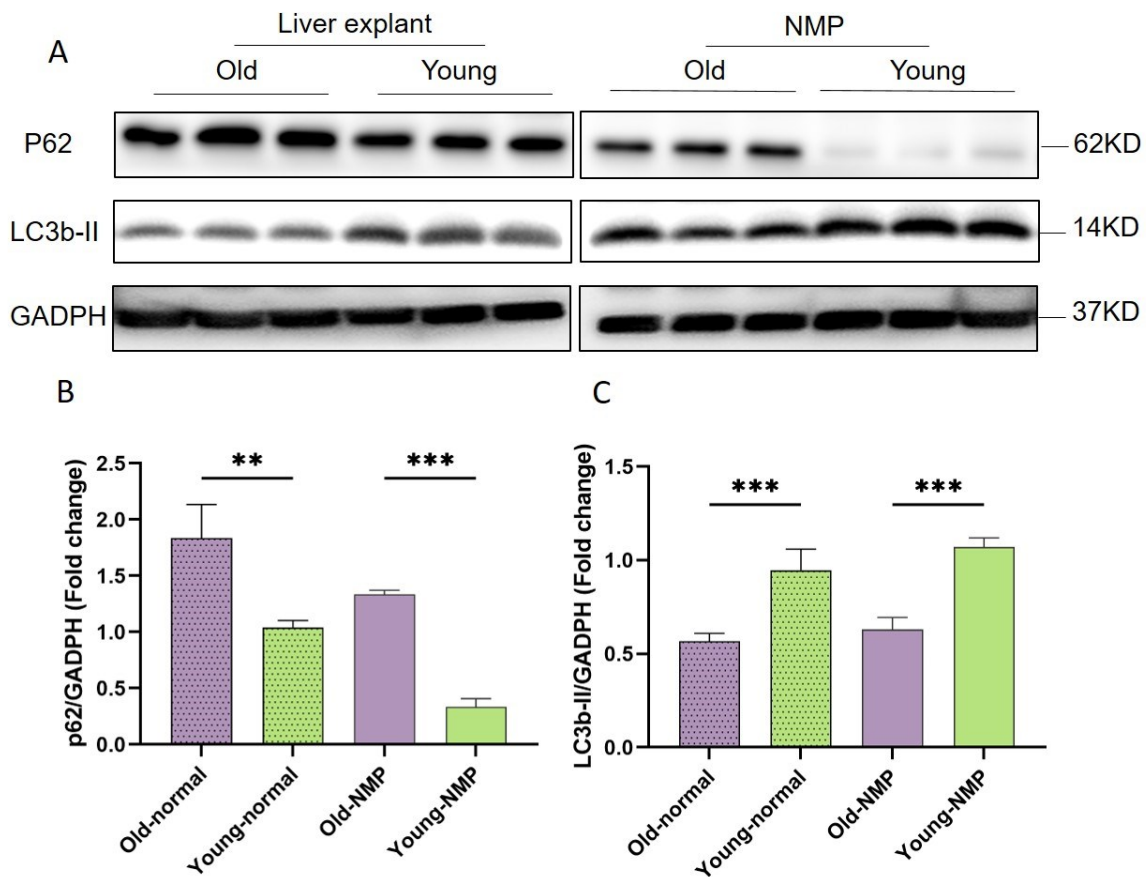


**Figure 31. Impact of age on autophagy markers.** (A) The western blot and quantitative analysis of expression of p62 protein (B) and LC3b-II protein (C) in normal and NMP livers (n = 3). Data expressed as mean  $\pm$  SD, one-way ANOVA followed by Tukey's post-hoc test. \*\*P < 0.01, \*\*\*P < 0.001, and ns = not significant.

Furthermore, to explore the role of autophagy in ischemia-reperfusion injury during NMP, the expression of P62 and LC3b-II were detected at 2h, 4h, and 6h NMP in both age and young groups (**Figure 32**). The results showed that the expression of P62 decreased over time, whereas the expression of LC3b-II increased in parallel with the perfusion time. Again, this eccentric was more pronounced in aged livers, suggesting an NMP-related augmentation of the age-related impairment of autophagy.

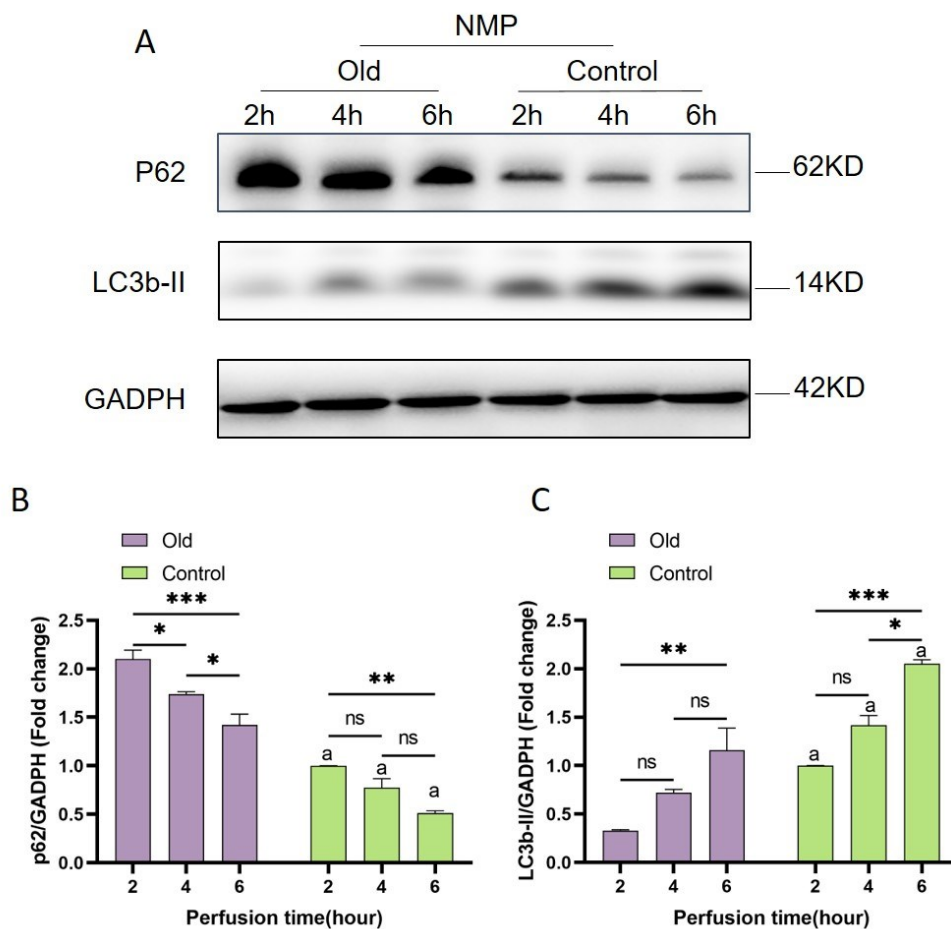


**Figure 32. Impact of age on expression of autophagy markers in livers subjected to NMP.** (A) Western blot and quantitative analysis of expression of p62 protein (B) and LC3b-II protein (C) in NMP livers. Data expressed as mean  $\pm$  SD, one-way ANOVA followed by Tukey's post-hoc test. \*\*\*P < 0.001 and ns = not significant. a: compared to control, there is significantly difference.

## 5.2 Part II: LTx study

### 5.2.1 Establishment of rat LTx

In Step I, to establish rat liver transplantation, the training was divided into 6 phases (**Table 3**). Phase A: handling exercise, Phase B1: cadaver vessel anastomosis, Phase B2: whole cadaver LTx anastomosis training, Phase C1: living animal technique training (n=27), Phase C2: 24h survival training (n=12), Phase C3: planned short term observation (n=14) and Phase C4: evaluation of optimized flushing conditions (n=3).



**Table 3. The overview for establishment of the rat LTx model**

Step I	Purpose	Number	Result
<b>Handling exercises (Phase A)</b>			
Phase A	handling exercise	-	
<b>Cadaver training (Phase B, n=18)</b>			
Phase B1	cadaver vessel anastomosis	11	
Phase B2	whole cadaver LTx anastomosis training	7	
<b>Living animal training (Phase C, n= 44)</b>			
Phase C1	technique training	15	
Phase C2	24h survival training (flow rate controlled flushing 10ml/min/animal with 100ml saline using pump)	12	6 surviving rats with homogenous reperfusion used for comparison with formal study
Phase C3	Planned short term observation (volume controlled flushing with 100ml saline using 80cm water column =>causing reperfusion problems)	14	6 intraoperative death, 4 sacrificed at 1h with 4 heterogenous reperfusion, 4 homogenous reperfusion (no HD)
Phase C4	Evaluation of optimized flushing conditions (pressure controlled flushing with 0.2ml Ringer lactate per body weight using 20cm water column)	3	homogenous reperfusion (but no HD)

HD: hemodynamic monitoring

First, Phase A was designed to practice suturing gauze and anastomosis on silicone tubes to improve handling of microsurgery instruments and to train the steps of vessel anastomosis.

Second, Phase B1 was designed to train suturing cadaver vessels (IHVC) to get used to the tissue properties of actual vessels (see **Table 4**). We recorded the time of suturing the back and front walls of the vessels, total anastomosis time, and success rate. Successful IHVC anastomosis was defined as no leakage and no stenosis. A total of 11 cases of IHVC anastomosis were performed. The total time was  $9.9 \pm 1.6$  min. The success rate of suturing was 63.6% (7/11) with errors occurring during the first exercises.

**Table 4. Vessel anastomosis practice in cadaver**

Replicate case	Back wall time	Front wall time	Total time	Results
Rep#1	8min	6min	14min	Stenosis
Rep#2	7min	4min	11min	Leakage from left corner
Rep#3	6min	4min	10min	Stenosis
Rep#4	4min	4min	8min	Leakage from left corner
Rep#5	4min	4min	8min	No leakage or stenosis
Rep#6	5min	4min	9min	No leakage or stenosis
Rep#7	5min	4min	9min	No leakage or stenosis
Rep#8	6min	4min	10min	No leakage or stenosis
Rep#9	6min	4min	10min	No leakage or stenosis
Rep#10	6min	4min	10min	No leakage or stenosis
Rep#11	5min	5min	10min	No leakage or stenosis
Summary	5.6 ± 1.2	4.2 ± 0.6	9.9 ± 1.6	7/11

Third, Phase B2 was designed to practice the anastomosis of SHVC, PV, and BD in cadavers to handle all the anastomosis techniques needed for LTx (see Table 5). A total of 7 cases of SHVC, PV, and BD anastomosis were performed. The anastomosis times of SHVC, PV, and BD were  $18.2 \pm 3.1$  min,  $7.7 \pm 1.7$  min, and  $6.8 \pm 1.2$  min, respectively. However, 2 of seven cases of SHVC anastomosis developed leakage, and in one case had stenosis occurred. In 2 out of cases PV anastomosis was twisted. None of complication occurred in BD anastomosis training.

**Table 5. SHVC, PV, and BD anastomosis practice in cadaver**

Replicate case	Time (min)			Results
	SHVC anastomosis	PV anastomosis	BD anastomosis	
Rep#1	25	10	8	Leakage of SHVC, twisting of PV
Rep#2	20	10	9	Leakage of SHVC
Rep#3	18	8	7	Stenosis of SHVC, twisting of PV
Rep#4	17	8	6	No leakage or stenosis
Rep#5	17	6	7	No leakage or stenosis
Rep#6	15	7	5	No leakage or stenosis
Rep#7	16	5	6	No leakage or stenosis
Summary	18.2 ± 3.1	7.7 ± 1.7	6.8 ± 1.2	SHVC: 4/7; PV:5/7; BD:7/7

SHVC, suprahepatic vena cava, PV, portal Vein, BD, bile duct

Finally, in Phase C, the full-procedure rat LTx was practiced in living animals. As shown in Table 6, 27 pairs of living Wistar rats were used for training. Fifteen cases were used for technical training (Phase C1) and 12 for observing 24-hour survival (Phase C2). During the technical training, the animals were sacrificed immediately after completing the implantation procedure using an overdose of isoflurane. The goal was to reach a stable anhepatic time under 25 minutes, as recommended prerequisite for survival (t Hart et al., 2004). In Phase C2, postoperative recovery was observed for the first 24h to determine the 24h survival rate.

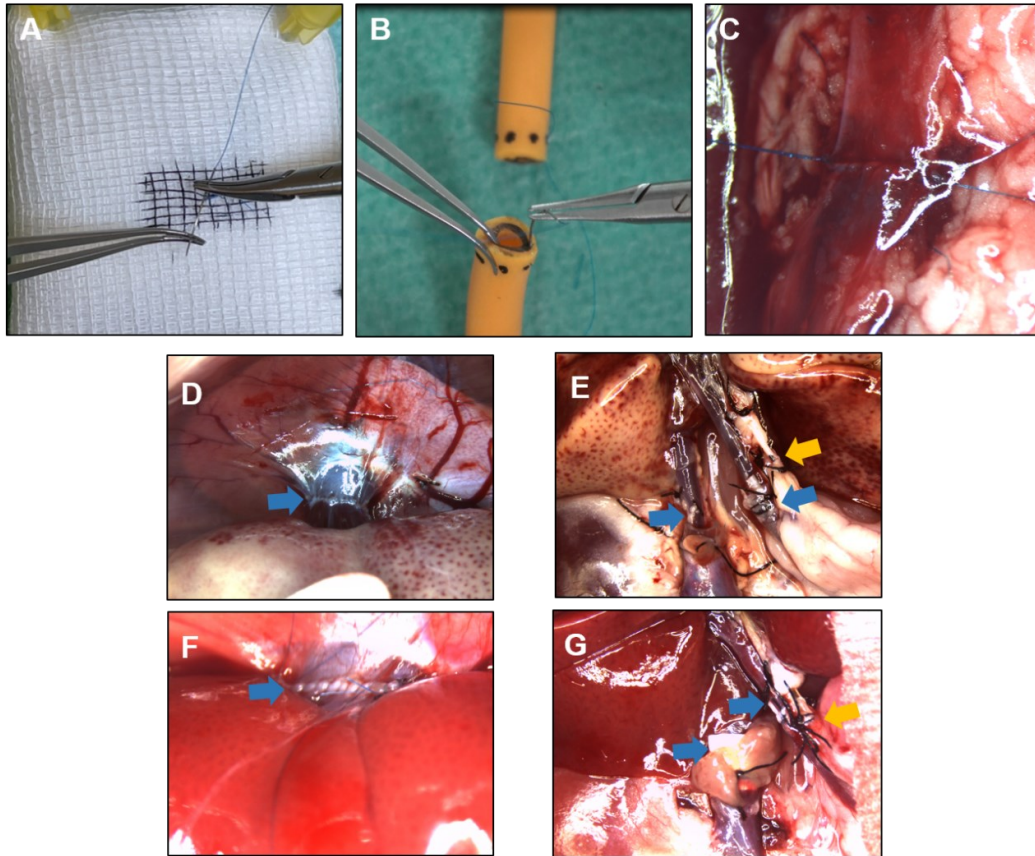


**Figure 33. Illustration of the phases needed for establishing rat LTx model.** Phase A: practice suturing glove (A) and tube anastomosis (B). (C) Phase B1: cadaver vessel anastomosis. (D-E) Phase B2: cadaver Ltx training of SHVC, IHVC, PV, and BD anastomosis. (E-F) Phase C1: Living Ltx training of SHVC, IHVC, PV, and BD anastomosis.

As shown in **Table 6**, the targeted anhepatic time was achieved in 7/15 procedures equivalent to a success rate of 47%. However, anhepatic time of below 25min was achieved for the last 4 consecutive cases. In the following survival training, half of the animals (6/12) reached the end of the planned observation time of 24h. All animals did recover from anesthesia within a few minutes, but deteriorated between 4-12 h postoperatively due to delayed bleeding from suprahepatic cava, or due to severe IRI because of inhomogenous reperfusion.

During the survival training, the liver was flushed with 100ml cold saline with 100IU heparin using a flow rate of 10ml/min. The time of each anastomosis was recorded to compare with the previous results achieved in phase B2. The anastomosis time in Phase C1 was shorter than in Phase C2 (see **Table 6**). Further improvement became visible when comparing the time for distinct surgical procedures in technical training and survival training. The analysis revealed that the time needed for the donor procedure ( $82.1 \pm 6.2$  min vs.  $68.6 \pm 4.3$  min) was significantly shortened as well as the time needed for the recipient procedure ( $113 \pm 12.5$  min vs.  $97.1 \pm 5.5$  min), the back table procedure ( $38.3 \pm 3.7$  min vs.  $30 \pm 2.2$  min), and also the anhepatic time ( $26.5 \pm 3.4$  min vs.  $23 \pm 1.7$  min). However, the anastomosis times of the SHVC,

PV, IHVC, and BD were not significantly different, but the time needed to position the liver was shortened from 8min to 5min.

**Table 6. The time of needed of each surgical step including the anastomosis in Phase B1, Phase C1, Phase C2**

Phase	Nr of S/T	Time (min)							
		Donor	Recipient	Back table	Anhepatic time	SHVC	PV	IHVC	BD
Phase B2	SHVC:4/7; PV:5/7; BD:7/7	NA	NA	NA	NA	18.2 ± 3.1	7.7 ± 1.7	NA	6.8 ± 1.2
Phase C1	7/15	82.1 ± 6.3	112 ± 12.5	38.4 ± 3.7	26.5 ± 3.4	13.5 ± 3*	5.9 ± 1.1*	7.2 ± 1.6	4.9 ± 1.6*
Phase C2	6/12	69 ± 4.3#	97 ± 5.5#	30 ± 2.2#	23 ± 1.7#	12 ± 2.3*	5 ± 0.8*	6 ± 1.8	5 ± 1.3*

Nr of S/T: number of success/total animals, \*: significant difference compared to phase B2, #:significant difference compared to Phase C1, NA: not applicable.

Additionally, to visualize the learning curve, we plotted the consecutive number of all procedures versus the anhepatic time, see **Figure 34**. It became visible, that after the first 10 procedures in living animals, the targeted anhepatic time of less than 25 min was reached in 16/17 cases.

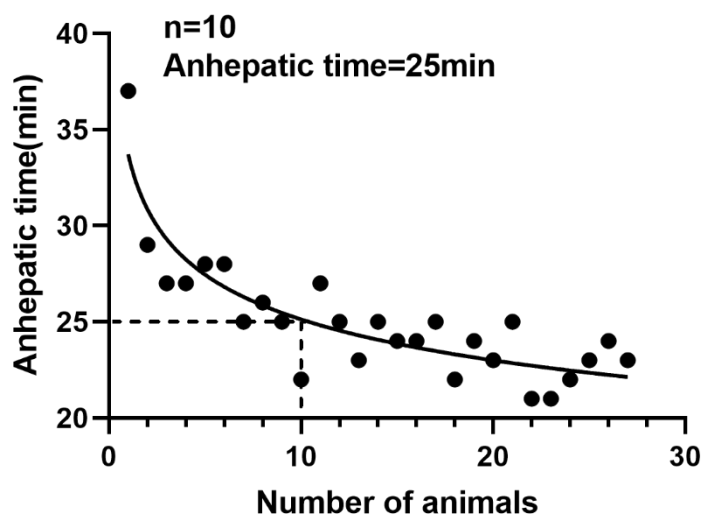


**Figure 34. Learning curve for establishing stable rat LTx.** After practicing 10 procedures, the anhepatic time became relatively stable  $\leq 25$  minutes.

As shown in **Figure 35**, the remaining 6 rats were sacrificed at the end of the planned 24h observation in clinically good condition (postoperative score = 0). Nevertheless, we observed that 1 case presented with heterogenous reperfusion (**Figure 35A-B**) requiring exclusion from further analysis. The remaining 5 cases presented with homogenous reperfusion but with a small area of necrosis in the hepatoduodenal ligament around the bile duct stent with a maximal diameter of 5mm (**Figure 35C**). In 2 cases we observed in addition a small necrosis in the edge

of the left lateral lobe. Therefore, these animals were included in the subsequent comparison of early and late IRI. Blood and tissue samples of those 5 animals were subjected to clinical chemistry and histology assessment. Results are described in chapter 5.2.4 to 5.2.6.

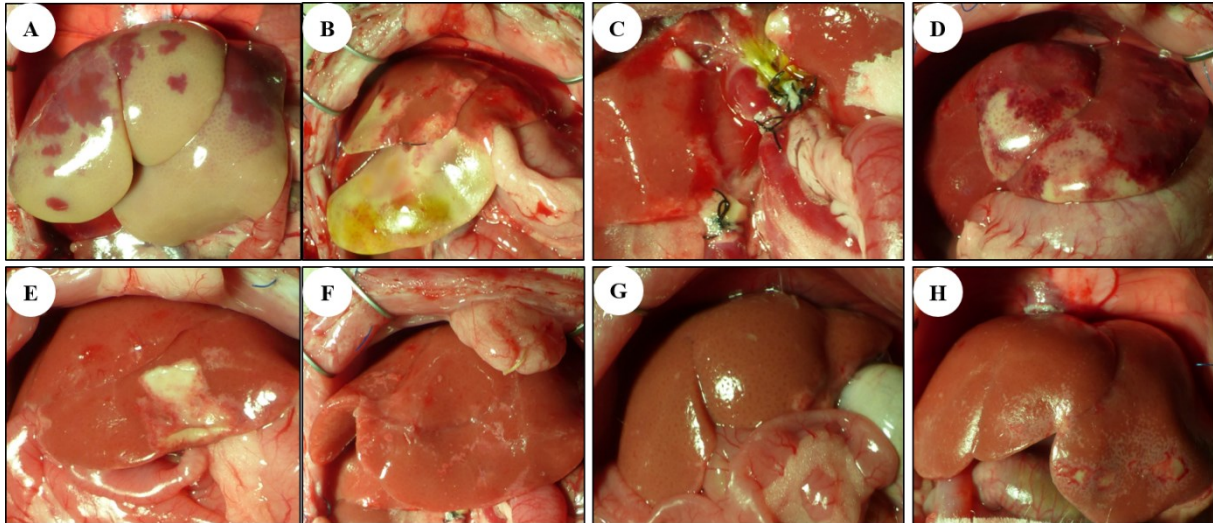


**Figure 35. Illustration of six cases of LTx survival at 24h.** (A) Heterogenous reperfusion around 30min reperfusion and the liver after 24h reperfusion (B). (C) small area of necrosis in the hepatoduodenal ligament around the bile duct stent with a maximal diameter of 5mm. (D-H) Included cases (n=5) for comparison study as 24h group.

### 5.2.1.1 Improvement of reperfusion quality in rat LTx

Based on the relatively stable technique for the LTx model at Phase C1 to Phase C2 (anhepatic phase:  $23 \pm 1.7$  min), we continued to perform 14 cases to evaluate hepatic microcirculation in the planned short term observation in Phase C3. During this phase, the anhepatic phase was  $24.4 \pm 2.1$  min (**Table 7**). However, 6 of the rats died intraoperatively due to technical complications such as air embolism (n=3) bleeding from hepatic artery (n=1) and bleeding of SHVC anastomosis (n=2). In addition, in the last four cases we observed a rather heterogenous reperfusion in the early postoperative phase (see **Figure 36A-B**). During this phase, we performed gravity controlled (80cm water column) flushing of the donor livers with a fixed volume of 100ml saline.

**Table 7. The time of each procedure and anastomosis in Phase C3 and Phase C4**

Group	Time (min)							
	Back table	Anhepatic time	SHVC	PV	IHVC	CBD	Donor	Recipient
Phase C3	28±2.1	24±3.3	14±2.9	5±0.4	7±0.8	6±1.9	66.2±5.2	96.3±5.4
Phase C4	25±1.3	24.4±1.4	14±0.8	5±0.5	7±0.7	6.4±0.8	72.4±2.5	94.3±3.3

SHVC: superior hepatic vena cava anastomosis; PV: portal vein anastomosis; IHVC: Inferior hepatic vena cava; CBD: common bile duct anastomosis.

Therefore, we went back to training (phase C4, n=3) to improve reperfusion quality. We reinstalled pressure controlled flushing with 0.2ml Ringer lactate per gr body weight using 20cm water column. After that, three consecutive cases of reperfusion were homogenous (**Figure 36C-D**), and none of the animals died intraoperatively. The anhepatic time was 24.4±1.4 min.

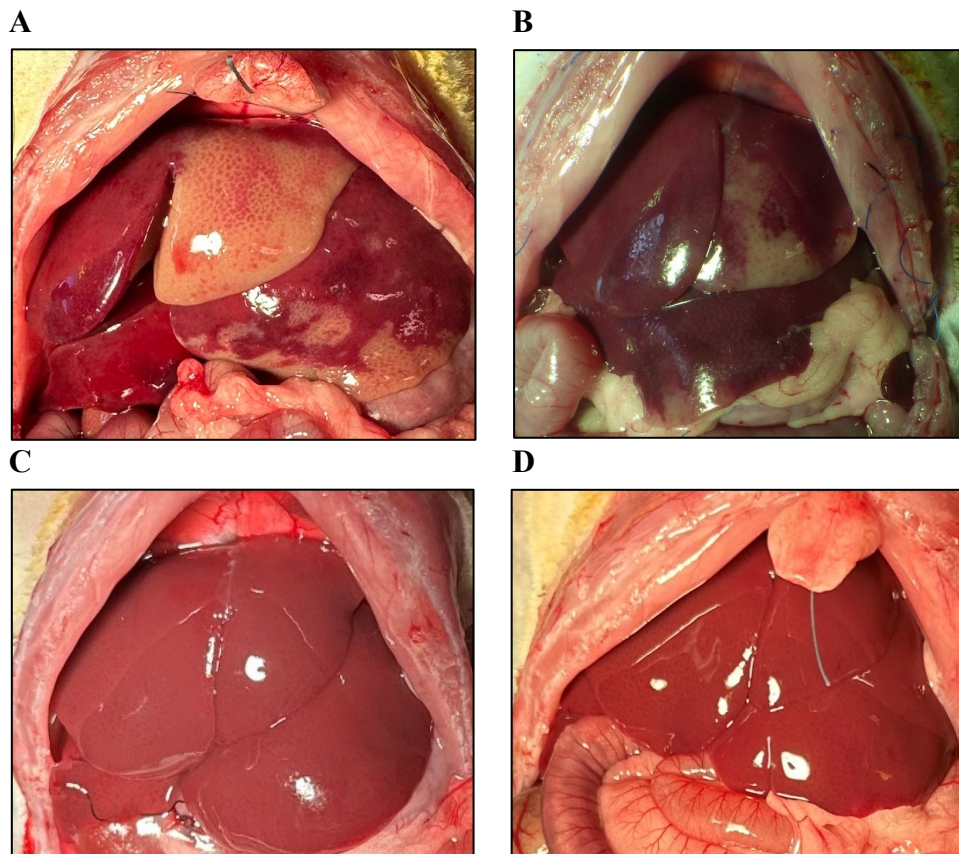


**Figure 36. Illustration of improvement of reperfusion quality for rat LTx model.** (A-B) Heterogenous reperfusion after flushing the liver with 100ml cold saline supplemented with 1IU/ml heparin at 80cm water column after reperfusion 15min (A) and 1h (B). Homogenous reperfusion after flushing the liver with 0.2ml/gr body weight of cold ringer lactate with 1 IU/gr body weight of heparin using a pressure of 20cm water column after reperfusion 15min (C) and 1h (D).

### 5.2.2 Characterisation of early hepatic IRI

A total of 6 cases of LTx were included in Step II to explore the early liver IRI and liver microcirculation. As shown in **Figure 37**, all transplantation procedures were performed smoothly and without obvious technical errors. No obvious torsion or stenosis was found in any of the anastomoses. Reperfusion became completely homogenous within 15 minutes and remained homogenous throughout the first hour as assessed visually.

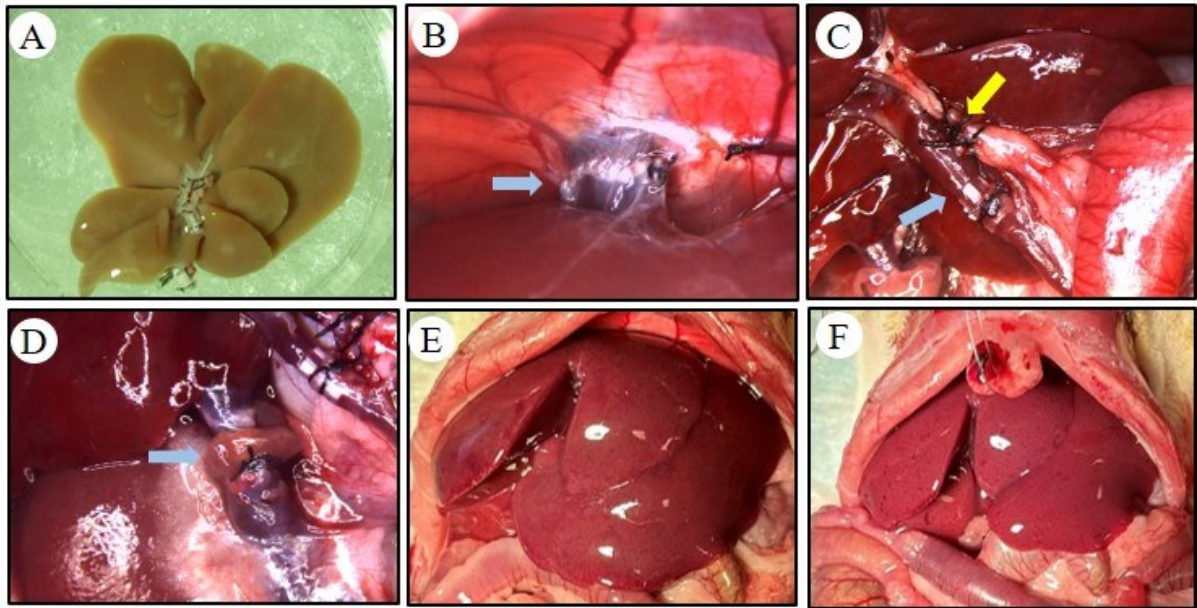


**Figure 37. Stepwise illustration of LTx procedures.** A: Donor graft after flushing; B: SHVC anastomosis; C: PV (blue arrow) and CBD (yellow arrow) anastomosis; D: IHVC anastomosis; E: Reperfusion 15min; F: Reperfusion 1h.

As shown in **Table 8**, the times of donor and recipient procedures were  $64.5 \pm 5.6$  min and  $91.9 \pm 4.4$  min, respectively. The anhepatic time was  $23.4 \pm 1.2$  min. There was no significant difference in anhepatic time between the LTx 1h and the LTx 24h group ( $23 \pm 1.4$  min vs  $23.4 \pm 1.1$  min,  $p=0.412$ ). Similarly, the time needed for other anastomoses were relatively stable.

**Table 8. The time of each procedure of LTx for comparison study**

Group	Time (min)							
	Back table	Anhepatic time	SHVC	PV	IHVC	CBD	Donor	Recipient
<b>Total (n=11)</b>	28.7±2.7	23.4±1.1	11.7±1.7	5.1±0.7	5.4±0.9	4.4±1.2	64.5±5.6	91.9±4.4
<b>LTx 24h (n=5)</b>	30.6±1.1	23±1.4	11.2±2.1	5±0.9	5.2±1	5±1.4	69.4±4.1	93.2±4.5
<b>LTx 1h (n=6)</b>	28.7±2.7	23.4±1.1	11.7±1.7	5.1±0.7	5.4±0.9	4.4±1.2	64.5±5.6	91.9±4.4

SHVC: superior hepatic vena cava anastomosis; PV: portal vein anastomosis; IHVC: Inferior hepatic vena cava; CBD: common bile duct anastomosis.

### 5.2.2.1 Impact of IRI on hepatic hemodynamic, perfusion and microcirculation

Assessment of the perfusion situation of the liver was done in 4 steps. As a first step, we determined PVP (expressed in mmHg) and PVF (expressed as ml/min). In the second step, we performed spectrophotometric determination of tissue oxygenation ( $SO_2$ , expressed in %), tissue hemoglobin (rHB, expressed in arbitrary units), and the volume flow (Flow, expressed

in arbitrary units. In the third step, microcirculation was visualized using CytoCam. After sacrificing the animal, liver stiffness was measured *ex vivo*.

The PVP and PVF were measured before and after reperfusion to monitor the hepatic hemodynamic changes induced by early IRI. As shown in **Figure 38**, the PVF decreased from  $17.5 \pm 4.8$  to  $12.8 \pm 0.8$  ml/min after 1 hour of transplantation. The PVP had a similar trend, decreasing from  $13.7 \pm 2.1$  mmHg to  $7.5 \pm 0.8$  mmHg, possibly reflecting partial recovery from the severe cardiovascular depression during the anhepatic phase.

In addition, the spectrometric device (O2C) allows for quantifying non-invasively tissue perfusion. This sensor was applied intraoperatively on the left lateral liver lobe to assess hepatic perfusion and microcirculatory alterations early after LTx. Therefore, we monitored the alteration of hepatic microcirculation before and post-transplant using O2C for real-time and visual evaluation of early IRI in transplantation. As shown in **Figure 38**, the level of capillary-venous oxygen saturation decreased from  $49 \pm 4.3$  % to  $33.4 \pm 7.4$  % after 1 hour of transplantation, again possibly reflecting partial recovery from cardiovascular depression during the anhepatic phase. In parallel, relative tissue hemoglobin concentration was increased from  $33.8 \pm 1.6$  AU to  $46 \pm 11.1$  AU, possibly related to a putative loss of volume. As shown in **Figure 38**, the microvessel perfusion flow of the liver significantly decreased to half of the value observed before transplantation, corresponding to a similar decrease in PVF.



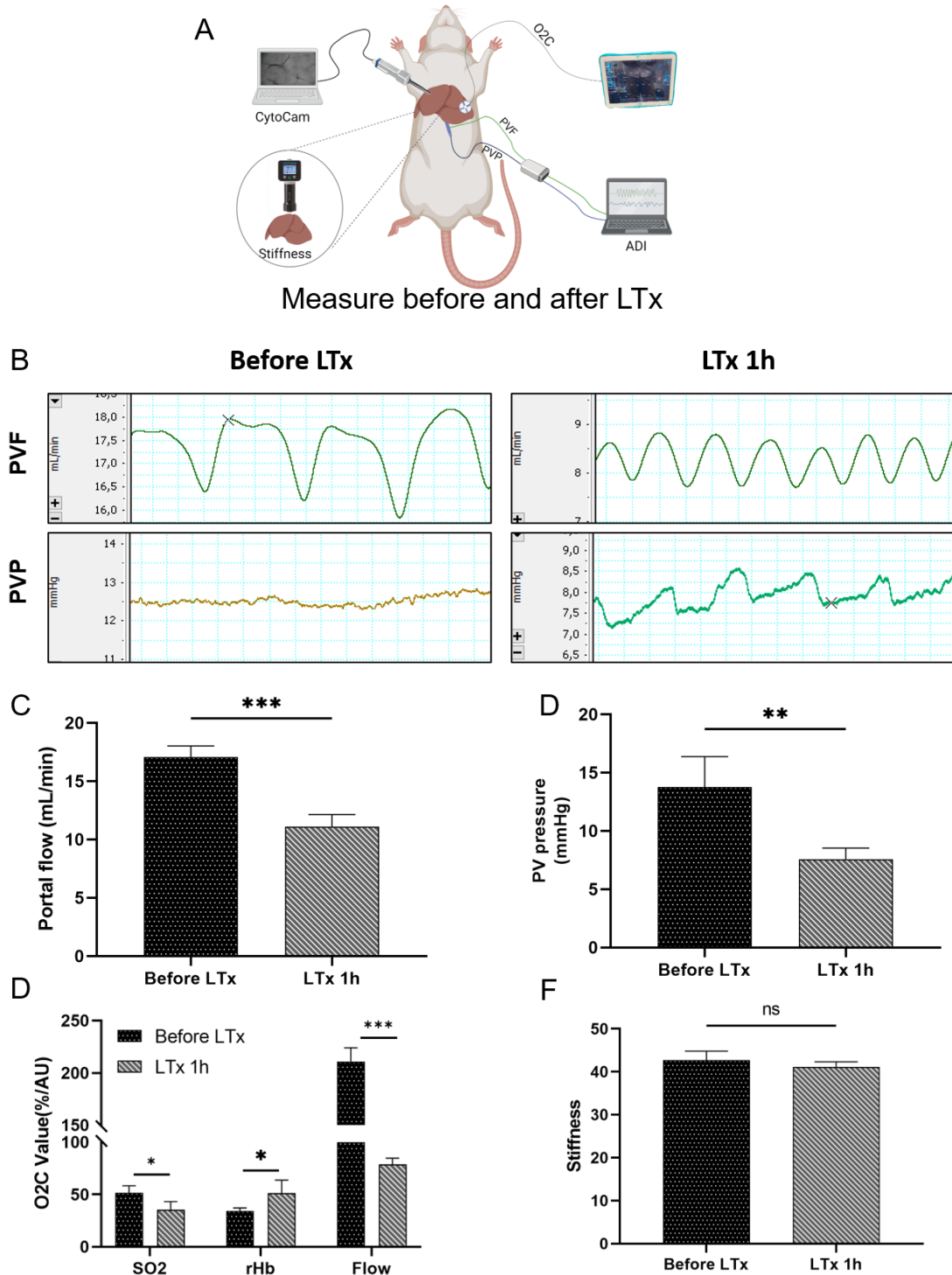


**Figure 38. Impact of reperfusion on hepatic hemodynamics.** Reduction in liver reperfusion 1 hour after reperfusion. (A) Time point of monitoring liver hemodynamics and liver microcirculation. (B-D) PVF and PVP before and 1h after LTx. (D) SO<sub>2</sub>, rHb, and Flow before and 1h after LTx. (E) Liver stiffness before and after 1h LTx. Data expressed as mean  $\pm$  SD, one-way ANOVA followed by Tukey's post-hoc test. \*P < 0.05, \*\*P < 0.01, \*\*\*P < 0.001, and ns = not significant.

The introduction of handheld microscopes provides a non-invasive modality for the direct assessment and visualization of the hepatic sinusoidal angioarchitecture. The technique allows

visualization of microcirculation based on the flow of red blood cells vessels and sinusoids of the liver.

Therefore, we monitored the hepatic microcirculation using the CytoCam device to quantify the perfused hepatic microvessels before and after reperfusion. The software allows for separate analysis of capillaries and larger non-capillary vessels. The capillaries and non-capillary vessels are defined by a diameter from 6 to 15.99  $\mu\text{m}$  and from 16 to 47.99  $\mu\text{m}$ , respectively.

As a first step of the automated analysis, the static parameters, such as the number of capillary segments, the total capillary length, the average capillary length, and the overall capillary density, were determined. As expected, IRI did not affect any of the parameters. Before and after reperfusion, a total number of  $1104.2 \pm 467$ , respectively,  $1077.7 \pm 475.9$  capillary segments were determined. IRI did also not affect total capillary length. Before and after reperfusion, the total capillary length was measured as  $31.1 \pm 12.6$  mm, respectively  $29.1 \pm 12.7$  mm. The average capillary length was  $28.7 \pm 4.1$   $\mu\text{m}$  and  $27.1 \pm 3.7$   $\mu\text{m}$  in normal and 1 hour post-transplant. The overall capillary density was  $17.8 \pm 7.23$  mm/mm<sup>2</sup> before transplantation and  $16.6 \pm 7.3$  mm/mm<sup>2</sup> after transplantation.

In the second step of the analysis, the dynamic parameters affected by IRI, such as the perfused capillary density and proportion of capillary density, were assessed (**Figure 39**). As expected, the perfused capillary density significantly decreased 1 hour after LTx, from  $2.8 \pm 2.4$  mm/mm<sup>2</sup> to  $0.91 \pm 0.5$  mm/mm<sup>2</sup>, reflecting the reduction of convective and diffusive properties of the visualized microcirculatory bed. The proportion of perfused capillaries had the same trend, decreasing from  $16.5 \pm 10.8$  % to  $6.3 \pm 3.9$  %. This finding corresponded to the reduction of PVP and PVF, but also to the reduced tissue oxygenation and reduced flow, all together reflecting the incomplete recovery from cardiovascular depression during early IRI.

After liver explantation, we measured the stiffness of the ex-vivo to determine the potential mechanical effect of reperfusion on the organ. However, the liver stiffness expressed in arbitrary units did not change after transplantation. ( $42.7 \pm 2.1$  and  $41.1 \pm 1.2$ , respectively, **Figure 38**).

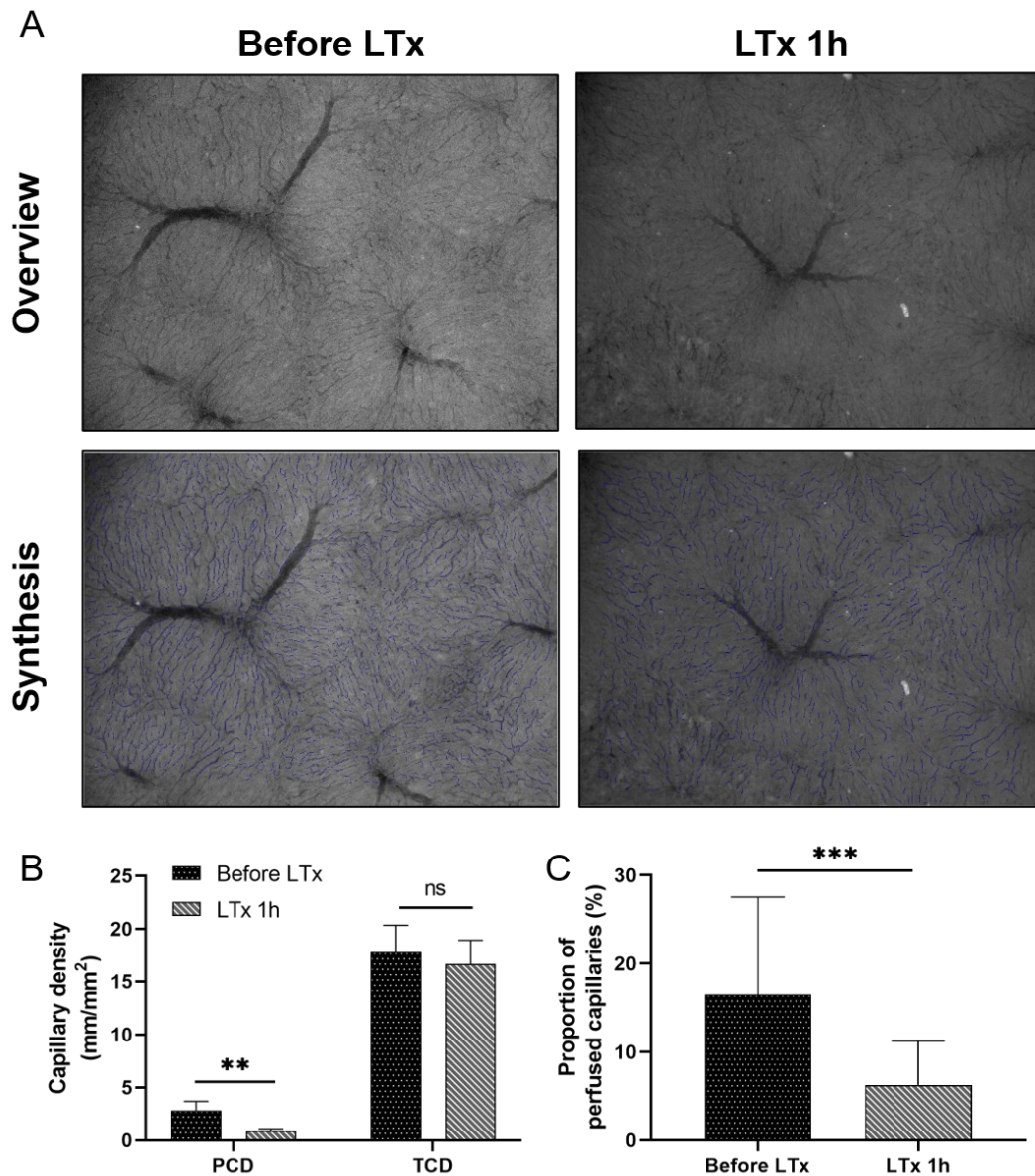


**Figure 39. Impact of early perfusion injury on hepatic microcirculation.** Reduction in liver reperfusion 1 hour after reperfusion. (A) Images of the microvessels before and 1h after LTx. The blue color is fitted microvessels. The capillary density (B) and proportion of perfused capillaries before and 1h after LTx. Data expressed as mean  $\pm$  SD, one-way ANOVA followed by Tukey's post-hoc test. \*\*P < 0.01, \*\*\*P < 0.001, and ns = not significant. PCD, perfused capillary density; TCD, total capillary density. The blue lines indicate the vessels smaller than 16  $\mu$ m and represent the TCD within the entire image.

### 5.2.2.2 Impact of IRI on liver damage in terms of liver enzymes and blood count

To evaluate the severity of early IRI, the release of liver enzymes was determined in liver donors prior to explantation and in liver graft recipients 1 hour and 24 hours after LTx. As shown in **Figure 40**, IRI caused an immediate strong release of liver enzymes within 1h of reperfusion, which recovered partially within 24h. As an example, normal ALT levels range between 10 and 50 IU/L; immediately after LTx the levels increased to  $1827.2 \pm 744.9$  IU/L

but recovered within 24 h to a level of  $662.8 \pm 407.5$  IU/L. The levels of AST, and LDH at 1 hour LTx with  $1684.1 \pm 791.6$  IU/L and  $4708.6 \pm 1909.2$  IU/L, respectively, and decreased to  $1497.4 \pm 583.9$  IU/L, and  $1891.8 \pm 694.8$  IU/L at 24 hours LTx.

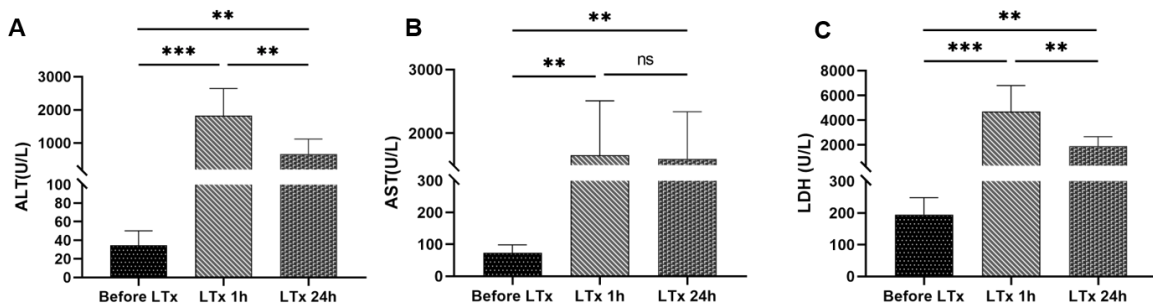


**Figure 40. Impact of transplant on liver function.** Substantial enzyme release after reperfusion. The levels of ALT (A), AST (B), and LDH (C) before LTx and after LTx. Data expressed as mean  $\pm$  SD, one-way ANOVA followed by Tukey's post-hoc test. \*\* $P < 0.01$ , \*\*\* $P < 0.001$ , and ns = not significant.

We investigated the alteration of blood count before and after early LTx. As shown in **Figure 41**, the levels of WBC and PLT significantly increased to  $11.9 \pm 4.6 \times 10^3/\text{mm}^3$  and  $1163 \pm 413 \times 10^9/\text{L}$ , respectively, after 1 hour of reperfusion. In addition, the levels of RBC, HGB, and HCT increased after reperfusion, possibly due to intraoperative loss of volume resulting in slight hemoconcentration. As expected, the levels of MCH, MCHC, and MCV were relatively stable after transplantation (data not shown).

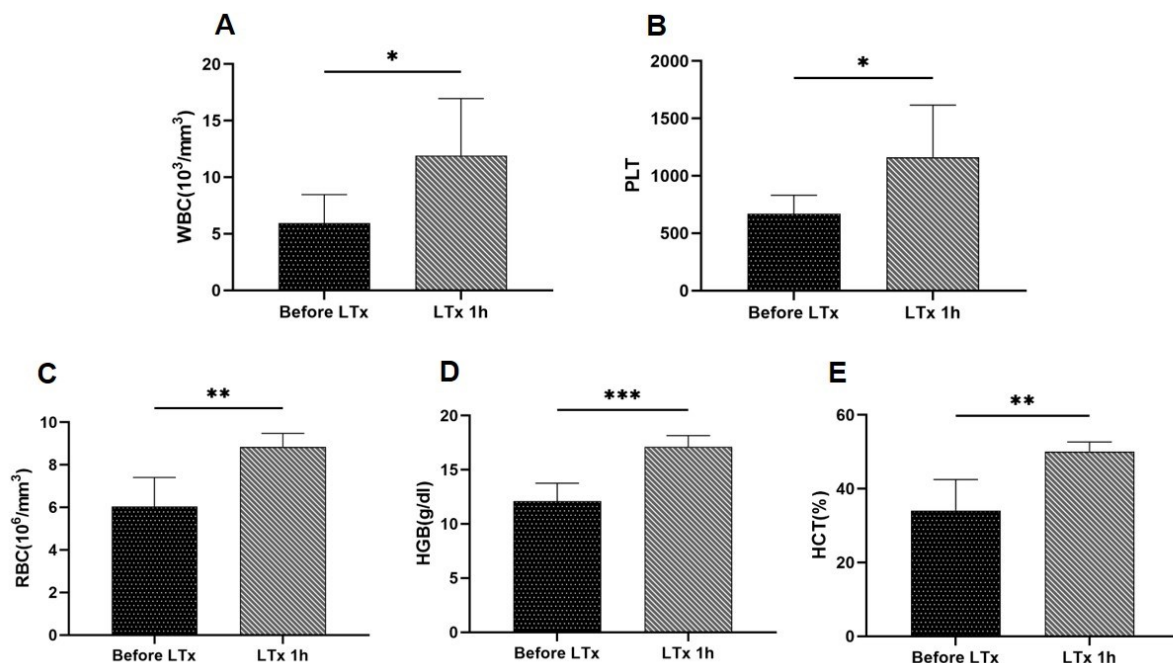


**Figure 41. The blood count after early LTx.** Increasing of WBC and PLT early after LTx. The levels of WBC (A), PLT (B), RBC (C), HGB (D), and HCT (D) before LTx and after LTx 1h. Data expressed as mean  $\pm$  SD, one-way ANOVA followed by Tu'y's post-hoc test. \* $P < 0.05$ , \*\* $P < 0.01$ , \*\*\* $P < 0.001$ , and ns = not significant.

### 5.2.2.3 Impact of IRI on liver morphology

Moreover, we assessed hepatic morphological changes over the course of early reperfusion. As expected, within the first hour of reperfusion we could only detect minor changes. As shown in **Figure 42**, the predominant finding was vacuolization of hepatocytes and was predominantly located in the pericentral area resulting in a Suzuki score of  $0.61 \pm 0.69$ . With time, the pattern of morphological damage changed. As a key finding, we observed some pericentral confluent necrosis (mild necrosis) affecting between 5% and 20% of the parenchymal tissue within a section, resulting in a Suzuki Score of about  $2.8 \pm 0.8$ .

As described before, HMGB1 acts as an alarmin, an alarm protein signal that initiates the inflammatory response resulting from liver IRI and is considered a marker of ischemic damage. Therefore, the translocation of HMGB1 was used as additional parameter to evaluate the severity of hepatic IRI (**Figure 42**). In contrast to the results obtained in NMP, we did not observe substantial differences in HMGB1 translocation when comparing periportal and pericentral regions. However, translocation was more pronounced 24h after transplantation compared to 1h after LTx.

In addition, we used CYP1A2 expression as an indirect parameter of hepatic metabolic function. As shown in **Figure 42**, CYP1A2 enzymes were expressed in the pericentral region, as expected. We observed a strong signal in the first 2–3 layers of hepatocytes surrounding the central vein and signals of moderate intensity in the remaining pericentral area of the lobule, representing about 30% of the total surface of the section. Extent of expression remained similar in the early phase after transplantation compared to normal but was reduced to about 20% within the first 24h after transplantation. This finding may suggest a transient reduced drug-metabolizing function.

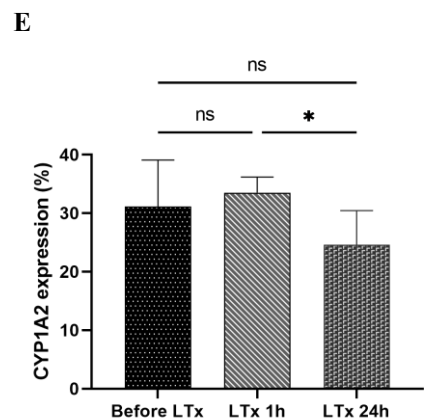
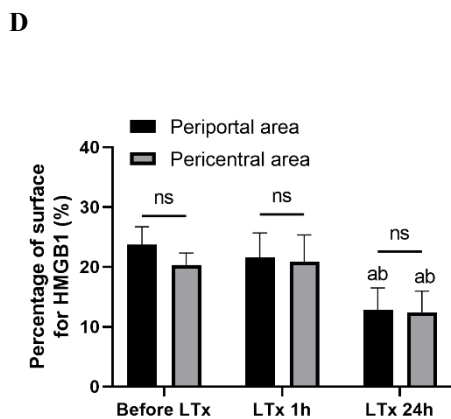
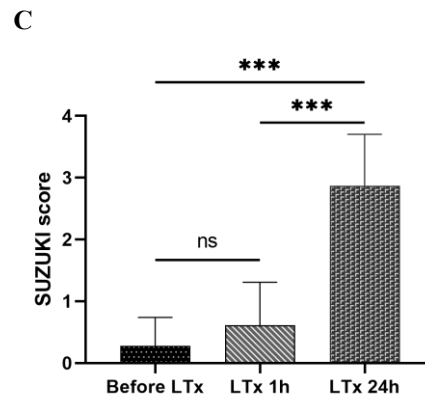
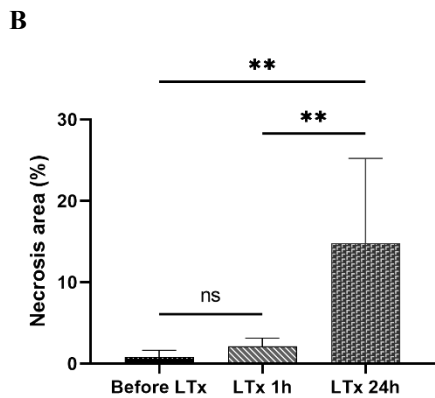
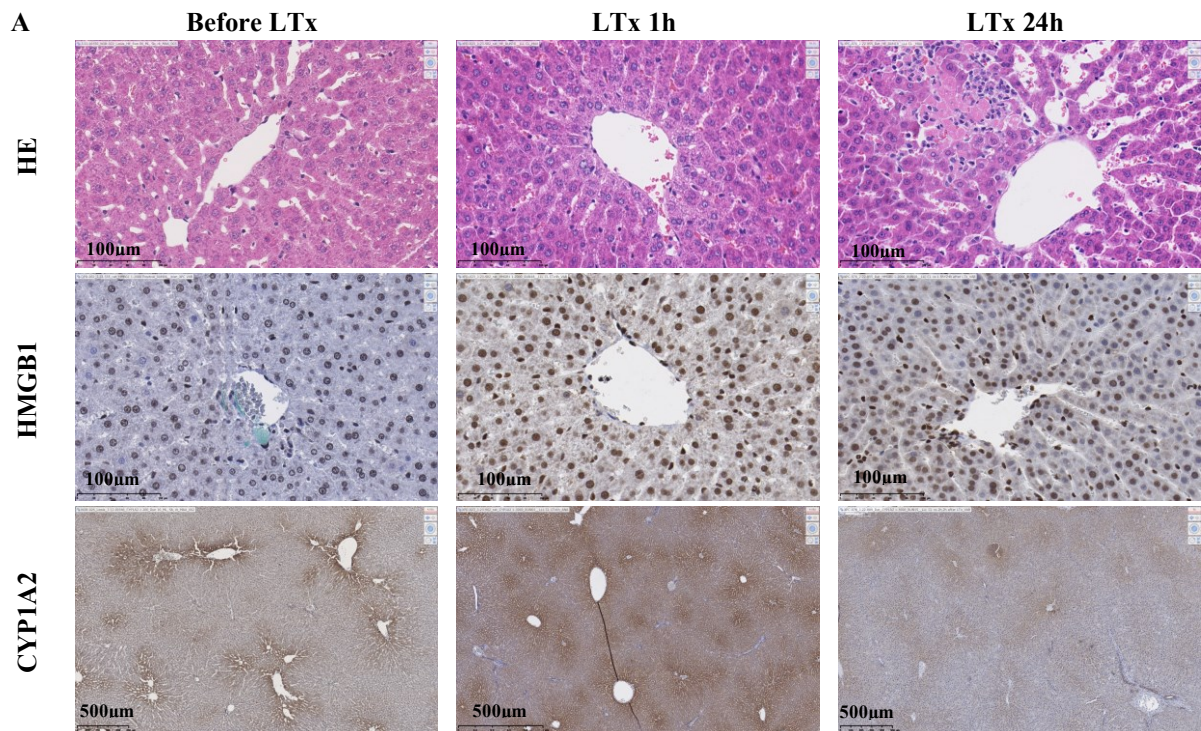


**Figure 42. Morphological damage, HMGB1 translocation, and CYP1A2 expression early after LTx.** (A) HE, HMGB1, and CYP1A2 staining. (B) Quantification of necrosis in percent of the surface early after LTx. (C) Quantification of morphological damage using Suzuki score. (D) Quantification of HMGB1 translocation after early LTx. (E) Quantification of CYP1A2 expression early after LTx. Data expressed as mean  $\pm$  SD, one-way ANOVA followed by Tukey's post-hoc test. \* $P < 0.05$ , \*\* $P < 0.01$ , \*\*\* $P < 0.001$ , and ns = not significant. a: compared to before LTx, there is a significant difference. b: compared to LTx 1h, there is a significant difference.

### 5.2.3 Correlation of hepatic microcirculation with alterations of liver function, liver damage, and blood count after reperfusion.

To investigate the potential correlation between liver microcirculation and liver damage, liver function, and alteration of blood components after reperfusion, we determined the Pearson product-moment correlation coefficient.

As shown in **Figure 43**, the levels of ALT and the proportion of perfused capillaries showed a significant inverse correlation ( $r=-0.76$ ,  $P < 0.01$ ), AST ( $r=-0.66$ ,  $P < 0.05$ ), and LDH ( $r=-0.79$ ,  $P < 0.01$ ). In other words, the higher the proportion of perfused capillaries, the lower enzyme release was observed.

A similar inverse correlation was found between the proportion of perfused capillaries and the number of WBC and platelets. The higher the PLT and WBC, the lower the proportion of perfused capillaries ( $r=-0.54$ ,  $P < 0.05$ ;  $r=-0.57$ ,  $P < 0.05$ ).

These preliminary results revealed significant correlations between hepatic hemodynamics, perfusion and microcirculation and liver damage in early IRI. Further investigations are needed to better understand the impact of hepatic perfusion impairment on the severity of IRI in terms of liver enzymes.

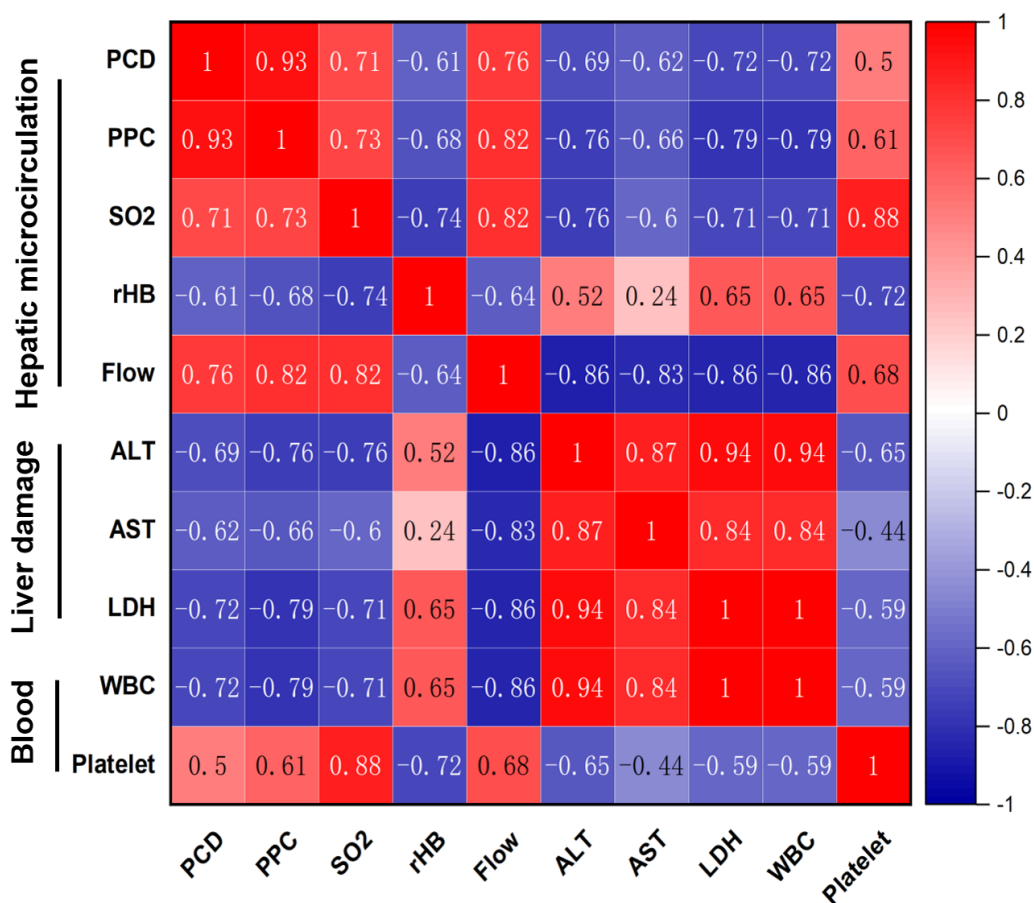


Figure 43. The correlation between liver microcirculation and liver damage and blood count.

## 6 DISCUSSION

In this thesis, we focussed on two complementary issues in IRI: the machine perfusion to reduce IRI of marginal livers and the assessment of hepatic microcirculation early after LTX correlates with the severity of hepatic IRI.

In the following chapters, we want to discuss the central aspects of our findings.

### 6.1 Part I: NMP study

We successfully established a stable NMP model using a clinically relevant model of cardiac death. We confirmed that slight hyperperfusion is needed to compensate for the limited oxygen content when using an oxygenated, but oxygen-carrier-free medium as perfusate. We also determined the benefits of female donor gender and short WIT on organ preservation in contrast to the detrimental effect of high donor age. We confirmed that old age is associated with an impairment of autophagy, which is partially restored during NMP.

#### 6.1.1 Advantage of CO<sub>2</sub> inhalation to induce cardiac death in liver graft donors

There are two principal types of DCD: controlled and uncontrolled (**Table 9**) (Lazzeri et al., 2020). Uncontrolled DCD refers to organ retrieval after a cardiac arrest that is unexpected and from which the patient cannot or should not be resuscitated (Maastricht I and II). In contrast, controlled DCD follows the planned withdrawal of life-sustaining treatments that have been considered to be of no overall benefit to a critically ill patient in the ICU or in the Emergency Department (Maastricht III and IV) (Limkemann et al., 2016). Unlike most of other strategies to induce cardiac death prior to organ procurement, we induced the DCD via CO<sub>2</sub> inhalation. 90% of previously published (**Table 10**) studies performed phrenotomy, sternotomy, external compression of the heart, or injection of potassium chloride. Here, most of the authors heparinized the living donor prior to inducing cardiac deaths, thereby facilitating complete flushing.

**Table 9. The category of DCD and the Maastricht classification.**

Category	Type	Circumstances	Typical location
Maastricht I	Uncontrolled	Dead on arrival	Emergency Department
Maastricht II	Uncontrolled	Unsuccessful resuscitation	Emergency Department
Maastricht III	Controlled	Cardiac arrest follows planned withdrawal of life-sustaining treatments	Intensive Care Unit
Maastricht IV	Either	Cardiac arrest in a patient who is brain-dead	Intensive Care Unit

In our model of DCD, after assurance of complete cessation of both cardiac heart and respiratory movements as tested by palpation, the rat was subjected to warm ischemia in situ for around 30 minutes, equal to the time needed for explanting the organ. After flushing and



explanting the liver, the graft was connected to the NMP system. In other published studies (see **Table 10**), over 50% preferred systemic heparinization before induction of DCD to prevent heterogeneous flushing and perfusion caused by micro-thrombosis. However, it is difficult to perform systemic heparinization in uncontrolled DCD in a clinical setting. In comparison, our induction of DCD models is more strict and closer to the clinical reality of uncontrolled DCD without systemic heparinization before inducing DCD.

**Table 10. The literature work-up of ways to induce DCD for liver machine perfusion model**

Way to induce DCD	WIT	Systemic heparinization	Reference
CO2 inhalation	30min	Yes	(Bae et al., 2014)
External compression of the heart (exogenous tamponade) until contractions ceased	30min	No	(Westerkamp et al., 2015)
Incision of the infrarenal aorta	30min	Yes	(Bruggenwirth et al., 2018; Niu et al., 2014; Op den Dries et al., 2016)
Injection of potassium chloride	20min	No	(von Horn et al., 2017)
	45min	Yes	(von Horn & Minor, 2020; von Horn et al., 2022)
		No	(Carnevale et al., 2013)
		No	(Abraham et al., 2022; Bessems, Doorschodt, van Marle, et al., 2005; Cheng et al., 2021; He et al., 2018; Luer et al., 2010; Minor et al., 2011; Minor et al., 2006; Saad & Minor, 2008; Schlegel et al., 2013; Schlegel et al., 2014; Schlegel et al., 2020; Stegemann et al., 2009; L. Yang et al., 2020; Zhou et al., 2022)
Induction of hypoxia via phrenotomy and sternotomy	30min	No	(Bessems et al., 2006; Bessems, Doorschodt, van Vliet, et al., 2005; Cao et al., 2021; Cao et al., 2020; Ferrigno et al., 2017; Ferrigno et al., 2011; Gassner et al., 2019; Lee et al., 2003; Liu et al., 2021; Sun et al., 2021; Wu et al., 1997; Xue et al., 2018; Zeng et al., 2017; Zeng, Li, et al., 2019; Zeng, Wang, et al., 2019)
	45min	Yes	(Dutkowski et al., 2006)
		No	(Tolboom et al., 2012)
	60min	No	(Lauschke et al., 2003; Oldani et al., 2019; Olschewski et al., 2010)

---

Yes	(De Stefano et al., 2021; Jain et al., 2008; Tolboom et al., 2008; Uygun et al., 2010)
-----	--

---

### **6.1.2 Balancing oxygen supply and waste removal resulting in optimal perfusion condition**

Regarding the optimal balance of supply and waste removal in NMP, we raised two hypotheses. We postulated that slight hyperperfusion is needed to compensate for the limited oxygen supply when using oxygenated medium without oxygen carriers as perfusate. We also postulated that partial medium change improves graft integrity and function due to waste removal.

#### **6.1.2.1 Increased oxygen supply by slight hyperperfusion beneficial for organ preservation in oxygen-carriers-free NMP**

We established an ex-vivo rat liver NMP system using an oxygenated complete hepatocyte culture medium with 20% FCS. However, at this stage, we did not use artificial oxygen carriers or erythrocytes for the sake of system simplicity. We evaluated the flow rate as one important factor potentially affecting organ preservation.

In contrast to previous studies, which chose 1 or 2ml/min/g liver weight as the perfusion flow rate due to closer to the physiological PV flow rate (see **Table 11**) (Liu et al., 2021; Schlegel et al., 2014; Uygun et al., 2010), we used 3ml/min/gr liver. We observed that the higher flow rate (3ml/min/g liver weight) caused less damage and preserved morphology and function substantially better than the lower flow rate. Hyperperfusion of the liver was associated with substantially higher enzyme release, higher damage score, and less bile production.

The studies favouring lower flow rates used perfusate supplemented with artificial oxygen carriers or rat blood (Schlegel et al., 2014), respectively, discarded human erythrocytes (Uygun et al., 2010). All these additives might increase the viscosity of the perfusate, which may affect the resistance of the system. Higher resistance in return may increase the risk of damaging the hepatic sinusoidal structure. In addition, the utilization of outdated human RBCs resulted in hemolysis and microvascular obstructions (Okamura et al., 2017). Therefore, we suspect that the medium viscosity and the hemolysis are the main reasons for this difference in perfusion flow rate selection. In our NMP system, we did not add oxygen carriers. However, oxygen has limited solubility in the perfusate without additives, which means hepatocytes take up constant amounts of oxygen. In comparison, a higher flow rate speeds up the perfusion cycle, and more newly dissolved oxygen in the perfusate is taken up by the hepatocytes, achieving a better outcome in our hyperperfusion NMP model.

**Table 11. Physiological portal vein flow in rats**

Reference	Strain of rat	Body weight	Physiological portal vein flow
(Daemen et al., 1989)	Wistar	350-450g	1.53 ± 0.19 ml/min/g liver
(Kassissia et al., 1994)	SD	300-400g	1.25+0.04 ml/min/g liver
(Nakajima et al., 1990)	Fischer	250-350g	1.32+0.06 ml/min/g liver
(Um et al., 1994)	SD	319 ± 5g	1.5 ml/min/g liver
(Katsuta et al., 2005)	SD	341 ± 15g	7.18+0.65 ml/min/100g BW
(H. Li et al., 2017)	Wistar	300-350g	2.52+0.23 ml/min/100g BW
(Figueira et al., 2014)	Wistar	185-300g	11.6+2.2 ml/min

### 6.1.2.2 Waste removal by perfusate replacement beneficial for organ preservation in oxygen-carriers-free NMP

Furthermore, we observed that the enzyme levels in the perfusate, as well as the potassium levels, increased in parallel with the duration of NMP, especially after the 3rd hour. Those accumulated metabolites, such as lactate and potassium, can lead to persistent metabolic acidosis, exacerbating liver injury (Vitin et al., 2017). Therefore, waste removal during NMP is one option to improve organ preservation. For this purpose, we evaluated the effect of replacing half of the medium either once or twice during the perfusion process and observed that in our hands, replacing half of the medium once was sufficient. Other studies evaluated the use of dialysis. Dialysis has been shown to be necessary in previous studies to maintain physiological perfusion conditions (Gassner et al., 2019; Nosser et al., 2020). NMP without dialysis resulted in non-physiological potassium levels and rising ALT levels compared to NMP with dialysis, consistent with our findings. A reason for the necessity to use dialysis in an experimental ex-vivo liver machine perfusion could be an adverse liver-weight to perfusate-volume ratio in comparison to large animal and human liver perfusion systems, which results in a higher extracellular potassium due to the lower potassium uptake by the hepatocytes in ex vivo rat liver perfusion (Nosser et al., 2020).

### 6.1.3 Impact of donor properties on outcome of NMP

Regarding the impact of donor properties on NMP, we postulated that livers from female donors and livers from male donors subjected to shorter WIT had a better outcome after NMP. We also hypothesized livers from aged donors had an inferior outcome due to structural impairment.

#### 6.1.3.1 Female gender beneficial for organ preservation

In addition to the duration of warm ischemia, we found that donor properties impact the outcome of NMP. Several studies suggest that female livers exhibit greater tolerance to stress

conditions compared to male livers (de Vries et al., 2013; Han et al., 2022). Li et al. revealed that estrogen protecting the liver from hepatic I/R injury depends on G protein-coupled estrogen receptor (GPER) and the influence of GPER activation on hepatocyte necroptosis via clamping the portal vein and hepatic artery to construct an IRI model (Li et al., 2022). It was repeatedly reported for experimental and clinical liver transplantation that recipients of livers from female donors exhibited more favorable graft survival than those receiving a liver graft from male donors (Lai et al., 2018). Similarly, our findings revealed that female DCD livers produced more bile, released less enzymes, and showed less morphological damage during NMP compared to the male livers. Hormonal factors have been postulated to lead to a reduction in susceptibility to ischemia-reperfusion injury in women. The proposed mechanisms for the protective effect of estrogens on liver I/R injury include inhibition of apoptosis, an increased serum level of nitric oxide, a decreased serum level of tumor necrosis factor  $\alpha$ , regulation of heat shock protein expression, and selective modulation of MAPK kinase activities (Guo et al., 2015).

#### **6.1.3.2 Shorter WIT beneficial for organ preservation**

Previous studies have already extensively investigated the adverse effects of prolonged WIT (Ali et al., 2015; Schlegel et al., 2014). Schlegel et.al (Schlegel et al., 2014) revealed that DCD livers subjected to 60 minutes in situ WIT followed by 4 hours NMP exhibited more severe damage compared to those with 30 min WIT, though bile production did not differ. However, no studies have explored the potential beneficial effects of short WIT (less than 30min) during NMP. Therefore, we examined whether shorter WIT (mean time: 20 min) could improve outcomes in DCD-NMP. Our findings indicated that even a reduction of WIT by as little as 10 minutes significantly improved organ preservation. Prolonged WIT leads to the accumulation of acidic metabolites, possibly due to reduced ATP supply, primarily impairing cellular functions such as homeostasis, signalling interactions, and sodium/potassium ATPase (Na<sup>+</sup>/K<sup>+</sup>-ATPase) activity, resulting in mitochondrial damage, microcirculation failure, and cellular destruction (Kalogeris et al., 2012).

It is interesting to note that bile production of the sWIT liver significantly increased at the beginning of 3 hours, but there was no difference after the 3rd hour. This suggests that shorter WIT may affect bile production to a greater extent in the first three hours.

#### **6.1.3.3 Old age detrimental for organ preservation**

Age is another risk factor influencing IRI tolerance. Aging causes liver structural changes, such as a reduction in liver volume and an increase in hepatocyte volume (Schmucker, 2005). Aging livers typically undergo a 20% to 40% reduction in volume and exhibit a hardened

texture indicative of fibrosis (Kim et al., 2015). In our study, we observed the increase in stiffness possibly reflecting the fibrotic changes.

Additionally, hepatic arteriolar walls thicken, endothelial cell fenestration decreases, and liver blood flow declines, accompanied by reduced bile acid secretion (Nasiri-Ansari et al., 2022). These findings explain the detrimental impact of older donor age on early mortality post-transplant, as reported by Dayoub et al. (Dayoub et al., 2018). A seminal study from the United States indicated that the 95% confidence interval for adjusted 1-year post-transplant survival estimates dropped from 85–86% to 61–76% for donors younger than 40 years of age vs. donors over 70 years of age, respectively (Durand et al., 2019).

Our findings showed that livers from senescent donors produced less bile and experienced more severe liver damage during NMP. Furthermore, we observed higher wedged hepatic vein pressure during NMP. This finding can be attributed to the described structural age-dependent changes in hepatic sinusoids, such as thickened endothelial layers and reduced fenestration. These changes may contribute to elevated hepatic sinusoidal pressure indirectly observed through measurements of wedged hepatic vein pressure.

Our study revealed in addition, that hepatic sinusoidal pressure increased with NMP duration in older livers, likely due to an increase in resistance over time. This increase in resistance might be explained by hyperperfusion related endothelial injury and subsequent edema. (Li et al., 2023).

#### **6.1.4 Impact of age on autophagy in native and machine perfusion livers**

Autophagy is an essential recycling mechanism of cellular components, which plays a crucial role in maintaining liver metabolism (Mizushima, 2007). Several studies indicated that autophagy is substantially lower in the aged liver compared to the young liver (Kim et al., 2022; Mao et al., 2023; Xu et al., 2020). To confirm this, the autophagy markers, including LC3b-II and p62, were detected via western blot in normal young and old livers obtained from the liver explant in our present study. We observed that the expression of p62 decreased with the increase of LC3b-II in aged livers, indicating autophagy was impaired in the aged livers, which was consistent with previous studies.

In addition, autophagy plays an important role in hepatic IRI. However, few studies explore the impact of autophagy on liver IRI in machine perfusion (Luo et al., 2023; Ohman et al., 2022; Zeng, Wang, et al., 2019). Therefore, we explored the expression of autophagy in the liver subjected to NMP. We observed that the expression of LC3b-II increased and P62 decreased in parallel with the perfusion time, suggesting an enhancement of autophagy in NMP. Moreover, based on the publications, most of them indicated the reduction of autophagic flux in the aged

liver. Similarly, we observed that the autophagy in the aged liver subjected to NMP was impaired, with more severe liver damage and lower preservation of hepatic function as indicated by lower bile production. Furthermore, in liver subjected to NMP, the expression of autophagy increased over time, interestingly both in livers from young but also from old donors. A growing number of studies suggested that autophagy protects hepatocytes from death during and after hepatic IRI (Gotoh et al., 2009; Mao et al., 2023). A study in 26-month-old mice demonstrated that the loss of atg4b in aged livers led to a reduction of LC3 activity, which resulted in a reduced autophagic flux and a more severe IRI. Compared to those from young mice, hepatocytes from old mice presented a highly reduced autophagy response after IRI simulation (Wang et al., 2011). Therefore, we assumed that the reduced autophagic flux in the aged liver leads to an aggravated hepatic I/R injury. According to these findings, modulation of autophagy might be another promising strategy to reduce IRI in NMP.

## **6.2 Part II: LTx study**

We successfully established a stable LTx model which was further improved by optimising flushing conditions to achieve homogenous reperfusion reproducibly. In a preliminary liver transplant experiment, we explored the correlation between parameters of hepatic hemodynamics, perfusion, and microcirculation on the one hand and damage parameters on the other hand.

### **6.2.1 Impact of pressure-controlled and volume-controlled flushing on the reperfusion in LTx model**

We established a relatively stable rat LTx model by following the recommendation of Jin Hao (Jin et al., 2012) consisting of “dry exercise”, cadaver training, and living animal training. We found that by practicing in this sequence, only 10 LTx procedures using living animals were needed to achieve the anhepatic phase below 25min. However, we encountered severe heterogeneous reperfusion when performing volume-controlled flushing of the liver with 100ml saline in about 4-5min. Under this flushing condition, reperfusion was heterogeneous in about half of the cases. We speculate that this result may be due to a pressure induced injury of the hepatic sinusoidal structure as a result of the non-physiological flow rate during flushing (physiological portal pressure: 5mmHg-10mmHg). Therefore, we improved the flushing condition with pressure-controlled flushing with 0.2ml Ringer lactate per body weight using a 20cm water column. When flushing the liver under physiological pressure conditions, reperfusion became completely homogenous within 15 minutes and remained homogenous throughout the first hour as assessed visually.

### **6.2.2 Asynchronous alteration of liver enzyme release and morphological damage in transplantation**

Liver enzyme activity levels represent a well-established parameter for estimating hepatic injury following organ procurement, preservation, and transplantation (Panconesi et al., 2021). Nonetheless, liver enzyme levels alone are not predictive of initial non- or poor graft function (Bolondi et al., 2016). A drastic increase in serum activities of “liver enzyme markers” does not necessarily have to reflect liver cell death (Contreras-Zentella & Hernández-Muñoz, 2016).

We observed that hepatic damage in terms of enzyme release occurred in the early posttransplantation phase. As expected, the morphological changes became visible at a later point in time, where enzyme release already partially recovered. Here, vacuolization in the pericentral area was the most prominent feature which developed in the within the first hour of reperfusion. In contrast confluent necrosis in the pericentral region was the most obvious change which occurred within 24-hour after transplantation mainly, reaching almost 15%.

### **6.2.3 Impairment of liver microcirculation after reperfusion in LTX**

We assessed hepatic hemodynamics, perfusion and microcirculation 1h postreperfusion. Despite intensive research in the field of IRI and microcirculation, there is only little information available regarding the early phase after rat liver transplantation. As reported in 1996 by Walcher (Walcher et al., 1996), the anhepatic phase in rat liver transplantation causes a severe cardiovascular depression due to clamping of the inferior cava. Despite intensive volume resuscitation the mean arterial pressure at 1h postreperfusion did not recover but remained between 60 – 80mmHg, which is at the edge of being critical for a rat.

In our experiment we did not perform any volume resuscitation, which gives rise to the assumption, that the mean arterial pressure during the anhepatic phase was even lower. Nevertheless, we observed that portal pressure and flow was only reduced by 30% - 40% compared to normal values. We measured a mean PVP of almost 13mmHg compared 17-18mmHg and a portal flow of 7-8ml/min compared to 18ml/min, which we considered to be indicative of partial recovery from systemic cardiovascular depression.

Similarly, we observed a severe reduction of perfusion parameters such as capillary-venous oxygen saturation and microvessel perfusion flow, which we also considered to be indicative of the recovery process after revascularization. Furthermore, we visualized and quantified postischemic microvascular architecture and perfusion. As expected, all static parameter remained similar compared to normal. In contrast, the dynamic parameters such as the perfused capillary density and proportion of perfused capillary density did not yet recover to normal.

We were interested to elucidate the relationship between impairment of hepatic perfusion in the early reperfusion phase and the corresponding damage in terms of enzyme release. We also wanted to know which parameter is best suited for real-time intra-operative assessment.

A previous study indicated that an important fraction of the released hepatic enzymes depends largely on hemodynamic changes in the rat liver (Puhl et al., 2005). We observed that all parameters used to describe and quantify hepatic perfusion were correlated with enzyme liver microcirculation which is correlated with the release of liver enzymes. Similar results were obtained by several groups in the past (Sindram et al., 2000; Vollmar & Menger, 2009), but require a rather time-consuming analysis of the raw data. Our devices allow acquisition of data in real-time, even within the operation room. Based on the ease of measurement, we currently favor the O2C-device, since this method only require the placing of sensor on the surface of the liver.

### **6.3 Part III: Comparison of morphological changes in different models of hepatic IRI**

Zonated morphological damage was observed in both of the models possibly associated to intralobular gradient of oxygen distribution, corresponding to the HMGB1 translocation and CYP1A2 expression.

#### **6.3.1 Zonated morphological damage pronounced in NMP but not in LTx**

We observed, for the first time in a NMP model, that the extent and type of hepatocyte injury differed significantly between the periportal and pericentral areas. In other words, we observed zonated morphological damage in our rat model of NMP. Furthermore, we realized that the extent and severity of the damage seemed to be flow rate dependent.

In the periportal area, we observed almost no damage when using a flow rate of 1ml/min/gr liver. Using this flow rate, we could not clearly discriminate the periportal areas from the midzonal area. However, when hyperperfusing the liver using a flow rate of 3ml/min/gr, we observed pressure related damage (vacuolization) in the periportal region.

In the pericentral region, we observed severe ischemic damage as indicated by nuclear pyknosis and vacuolization. The extent of ischemic damage seemed to be flow rate and perfusion time dependent.

Pericentral ischemic damage of the hepatocytes increased in all groups along with the perfusion time. However, the size of the damaged pericentral region became smaller when increasing the flow rate and even smaller when removing waste products by replacing half of the medium. Here, we speculate that increasing the flow rate above the physiological range probably increased the oxygen supply along the sinusoids, with more oxygen remaining for hepatocytes located closer to the central vein, **see Figure 44**. Therefore, we believe that in our



model of oxygenated NMP, but without oxygen carriers, hyperperfusion reduced ischemic injury of pericentral hepatocyte and preserved function, but caused some pressure related damage in the periportal area. Here, we assume that adding oxygen carriers to the medium would call for reducing the flow rate to achieve best prevention from pressure related damage in the periportal region and ischemic damage in the pericentral region.

To the best of our knowledge, none of the previous studies reported this zoned morphological impairment after NMP, possibly due to the short perfusion duration or the use of oxygen carrier enriched perfusate. Our finding can be well explained with the concept of metabolic zonation. A recent work by Xin and colleagues showed in a 70 % portal vein ligation model in rats that the pericentral area is more sensitive to IRI compared with the periportal area (Xin et al., 2023). The discrepancy in zonation might be related to the liver microanatomy and the intralobular gradient of **oxygen distribution** (Kietzmann, 2017; Manco & Itzkovitz, 2021; Soto-Gutierrez et al., 2017), see **Figure 44** Under physiological conditions, the oxygen decreases from about 60–65 mm Hg (84–91  $\mu\text{mol/L}$ ) in the periportal blood to about 30–35 mm Hg (42–49  $\mu\text{mol/L}$ ) in the perivenous blood (Kietzmann et al., 2006). This intralobular gradient distribution of oxygen leads to the spatial distribution of metabolic function throughout the liver lobule, a phenomenon called **metabolic zonation** (Kietzmann, 2017; Manco & Itzkovitz, 2021; Soto-Gutierrez et al., 2017).

The liver lobule is divided into three functional zones specialized in carrying out specific metabolic functions, including metabolism, detoxification, and bile generation (Kietzmann et al., 2006). The periportal zone, also known as Zone 1, is closest to the arterioles and bile duct. It is primarily responsible for oxygen-requiring metabolic processes, such as gluconeogenesis, cholesterol biosynthesis, ureagenesis, and fatty acid  $\beta$ oxidation. The midzone, also known as Zone 2, performs various functions, including maintaining iron homeostasis and regulating insulin-like growth. The pericentral zone, or Zone 3, surrounds the central vein and is primarily responsible for low-oxygen-requiring processes, such as glycolysis, bile-acid biosynthesis, glutamine synthesis, lipogenesis, and xenobiotic metabolism (Jungermann & Kietzmann, 1996; Soto-Gutierrez et al., 2017).

Zonated morphological damage was also observed in livers after transplantation, but much less pronounced. In our transplantation model, we observed mild vacuolization of pericentral hepatocytes 1 hour after reperfusion, as well as confluent necrosis and dilatation of hepatic sinusoids 24 hours after reperfusion in the pericentral region. This difference between NMP and Ltx can be well related to the different levels of oxygen and nutrient supply in the two

models. NMP was performed with oxygenated protein enriched cell culture medium without oxygen carriers, whereas transplanted livers were obviously reperfused with whole blood.

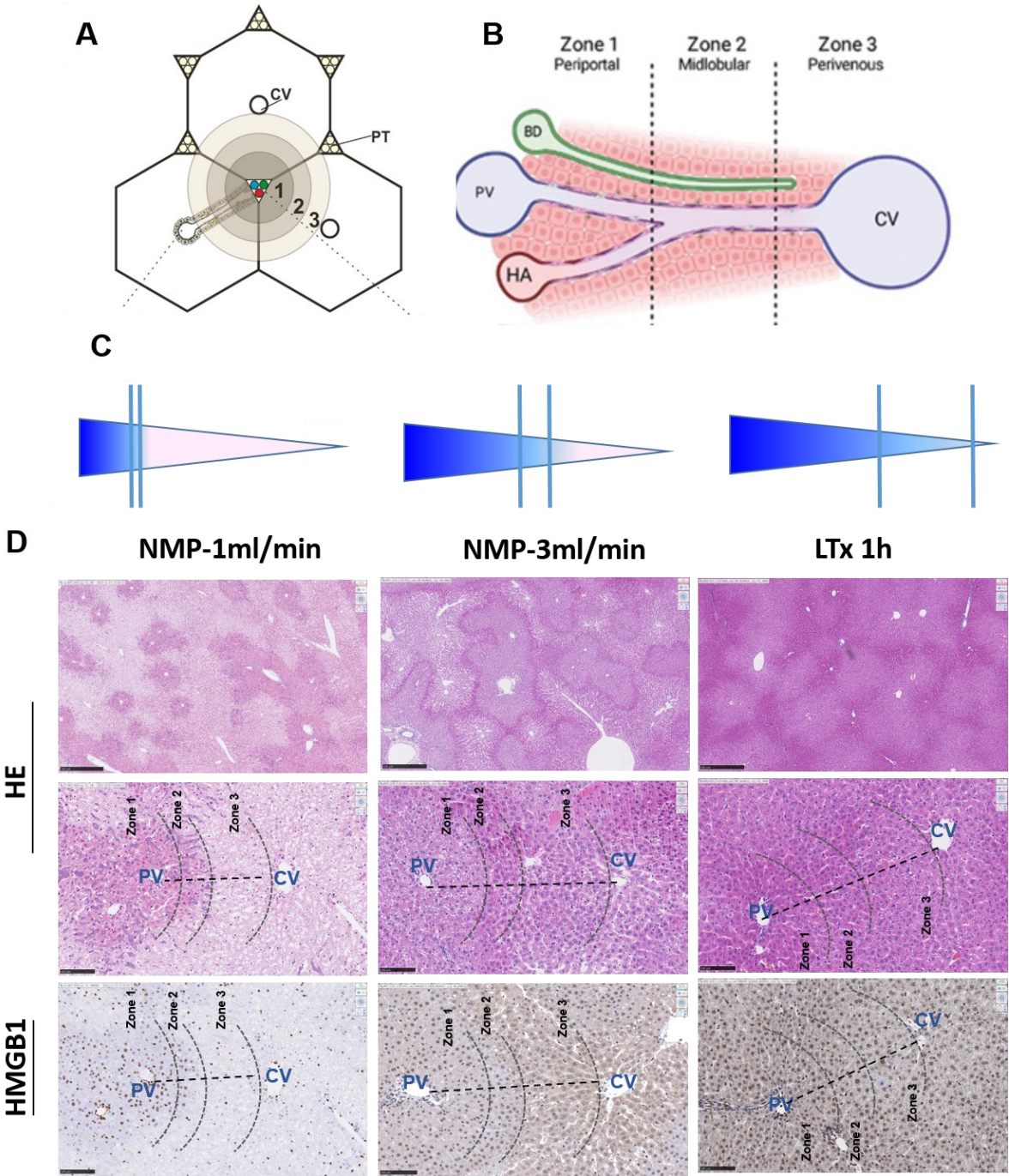


**Figure 44. Liver microarchitecture, oxygen gradient, and HE and HMGB1 staining different flow rate NMP, and transplantation livers.** (A) Classic hexagonal shaped liver lobule with a central vein (CV) in the middle and portal triad (PT) corners with the branch from the portal vein also called terminal portal vein (TPV, blue dot), and a branch from the hepatic artery also called terminal hepatic arteriole (THA, red dot) as well as a bile duct (BD, green dot). (B) Three zones can be distinguished. 1, the periportal zone; 2, the midlobular zone or midzone; 3, the perivenous, pericentral, or centrilobular zone. (C) Oxygen gradient in different experimental conditions. (D) The HE results of livers subjected to different flow rate of NMP and LTx 1h. This figure A and B copied from Panday and Kietzmann (Kietzmann, 2017; Panday et al., 2022) with friendly permission.

### **6.3.2 Pericentral translocation of HMGB1 and reduced expression of CYP1A2 pronounced in NMP but not in LTx**

HMGB1 is an alarm protein that initiates inflammation in response to hepatic IRI. (Ni et al., 2021). Upon ischemic injury, HMGB1 translocates from the nucleus to the cytoplasm and further to the extracellular space. In a previous study, our group showed in a warm ischemia model, that HMGB1 translocation was visible as early as after 0.5h, and HMGB1 translocation and expression were increased in a time-dependent manner and peaked at 24 h (Liu et al., 2011).

In the NMP model, we observed that the HMGB1 translocation was more pronounced in the pericentral area compared to the periportal area. This finding is indicative of ischemic damage in the pericentral region, as suspected by the morphological assessment. In contrast, the nuclear HMGB1-signal persisted throughout the 6h of NMP in the periportal region (**Figure 44**). This finding suggests that eventual damage in this region, as observed in the hyperperfused livers, cannot be attributed to ischemia and supports the interpretation of pressure related damage.

Pericentral HMGB1 translocation was also significantly increased after transplantation. Similarly, as in NMP and our previous study, translocation was not so pronounced in the early phase (1 h) after reperfusion but then increased within the subsequent 24h. Compared to the NMP study, zonated translocation but also extent of ischemic was less prominent after transplantation. We speculate that this difference in the zonated translocation may be primarily related to the quality of oxygen supply, possibly related to the presence or absence of erythrocytes.

Assessment of liver function can be done by investigating drug metabolizing enzymes belonging to the family of cytochrome P450 (CYP) enzymes. These enzymes play a vital role in clearing various compounds, including steroids, fatty acids, and xenobiotics (Almazroo et al., 2017). Therefore, we attempted to visualize and quantify the expression of CYP1A2 as an indirect indicator of metabolic function after reperfusion in both models, including NMP and LTx. A recent study demonstrated that determination of CYP1A2 activity via a modified LiMax assay showed a high correlation with damage parameters, especially histology. Therefore, the authors concluded that CYP activity can be used as a biomarker of liver function assessment during NMP (Schurink et al., 2021).

We observed that extent of pericentral CYP1A2-expression decreased during the course of NMP. This was most pronounced in aged livers, which are very sensitive to IRI due to the pre-existent age induced structural and functional impairment. In a next step we will assess CYP-activity to obtain a more comprehensive picture of the metabolic capacity of the liver subjected to machine perfusion.

## **6.4 Limitation**

Our study has several limitations. First, although our NMP model shows promise, previous research has shown that supplementation of the medium with oxygen carriers is beneficial, especially when prolonging the perfusion time further. As a result, our next plan is to add artificial oxygen carriers to the perfusate to assess and quantify the additional benefit. Second, we observed substantial effects of donor properties on the outcome of NMP, but did not yet conduct in-depth mechanistic studies. However, our first preliminary results show, that autophagy might play a key role deserving further attention. Third, our research focused only on changes in hepatic sinusoidal pressure in aged livers. However, we did not assess hepatic sinusoidal cell function or morphological changes post-NMP, which is a focus of our future research. Fourth, so far we only explored the relationship between autophagy and old age and did not explore the relationship between other donor properties and autophagy. Lastly, we did not yet monitor the real-time liver microcirculation by direct imaging via CytoCam because we were using an oxygen carrier-free medium for NMP. This is only possible when performing NMP using diluted blood as oxygen carriers as described by others.

There are two limitations in the LTx part. Firstly, we only focused on the liver microcirculation change after early liver transplantation, however, the long-term microcirculation change needs to be explored in a next step. Secondly, our donor grafts were only subjected to short cold ischemia times. However, the impact of longer cold ischemia on liver microcirculation still needs to be investigated.

## **7 CONCLUSION**

NMP using oxygenated Williams E medium without additional oxygen carriers can preserve rat liver morphology and function for at least 6h. Best preservation is achieved when balancing oxygen supply and waste removal. However, donor properties such as gender and age, as well as even a minimal extension of WIT, have a significant beneficial respectively detrimental effect on organ preservation. Further work is needed to understand the underlying pathophysiological mechanism between donor characteristics, NMP condition, and organ preservation.

Intraoperative assessment of liver hemodynamics, perfusion and microcirculation seems to reflect severity of early IRI. Further work is needed to identify the most relevant parameter to predict severity of IRI based on an “easy to determine” intra-operative measurement.

Taken together, addressing the complex topic of IRI from the side of NMP to prevent severe IRI and from a diagnostic point of view will contribute to better prevention of severe liver damage.

## 8 REFERENCE

- Abraham, N., Zhang, M., Cray, P., Gao, Q., Samy, K. P., Neill, R., Cywinska, G., Migaly, J., Kahan, R., Pontula, A., Halpern, S. E., Rush, C., Penaflo, J., Kesseli, S. J., Krischak, M., Song, M., Hartwig, M. G., Pollara, J. J., & Barbas, A. S. (2022). Two Compartment Evaluation of Liver Grafts During Acellular Room Temperature Machine Perfusion (acRTMP) in a Rat Liver Transplant Model. *Front Med (Lausanne)*, 9, 804834. <https://doi.org/10.3389/fmed.2022.804834>
- Almazroo, O. A., Miah, M. K., & Venkataramanan, R. (2017). Drug Metabolism in the Liver. *Clin Liver Dis*, 21(1), 1-20. <https://doi.org/10.1016/j.cld.2016.08.001>
- Aykut, G., Veenstra, G., Scorcella, C., Ince, C., & Boerma, C. (2015). Cytocam-IDF (incident dark field illumination) imaging for bedside monitoring of the microcirculation. *Intensive Care Med Exp*, 3(1), 40. <https://doi.org/10.1186/s40635-015-0040-7>
- Bae, C., Pichardo, E. M., Huang, H., Henry, S. D., & Guarrera, J. V. (2014). The benefits of hypothermic machine perfusion are enhanced with Vasosol and alpha-tocopherol in rodent donation after cardiac death livers. *Transplant Proc*, 46(5), 1560-1566. <https://doi.org/10.1016/j.transproceed.2013.12.050>
- Bai, Y., Shi, J. H., Liu, Q., Yang, D. J., Yan, Z. P., Zhang, J. K., Tang, H. W., Guo, W. Z., Jin, Y., & Zhang, S. J. (2023). Charged multivesicular body protein 2B ameliorates biliary injury in the liver from donation after cardiac death rats via autophagy with air-oxygenated normothermic machine perfusion. *Biochim Biophys Acta Mol Basis Dis*, 1869(5), 166686. <https://doi.org/10.1016/j.bbadis.2023.166686>
- Bessemers, M., Doorschodt, B. M., Albers, P. S., Meijer, A. J., & van Gulik, T. M. (2006). Wash-out of the non-heart-beating donor liver: a matter of flush solution and temperature? *Liver Int*, 26(7), 880-888. <https://doi.org/10.1111/j.1478-3231.2006.01295.x>
- Bessemers, M., Doorschodt, B. M., van Marle, J., Vreeling, H., Meijer, A. J., & van Gulik, T. M. (2005). Improved machine perfusion preservation of the non-heart-beating donor rat liver using Polysol: a new machine perfusion preservation solution. *Liver Transpl*, 11(11), 1379-1388. <https://doi.org/10.1002/lt.20502>
- Bessemers, M., Doorschodt, B. M., van Vliet, A. K., & van Gulik, T. M. (2005). Machine perfusion preservation of the non-heart-beating donor rat livers using polysol, a new preservation solution. *Transplant Proc*, 37(1), 326-328. <https://doi.org/10.1016/j.transproceed.2005.01.039>
- Blacker, T. S., & Duchon, M. R. (2016). Investigating mitochondrial redox state using NADH and NADPH autofluorescence. *Free Radic Biol Med*, 100, 53-65. <https://doi.org/10.1016/j.freeradbiomed.2016.08.010>
- Bodewes, S. B., van Leeuwen, O. B., Thorne, A. M., Lascaris, B., Ubbink, R., Lisman, T., Monbaliu, D., De Meijer, V. E., Nijsten, M. W. N., & Porte, R. J. (2020). Oxygen Transport during Ex Situ Machine Perfusion of Donor Livers Using Red Blood Cells or Artificial Oxygen Carriers. *Int J Mol Sci*, 22(1). <https://doi.org/10.3390/ijms22010235>
- Bolondi, G., Mocchegiani, F., Montalti, R., Nicolini, D., Vivarelli, M., & De Pietri, L. (2016). Predictive factors of short term outcome after liver transplantation: A review. *World J Gastroenterol*, 22(26), 5936-5949. <https://doi.org/10.3748/wjg.v22.i26.5936>
- Bruggenwirth, I. M. A., Moore, C., Mahboub, P., Thijssen, M. F., E, X., Leuvenink, H. G. D., Mandrekar, P., Wang, X., Kowalik, T. F., Porte, R. J., & Martins, P. N. (2018). A Comparative Study of Single and Dual Perfusion During End-ischemic Subnormothermic Liver Machine Preservation. *Transplant Direct*, 4(11), e400. <https://doi.org/10.1097/TXD.0000000000000840>
- Bruinsma, B. G., Berendsen, T. A., Izamis, M. L., Yarmush, M. L., & Uygun, K. (2013). Determination and extension of the limits to static cold storage using

- subnormothermic machine perfusion. *Int J Artif Organs*, 36(11), 775-780.  
<https://doi.org/10.5301/ijao.5000250>
- Cao, H., Wu, L., Tian, X., Zheng, W., Yuan, M., Li, X., Tian, X., Wang, Y., Song, H., & Shen, Z. (2021). HO-1/BMMSC perfusion using a normothermic machine perfusion system reduces the acute rejection of DCD liver transplantation by regulating NKT cell co-inhibitory receptors in rats. *Stem Cell Res Ther*, 12(1), 587.  
<https://doi.org/10.1186/s13287-021-02647-5>
- Cao, H., Yang, L., Hou, B., Sun, D., Lin, L., Song, H. L., & Shen, Z. Y. (2020). Heme oxygenase-1-modified bone marrow mesenchymal stem cells combined with normothermic machine perfusion to protect donation after circulatory death liver grafts. *Stem Cell Res Ther*, 11(1), 218. <https://doi.org/10.1186/s13287-020-01736-1>
- Carnevale, M. E., Balaban, C. L., Guibert, E. E., Bottai, H., & Rodriguez, J. V. (2013). Hypothermic machine perfusion versus cold storage in the rescuing of livers from non-heart-beating donor rats. *Artif Organs*, 37(11), 985-991.  
<https://doi.org/10.1111/aor.12235>
- Ceresa, C. D. L., Nasralla, D., Pollok, J. M., & Friend, P. J. (2022). Machine perfusion of the liver: applications in transplantation and beyond. *Nat Rev Gastroenterol Hepatol*, 19(3), 199-209. <https://doi.org/10.1038/s41575-021-00557-8>
- Chen, H., Dirsch, O., Albadry, M., Ana, P. H., & Dahmen, U. (2023). Normothermic Ex Vivo Liver Machine Perfusion in Mouse. *J Vis Exp*(199). <https://doi.org/10.3791/65363>
- Cheng, N., Shi, J. H., Jin, Y., Shi, Y. B., Liu, X. D., Zhang, H. P., Cao, S. L., Yang, H., Guo, W. Z., & Zhang, S. J. (2021). Pharmacological Activating Transcription Factor 6 Activation Is Beneficial for Liver Retrieval With ex vivo Normothermic Mechanical Perfusion From Cardiac Dead Donor Rats. *Front Surg*, 8, 665260.  
<https://doi.org/10.3389/fsurg.2021.665260>
- Chullo, G., Panisello-Rosello, A., Marquez, N., Colmenero, J., Brunet, M., Pera, M., Rosello-Catafau, J., Bataller, R., Garcia-Valdecasas, J. C., & Fundora, Y. (2024). Focusing on Ischemic Reperfusion Injury in the New Era of Dynamic Machine Perfusion in Liver Transplantation. *Int J Mol Sci*, 25(2). <https://doi.org/10.3390/ijms25021117>
- Contreras-Zentella, M. L., & Hernández-Muñoz, R. (2016). Is Liver Enzyme Release Really Associated with Cell Necrosis Induced by Oxidant Stress? *Oxid Med Cell Longev*, 2016, 3529149. <https://doi.org/10.1155/2016/3529149>
- Cursio, R., Colosetti, P., & Gugenheim, J. (2015). Autophagy and liver ischemia-reperfusion injury. *Biomed Res Int*, 2015, 417590. <https://doi.org/10.1155/2015/417590>
- Cursio, R., & Gugenheim, J. (2012). Ischemia-Reperfusion Injury and Ischemic-Type Biliary Lesions following Liver Transplantation. *J Transplant*, 2012, 164329.  
<https://doi.org/10.1155/2012/164329>
- Daemen, M. J., Thijssen, H. H., van Essen, H., Vervoort-Peters, H. T., Prinzen, F. W., Struyker Boudier, H. A., & Smits, J. F. (1989). Liver blood flow measurement in the rat. The electromagnetic versus the microsphere and the clearance methods. *J Pharmacol Methods*, 21(4), 287-297. [https://doi.org/10.1016/0160-5402\(89\)90066-1](https://doi.org/10.1016/0160-5402(89)90066-1)
- Dar, W. A., Sullivan, E., Bynon, J. S., Eltzschig, H., & Ju, C. (2019). Ischaemia reperfusion injury in liver transplantation: Cellular and molecular mechanisms. *Liver Int*, 39(5), 788-801. <https://doi.org/10.1111/liv.14091>
- De Stefano, N., Navarro-Tableros, V., Roggio, D., Calleri, A., Rigo, F., David, E., Gambella, A., Bassino, D., Amoroso, A., Patrono, D., Camussi, G., & Romagnoli, R. (2021). Human liver stem cell-derived extracellular vesicles reduce injury in a model of normothermic machine perfusion of rat livers previously exposed to a prolonged warm ischemia. *Transpl Int*, 34(9), 1607-1617. <https://doi.org/10.1111/tri.13980>
- de Vries, H. A., Ponds, F. A., Nieuwenhuijs, V. B., Morphet, A., Padbury, R. T., & Barritt, G. J. (2013). Evidence that estrogen receptors play a limited role in mediating

- enhanced recovery of bile flow in female rats in the acute phase of liver ischemia reperfusion injury. *Ann Hepatol*, 12(1), 130-137.
- Durand, F., Levitsky, J., Cauchy, F., Gilgenkrantz, H., Soubrane, O., & Francoz, C. (2019). Age and liver transplantation. *J Hepatol*, 70(4), 745-758. <https://doi.org/10.1016/j.jhep.2018.12.009>
- Dutkowski, P., Furrer, K., Tian, Y., Graf, R., & Clavien, P. A. (2006). Novel short-term hypothermic oxygenated perfusion (HOPE) system prevents injury in rat liver graft from non-heart beating donor. *Ann Surg*, 244(6), 968-976; discussion 976-967. <https://doi.org/10.1097/01.sla.0000247056.85590.6b>
- Fang, H., Liu, A., Dahmen, U., & Dirsch, O. (2013). Dual role of chloroquine in liver ischemia reperfusion injury: reduction of liver damage in early phase, but aggravation in late phase. *Cell Death Dis*, 4(6), e694. <https://doi.org/10.1038/cddis.2013.225>
- Ferrigno, A., Di Pasqua, L. G., Berardo, C., Siciliano, V., Rizzo, V., Mannucci, B., Richelmi, P., Croce, A. C., & Vairetti, M. (2017). Liver Graft Susceptibility during Static Cold Storage and Dynamic Machine Perfusion: DCD versus Fatty Livers. *Int J Mol Sci*, 19(1). <https://doi.org/10.3390/ijms19010109>
- Ferrigno, A., Rizzo, V., Boncompagni, E., Bianchi, A., Gringeri, E., Neri, D., Richelmi, P., Freitas, I., Cillo, U., & Vairetti, M. (2011). Machine perfusion at 20 degrees C reduces preservation damage to livers from non-heart beating donors. *Cryobiology*, 62(2), 152-158. <https://doi.org/10.1016/j.cryobiol.2011.02.004>
- Figueira, E. R., Rocha-Filho, J. A., Nakatani, M., Buto, M. F., Tatebe, E. R., Andre, V. O., Ceconello, I., & D'Albuquerque, L. A. (2014). Hepatic ischemic preconditioning increases portal vein flow in experimental liver ischemia reperfusion injury. *Hepatobiliary Pancreat Dis Int*, 13(1), 40-47. [https://doi.org/10.1016/s1499-3872\(14\)60005-9](https://doi.org/10.1016/s1499-3872(14)60005-9)
- Gaskell, H., Ge, X., & Nieto, N. (2018). High-Mobility Group Box-1 and Liver Disease. *Hepatol Commun*, 2(9), 1005-1020. <https://doi.org/10.1002/hep4.1223>
- Gassner, J., Nösser, M., Moosburner, S., Horner, R., Tang, P., Wegener, L., Wyrwal, D., Claussen, F., Arsenic, R., Pratschke, J., Sauer, I. M., & Raschzok, N. (2019). Improvement of Normothermic Ex Vivo Machine Perfusion of Rat Liver Grafts by Dialysis and Kupffer Cell Inhibition With Glycine. *Liver Transpl*, 25(2), 275-287. <https://doi.org/10.1002/lt.25360>
- GODT. (2023). *Intrnational report on Organ Donation and Transplantation Activities*. <https://www.transplant-observatory.org>
- Gotoh, K., Lu, Z., Morita, M., Shibata, M., Koike, M., Waguri, S., Dono, K., Doki, Y., Kominami, E., Sugioka, A., Monden, M., & Uchiyama, Y. (2009). Participation of autophagy in the initiation of graft dysfunction after rat liver transplantation. *Autophagy*, 5(3), 351-360. <https://doi.org/10.4161/auto.5.3.7650>
- Han, S., Kwon, J. H., Lee, K. W., Lee, S., Choi, G. S., Kim, J. M., Ko, J. S., Gwak, M. S., Kim, G. S., Ha, S. Y., & Joh, J. W. (2023). Abrogation of greater graft failure risk of female-to-male liver transplantation with donors older than 40 years or graft macrosteatosis greater than 5. *Sci Rep*, 13(1), 12914. <https://doi.org/10.1038/s41598-023-38113-w>
- Haque, O., Pendexter, C. A., Cronin, S. E. J., Raigani, S., de Vries, R. J., Yeh, H., Markmann, J. F., & Uygun, K. (2020). Twenty-four hour ex-vivo normothermic machine perfusion in rat livers. *Technology (Singap World Sci)*, 8(1-2), 27-36. <https://doi.org/10.1142/s2339547820500028>
- Harada, H., Pavlick, K. P., Hines, I. N., Hoffman, J. M., Bharwani, S., Gray, L., Wolf, R. E., & Grisham, M. B. (2001). Selected contribution: Effects of gender on reduced-size liver ischemia and reperfusion injury. *J Appl Physiol (1985)*, 91(6), 2816-2822. <https://doi.org/10.1152/jappl.2001.91.6.2816>



- He, W., Ye, S., Zeng, C., Xue, S., Hu, X., Zhang, X., Gao, S., Xiong, Y., He, X., Vivalda, S., Li, L., Wang, Y., & Ye, Q. (2018). Hypothermic oxygenated perfusion (HOPE) attenuates ischemia/reperfusion injury in the liver through inhibition of the TXNIP/NLRP3 inflammasome pathway in a rat model of donation after cardiac death. *FASEB J*, *fj201800028RR*. <https://doi.org/10.1096/fj.201800028RR>
- Ince, C. (2005). The microcirculation is the motor of sepsis. *Crit Care*, *9 Suppl 4*(Suppl 4), S13-19. <https://doi.org/10.1186/cc3753>
- Jain, S., Lee, S. H., Korneszczuk, K., Culberson, C. R., Southard, J. H., Berthiaume, F., Zhang, J. X., Clemens, M. G., & Lee, C. Y. (2008). Improved preservation of warm ischemic livers by hypothermic machine perfusion with supplemented University of Wisconsin solution. *J Invest Surg*, *21*(2), 83-91. <https://doi.org/10.1080/08941930701883657>
- Jimenez-Castro, M. B., Cornide-Petronio, M. E., Gracia-Sancho, J., & Peralta, C. (2019). Inflammasome-Mediated Inflammation in Liver Ischemia-Reperfusion Injury. *Cells*, *8*(10). <https://doi.org/10.3390/cells8101131>
- Jin, H., Huang, H., Dong, W., Sun, J., Liu, A., Deng, M., Dirsch, O., & Dahmen, U. (2012). Preliminary experience of a PDCA-cycle and quality management based training curriculum for rat liver transplantation. *J Surg Res*, *176*(2), 409-422. <https://doi.org/10.1016/j.jss.2011.10.010>
- Jungermann, K., & Kietzmann, T. (1996). Zonation of parenchymal and nonparenchymal metabolism in liver. *Annu Rev Nutr*, *16*, 179-203. <https://doi.org/10.1146/annurev.nu.16.070196.001143>
- Kang, J. W., Cho, H. I., & Lee, S. M. (2014). Melatonin inhibits mTOR-dependent autophagy during liver ischemia/reperfusion. *Cell Physiol Biochem*, *33*(1), 23-36. <https://doi.org/10.1159/000356647>
- Kassissia, I., Brault, A., & Huet, P. M. (1994). Hepatic artery and portal vein vascularization of normal and cirrhotic rat liver. *Hepatology*, *19*(5), 1189-1197. <https://www.ncbi.nlm.nih.gov/pubmed/8175141>
- Katsuta, Y., Zhang, X. J., Ohsuga, M., Akimoto, T., Komeichi, H., Shimizu, S., Kato, Y., Miyamoto, A., Satomura, K., & Takano, T. (2005). Arterial hypoxemia and intrapulmonary vasodilatation in rat models of portal hypertension. *J Gastroenterol*, *40*(8), 811-819. <https://doi.org/10.1007/s00535-005-1633-9>
- Kietzmann, T. (2017). Metabolic zonation of the liver: The oxygen gradient revisited. *Redox Biol*, *11*, 622-630. <https://doi.org/10.1016/j.redox.2017.01.012>
- Kietzmann, T., Dimova, E. Y., Flügel, D., & Scharf, J. G. (2006). Oxygen: modulator of physiological and pathophysiological processes in the liver. *Z Gastroenterol*, *44*(1), 67-76. <https://doi.org/10.1055/s-2005-858987>
- Kim, J. S., Chapman, W. C., & Lin, Y. (2022). Mitochondrial Autophagy in Ischemic Aged Livers. *Cells*, *11*(24). <https://doi.org/10.3390/cells11244083>
- Kim, J. S., He, L., Qian, T., & Lemasters, J. J. (2003). Role of the mitochondrial permeability transition in apoptotic and necrotic death after ischemia/reperfusion injury to hepatocytes. *Curr Mol Med*, *3*(6), 527-535. <https://doi.org/10.2174/1566524033479564>
- Kwong, A. J., Kim, W. R., Lake, J. R., Schladt, D. P., Schnellinger, E. M., Gauntt, K., McDermott, M., Weiss, S., Handarova, D. K., Snyder, J. J., & Israni, A. K. (2024). OPTN/SRTR 2022 Annual Data Report: Liver. *Am J Transplant*, *24*(2S1), S176-S265. <https://doi.org/10.1016/j.ajt.2024.01.014>
- Laing, R. W., Mergental, H., Yap, C., Kirkham, A., Whilku, M., Barton, D., Curbishley, S., Boteon, Y. L., Neil, D. A., Hubscher, S. G., Perera, M., Muiesan, P., Isaac, J., Roberts, K. J., Cilliers, H., Afford, S. C., & Mirza, D. F. (2017). Viability testing and transplantation of marginal livers (VITTAL) using normothermic machine perfusion:

- study protocol for an open-label, non-randomised, prospective, single-arm trial. *BMJ Open*, 7(11), e017733. <https://doi.org/10.1136/bmjopen-2017-017733>
- Lauschke, H., Olschewski, P., Tolba, R., Schulz, S., & Minor, T. (2003). Oxygenated machine perfusion mitigates surface antigen expression and improves preservation of predamaged donor livers. *Cryobiology*, 46(1), 53-60. [https://doi.org/10.1016/s0011-2240\(02\)00164-5](https://doi.org/10.1016/s0011-2240(02)00164-5)
- Lazzeri, C., Bonizzoli, M., Marra, F., Muiesan, P., Ghinolfi, D., De Simone, P., Nesi, M. G., Migliaccio, M. L., & Peris, A. (2020). Uncontrolled donation after circulatory death and liver transplantation: evidence and unresolved issues. *Minerva Anestesiol*, 86(2), 196-204. <https://doi.org/10.23736/s0375-9393.19.13746-7>
- Lee, C. Y., Jain, S., Duncan, H. M., Zhang, J. X., Jones, J. W., Jr., Southard, J. H., & Clemens, M. G. (2003). Survival transplantation of preserved non-heart-beating donor rat livers: preservation by hypothermic machine perfusion. *Transplantation*, 76(10), 1432-1436. <https://doi.org/10.1097/01.TP.0000088674.23805.0F>
- Li, C. H., Ge, X. L., Pan, K., Wang, P. F., Su, Y. N., & Zhang, A. Q. (2017). Laser speckle contrast imaging and Oxygen to See for assessing microcirculatory liver blood flow changes following different volumes of hepatectomy. *Microvasc Res*, 110, 14-23. <https://doi.org/10.1016/j.mvr.2016.11.004>
- Li, H., Lu, J., Zhou, X., Pan, D., Guo, D., Ling, H., Yang, H., He, Y., & Chen, G. (2017). Quantitative Analysis of Hepatic Microcirculation in Rabbits After Liver Ischemia-Reperfusion Injury Using Contrast-Enhanced Ultrasound. *Ultrasound Med Biol*, 43(10), 2469-2476. <https://doi.org/10.1016/j.ultrasmedbio.2017.06.004>
- Li, J., Lu, H., Zhang, J., Li, Y., & Zhao, Q. (2023). Comprehensive Approach to Assessment of Liver Viability During Normothermic Machine Perfusion. *J Clin Transl Hepatol*, 11(2), 466-479. <https://doi.org/10.14218/jcth.2022.00130>
- Li, Z., Chen, L., Chu, H., Wang, W., & Yang, L. (2022). Estrogen alleviates hepatocyte necroptosis depending on GPER in hepatic ischemia reperfusion injury. *J Physiol Biochem*, 78(1), 125-137. <https://doi.org/10.1007/s13105-021-00846-5>
- Limkemann, A., Lindell, S. L., Reichstetter, H., Plant, V., Parrish, D., Ramos, C., Kowalski, C., Quintini, C., & Mangino, M. J. (2016). Donor gluconate rescues livers from uncontrolled donation after cardiac death. *Surgery*, 159(3), 852-861. <https://doi.org/10.1016/j.surg.2015.10.022>
- Liu, A., Dirsch, O., Fang, H., Dong, W., Jin, H., Huang, H., Sun, J., & Dahmen, U. (2011). HMGB1 translocation and expression is caused by warm ischemia reperfusion injury, but not by partial hepatectomy in rats. *Exp Mol Pathol*, 91(2), 502-508. <https://doi.org/10.1016/j.yexmp.2011.05.005>
- Liu, W., Fan, Y., Ding, H., Han, D., Yan, Y., Wu, R., Lv, Y., & Zheng, X. (2021). Normothermic machine perfusion attenuates hepatic ischaemia-reperfusion injury by inhibiting CIRP-mediated oxidative stress and mitochondrial fission. *J Cell Mol Med*, 25(24), 11310-11321. <https://doi.org/10.1111/jcmm.17062>
- Lu, D., Xu, X., Wang, J., Ling, Q., Xie, H., Zhou, L., Yan, S., Wang, W., Zhang, M., Shen, Y., & Zheng, S. (2014). The influence of a contemporaneous portal and hepatic artery revascularization protocol on biliary complications after liver transplantation. *Surgery*, 155(1), 190-195. <https://doi.org/10.1016/j.surg.2013.06.056>
- Luer, B., Koetting, M., Efferz, P., & Minor, T. (2010). Role of oxygen during hypothermic machine perfusion preservation of the liver. *Transpl Int*, 23(9), 944-950. <https://doi.org/10.1111/j.1432-2277.2010.01067.x>
- Luo, J., Hu, Y., Qiao, Y., Li, H., Huang, J., Xu, K., Jiang, L., Wu, H., Hu, X., Jia, J., Zhou, L., Xie, H., Li, J., & Zheng, S. (2023). Hypothermic Oxygenated Machine Perfusion Promotes Mitophagy Flux against Hypoxia-Ischemic Injury in Rat DCD Liver. *Int J Mol Sci*, 24(6). <https://doi.org/10.3390/ijms24065403>

- Manco, R., & Itzkovitz, S. (2021). Liver zonation. *J Hepatol*, 74(2), 466-468. <https://doi.org/10.1016/j.jhep.2020.09.003>
- Manzia, T. M., Toti, L., Quaranta, C., Blasi, F., & Tisone, G. (2019). Liver transplantation with a normothermic machine preserved fatty nonagenarian liver: A case report. *Int J Surg Case Rep*, 57, 163-166. <https://doi.org/10.1016/j.ijscr.2019.03.033>
- Mao, B., Yuan, W., Wu, F., Yan, Y., & Wang, B. (2023). Autophagy in hepatic ischemia-reperfusion injury. *Cell Death Discov*, 9(1), 115. <https://doi.org/10.1038/s41420-023-01387-0>
- Marambio, A., Tunon, J. M. C., Gomez, L. M. M., Martinez, J. M. A., Bellido, C. B., Artacho, G. S., Franco, C. C., Pulido, L. B., Ruiz, F. J. P., & Bravo, M. A. G. (2018). Intraoperative Portal Vein Flow > 123 mL/min Per 100 g Predicts a Better Survival of Patients After Liver Transplantation. *Transplant Proc*, 50(10), 3582-3586. <https://doi.org/10.1016/j.transproceed.2018.06.032>
- Minor, T., Luer, B., & Efferz, P. (2011). Dopamine improves hypothermic machine preservation of the liver. *Cryobiology*, 63(2), 84-89. <https://doi.org/10.1016/j.cryobiol.2011.05.004>
- Minor, T., Manekeller, S., Sioutis, M., & Dombrowski, F. (2006). Endoplasmic and vascular surface activation during organ preservation: refining upon the benefits of machine perfusion. *Am J Transplant*, 6(6), 1355-1366. <https://doi.org/10.1111/j.1600-6143.2006.01338.x>
- Mizushima, N. (2007). Autophagy: process and function. *Genes Dev*, 21(22), 2861-2873. <https://doi.org/10.1101/gad.1599207>
- Muth, V., Gassner, J., Moosburner, S., Lurje, G., Michelotto, J., Strobl, F., Knaub, K., Engelmann, C., Tacke, F., Selzner, M., Pratschke, J., Sauer, I. M., & Raschzok, N. (2023). Ex Vivo Liver Machine Perfusion: Comprehensive Review of Common Animal Models. *Tissue Eng Part B Rev*, 29(1), 10-27. <https://doi.org/10.1089/ten.TEB.2022.0018>
- Nagrath, D., Xu, H., Tanimura, Y., Zuo, R., Berthiaume, F., Avila, M., Yarmush, R., & Yarmush, M. L. (2009). Metabolic preconditioning of donor organs: defatting fatty livers by normothermic perfusion ex vivo. *Metab Eng*, 11(4-5), 274-283. <https://doi.org/10.1016/j.ymben.2009.05.005>
- Nakajima, T., Osborn, J., Rhee, J. G., & Song, C. W. (1990). Effect of regional heating of upper body on the liver blood flow in rats. *Int J Hyperthermia*, 6(1), 1-14. <https://doi.org/10.3109/02656739009140800>
- Nasralla, D., Coussios, C. C., Mergental, H., Akhtar, M. Z., Butler, A. J., Ceresa, C. D. L., Chiocchia, V., Dutton, S. J., García-Valdecasas, J. C., Heaton, N., Imber, C., Jassem, W., Jochmans, I., Karani, J., Knight, S. R., Kocabayoglu, P., Malagò, M., Mirza, D., Morris, P. J., Pallan, A., Paul, A., Pavel, M., Perera, M., Pirenne, J., Ravikumar, R., Russell, L., Upponi, S., Watson, C. J. E., Weissenbacher, A., Ploeg, R. J., & Friend, P. J. (2018). A randomized trial of normothermic preservation in liver transplantation. *Nature*, 557(7703), 50-56. <https://doi.org/10.1038/s41586-018-0047-9>
- Nephew, L. D., Zia, Z., Ghabril, M., Orman, E., Lammert, C., Kubal, C., & Chalasani, N. (2021). Sex disparities in waitlisting and liver transplant for acute liver failure. *JHEP Rep*, 3(1), 100200. <https://doi.org/10.1016/j.jhepr.2020.100200>
- Ni, Y. A., Chen, H., Nie, H., Zheng, B., & Gong, Q. (2021). HMGB1: An overview of its roles in the pathogenesis of liver disease. *J Leukoc Biol*, 110(5), 987-998. <https://doi.org/10.1002/JLB.3MR0121-277R>
- Niu, X., Huang, W. H., De Boer, B., Delriviere, L., Mou, L. J., & Jeffrey, G. P. (2014). Iron-induced oxidative rat liver injury after non-heart-beating warm ischemia is mediated by tumor necrosis factor alpha and prevented by deferoxamine. *Liver Transpl*, 20(8), 904-911. <https://doi.org/10.1002/lt.23893>

- Ohman, A., Raigani, S., Santiago, J. C., Heaney, M. G., Boylan, J. M., Parry, N., Carroll, C., Baptista, S. G., Uygun, K., Gruppuso, P. A., Sanders, J. A., & Yeh, H. (2022). Activation of autophagy during normothermic machine perfusion of discarded livers is associated with improved hepatocellular function. *Am J Physiol Gastrointest Liver Physiol*, 322(1), G21-g33. <https://doi.org/10.1152/ajpgi.00266.2021>
- Oldani, G., Peloso, A., Slits, F., Gex, Q., Delaune, V., Orci, L. A., van de Looij, Y., Colin, D. J., Germain, S., de Vito, C., Rubbia-Brandt, L., Lacotte, S., & Toso, C. (2019). The impact of short-term machine perfusion on the risk of cancer recurrence after rat liver transplantation with donors after circulatory death. *PLoS One*, 14(11), e0224890. <https://doi.org/10.1371/journal.pone.0224890>
- Olschewski, P., Gass, P., Ariyakhagorn, V., Jasse, K., Hunold, G., Menzel, M., Schoning, W., Schmitz, V., Neuhaus, P., & Puhl, G. (2010). The influence of storage temperature during machine perfusion on preservation quality of marginal donor livers. *Cryobiology*, 60(3), 337-343. <https://doi.org/10.1016/j.cryobiol.2010.03.005>
- Op den Dries, S., Karimian, N., Westerkamp, A. C., Sutton, M. E., Kuipers, M., Wiersema-Buist, J., Ottens, P. J., Kuipers, J., Giepmans, B. N., Leuvenink, H. G., Lisman, T., & Porte, R. J. (2016). Normothermic machine perfusion reduces bile duct injury and improves biliary epithelial function in rat donor livers. *Liver Transpl*, 22(7), 994-1005. <https://doi.org/10.1002/lt.24436>
- Panconesi, R., Flores Carvalho, M., Mueller, M., Meierhofer, D., Dutkowski, P., Muiesan, P., & Schlegel, A. (2021). Viability Assessment in Liver Transplantation-What Is the Impact of Dynamic Organ Preservation? *Biomedicines*, 9(2). <https://doi.org/10.3390/biomedicines9020161>
- Panday, R., Monckton, C. P., & Khetani, S. R. (2022). The Role of Liver Zonation in Physiology, Regeneration, and Disease. *Semin Liver Dis*, 42(1), 1-16. <https://doi.org/10.1055/s-0041-1742279>
- Peralta, C., Jimenez-Castro, M. B., & Gracia-Sancho, J. (2013). Hepatic ischemia and reperfusion injury: effects on the liver sinusoidal milieu. *J Hepatol*, 59(5), 1094-1106. <https://doi.org/10.1016/j.jhep.2013.06.017>
- Perk, S., Izamis, M. L., Tolboom, H., Uygun, B., Berthiaume, F., Yarmush, M. L., & Uygun, K. (2011). A metabolic index of ischemic injury for perfusion-recovery of cadaveric rat livers. *PLoS One*, 6(12), e28518. <https://doi.org/10.1371/journal.pone.0028518>
- Petrovic, A., Vukadin, S., Sikora, R., Bojanic, K., Smolic, R., Plavec, D., Wu, G. Y., & Smolic, M. (2022). Anabolic androgenic steroid-induced liver injury: An update. *World J Gastroenterol*, 28(26), 3071-3080. <https://doi.org/10.3748/wjg.v28.i26.3071>
- Puhl, G., Schaser, K. D., Pust, D., Kohler, K., Vollmar, B., Menger, M. D., Neuhaus, P., & Settmacher, U. (2005). Initial hepatic microcirculation correlates with early graft function in human orthotopic liver transplantation. *Liver Transpl*, 11(5), 555-563. <https://doi.org/10.1002/lt.20394>
- Saad, S., & Minor, T. (2008). Short-term resuscitation of predamaged donor livers by brief machine perfusion: the influence of temperature. *Transplant Proc*, 40(10), 3321-3326. <https://doi.org/10.1016/j.transproceed.2008.06.058>
- Schlegel, A., Graf, R., Clavien, P. A., & Dutkowski, P. (2013). Hypothermic oxygenated perfusion (HOPE) protects from biliary injury in a rodent model of DCD liver transplantation. *J Hepatol*, 59(5), 984-991. <https://doi.org/10.1016/j.jhep.2013.06.022>
- Schlegel, A., Kron, P., Graf, R., Dutkowski, P., & Clavien, P. A. (2014). Warm vs. cold perfusion techniques to rescue rodent liver grafts. *J Hepatol*, 61(6), 1267-1275. <https://doi.org/10.1016/j.jhep.2014.07.023>
- Schlegel, A., Muller, X., Mueller, M., Stepanova, A., Kron, P., de Rougemont, O., Muiesan, P., Clavien, P. A., Galkin, A., Meierhofer, D., & Dutkowski, P. (2020). Hypothermic

- oxygenated perfusion protects from mitochondrial injury before liver transplantation. *EBioMedicine*, 60, 103014. <https://doi.org/10.1016/j.ebiom.2020.103014>
- Schmucker, D. L. (2005). Age-related changes in liver structure and function: Implications for disease? *Exp Gerontol*, 40(8-9), 650-659. <https://doi.org/10.1016/j.exger.2005.06.009>
- Schurink, I. J., de Haan, J. E., Willemse, J., Mueller, M., Doukas, M., Roest, H., de Goeij, F. H. C., Polak, W. G., Ijzermans, J. N. M., Dutkowski, P., van der Laan, L. J. W., & de Jonge, J. (2021). A proof of concept study on real-time LiMAX CYP1A2 liver function assessment of donor grafts during normothermic machine perfusion. *Sci Rep*, 11(1), 23444. <https://doi.org/10.1038/s41598-021-02641-0>
- Schwartz, J. J., Pappas, L., Thiesset, H. F., Vargas, G., Sorensen, J. B., Kim, R. D., Hutson, W. R., Boucher, K., & Box, T. (2012). Liver transplantation in septuagenarians receiving model for end-stage liver disease exception points for hepatocellular carcinoma: the national experience. *Liver Transpl*, 18(4), 423-433. <https://doi.org/10.1002/lt.23385>
- Shen, L., Uz, Z., Verheij, J., Veelo, D. P., Ince, Y., Ince, C., & van Gulik, T. M. (2020). Interpatient heterogeneity in hepatic microvascular blood flow during vascular inflow occlusion (Pringle manoeuvre). *Hepatobiliary Surg Nutr*, 9(3), 271-283. <https://doi.org/10.21037/hbsn.2020.02.04>
- Shen, M., Lu, J., Dai, W., Wang, F., Xu, L., Chen, K., He, L., Cheng, P., Zhang, Y., Wang, C., Wu, D., Yang, J., Zhu, R., Zhang, H., Zhou, Y., & Guo, C. (2013). Ethyl pyruvate ameliorates hepatic ischemia-reperfusion injury by inhibiting intrinsic pathway of apoptosis and autophagy. *Mediators Inflamm*, 2013, 461536. <https://doi.org/10.1155/2013/461536>
- Shonaka, T., Matsuno, N., Obara, H., Yoshikawa, R., Nishikawa, Y., Ishihara, Y., Bochimoto, H., Gochi, M., Otani, M., Kanazawa, H., Azuma, H., Sakai, H., & Furukawa, H. (2019). Impact of human-derived hemoglobin based oxygen vesicles as a machine perfusion solution for liver donation after cardiac death in a pig model. *PLoS One*, 14(12), e0226183. <https://doi.org/10.1371/journal.pone.0226183>
- Sindram, D., Porte, R. J., Hoffman, M. R., Bentley, R. C., & Clavien, P. A. (2000). Platelets induce sinusoidal endothelial cell apoptosis upon reperfusion of the cold ischemic rat liver. *Gastroenterology*, 118(1), 183-191. [https://doi.org/10.1016/s0016-5085\(00\)70427-6](https://doi.org/10.1016/s0016-5085(00)70427-6)
- Sinha, S., Hassan, N., & Schwartz, R. E. (2024). Organelle stress and alterations in interorganelle crosstalk during liver fibrosis. *Hepatology*, 79(2), 482-501. <https://doi.org/10.1097/hep.000000000000012>
- Siniscalchi, A., Gamberini, L., Laici, C., Bardi, T., Ercolani, G., Lorenzini, L., & Faenza, S. (2016). Post reperfusion syndrome during liver transplantation: From pathophysiology to therapy and preventive strategies. *World J Gastroenterol*, 22(4), 1551-1569. <https://doi.org/10.3748/wjg.v22.i4.1551>
- Soto-Gutierrez, A., Gough, A., Verneti, L. A., Taylor, D. L., & Monga, S. P. (2017). Pre-clinical and clinical investigations of metabolic zonation in liver diseases: The potential of microphysiology systems. *Exp Biol Med (Maywood)*, 242(16), 1605-1616. <https://doi.org/10.1177/1535370217707731>
- Stegemann, J., Hirner, A., Rauen, U., & Minor, T. (2009). Gaseous oxygen persufflation or oxygenated machine perfusion with Custodiol-N for long-term preservation of ischemic rat livers? *Cryobiology*, 58(1), 45-51. <https://doi.org/10.1016/j.cryobiol.2008.10.127>
- Sun, D., Yang, L., Zheng, W., Cao, H., Wu, L., & Song, H. (2021). Protective Effects of Bone Marrow Mesenchymal Stem Cells (BMSCs) Combined with Normothermic Machine Perfusion on Liver Grafts Donated After Circulatory Death via Reducing the

- Ferroptosis of Hepatocytes. *Med Sci Monit*, 27, e930258.  
<https://doi.org/10.12659/MSM.930258>
- Suzuki, S., Toledo-Pereyra, L. H., Rodriguez, F. J., & Cejalvo, D. (1993). Neutrophil infiltration as an important factor in liver ischemia and reperfusion injury. Modulating effects of FK506 and cyclosporine. *Transplantation*, 55(6), 1265-1272.  
<https://doi.org/10.1097/00007890-199306000-00011>
- van Hart, N. A., van der Plaats, A., Leuvenink, H. G., Wiersema-Buist, J., Olinga, P., van Luyn, M. J., Verkerke, G. J., Rakhorst, G., & Ploeg, R. J. (2004). Initial blood washout during organ procurement determines liver injury and function after preservation and reperfusion. *Am J Transplant*, 4(11), 1836-1844. <https://doi.org/10.1111/j.1600-6143.2004.00580.x>
- Tara, A., Dominic, J. L., Patel, J. N., Garg, I., Yeon, J., Memon, M. S., Gergal Gopalkrishna Rao, S. R., Bugazia, S., Dhandapani, T. P. M., Kannan, A., Kantamaneni, K., Win, M., Went, T. R., Yanamala, V. L., & Mostafa, J. A. (2021). Mitochondrial Targeting Therapy Role in Liver Transplant Preservation Lines: Mechanism and Therapeutic Strategies. *Cureus*, 13(7), e16599. <https://doi.org/10.7759/cureus.16599>
- Tolboom, H., Izamis, M. L., Sharma, N., Milwid, J. M., Uygun, B., Berthiaume, F., Uygun, K., & Yarmush, M. L. (2012). Subnormothermic machine perfusion at both 20 degrees C and 30 degrees C recovers ischemic rat livers for successful transplantation. *J Surg Res*, 175(1), 149-156. <https://doi.org/10.1016/j.jss.2011.03.003>
- Tolboom, H., Milwid, J. M., Izamis, M. L., Uygun, K., Berthiaume, F., & Yarmush, M. L. (2008). Sequential cold storage and normothermic perfusion of the ischemic rat liver. *Transplant Proc*, 40(5), 1306-1309.  
<https://doi.org/10.1016/j.transproceed.2008.03.100>
- Um, S. H., Nishida, O., Tokubayashi, M., Kimura, F., Takimoto, Y., Yoshioka, H., Inque, R., & Kita, T. (1994). Hemodynamic changes after ligation of a major branch of the portal vein in rats: comparison with rats with portal vein constriction. *Hepatology*, 19(1), 202-209. <https://www.ncbi.nlm.nih.gov/pubmed/8276356>
- Uygun, K., Tolboom, H., Izamis, M. L., Uygun, B., Sharma, N., Yagi, H., Soto-Gutierrez, A., Hertl, M., Berthiaume, F., & Yarmush, M. L. (2010). Diluted blood reperfusion as a model for transplantation of ischemic rat livers: alanine aminotransferase is a direct indicator of viability. *Transplant Proc*, 42(7), 2463-2467.  
<https://doi.org/10.1016/j.transproceed.2010.04.037>
- Uz, Z., Ergin, B., Shen, L., van Lienden, K. P., Rassam, F., Olthof, P. B., Bennink, R. J., Ince, C., & van Gulik, T. M. (2022). Increased Hepatic Microvascular Density, Oxygenation, and VEGF in the Hypertrophic Lobe following Portal Vein Embolization in Rabbits. *Eur Surg Res*, 63(1), 9-18.  
<https://doi.org/10.1159/000517025>
- Uz, Z., Ince, C., Shen, L., Ergin, B., & van Gulik, T. M. (2021). Real-time observation of microcirculatory leukocytes in patients undergoing major liver resection. *Sci Rep*, 11(1), 4563. <https://doi.org/10.1038/s41598-021-83677-0>
- van Golen, R. F., van Gulik, T. M., & Heger, M. (2012). Mechanistic overview of reactive species-induced degradation of the endothelial glycocalyx during hepatic ischemia/reperfusion injury. *Free Radic Biol Med*, 52(8), 1382-1402.  
<https://doi.org/10.1016/j.freeradbiomed.2012.01.013>
- Vollmar, B., & Menger, M. D. (2009). The hepatic microcirculation: mechanistic contributions and therapeutic targets in liver injury and repair. *Physiol Rev*, 89(4), 1269-1339. <https://doi.org/10.1152/physrev.00027.2008>
- von Horn, C., Baba, H. A., Hannaert, P., Hauet, T., Leuvenink, H., Paul, A., Minor, T., & partners, C. c. (2017). Controlled oxygenated rewarming up to normothermia for

- pretransplant reconditioning of liver grafts. *Clin Transplant*, 31(11).  
<https://doi.org/10.1111/ctr.13101>
- von Horn, C., & Minor, T. (2020). Transient hyperthermia during oxygenated rewarming of isolated rat livers. *Transpl Int*, 33(3), 272-278. <https://doi.org/10.1111/tri.13542>
- von Horn, C., Zlatev, H., Pletz, J., Luer, B., & Minor, T. (2022). Comparison of thermal variations in post-retrieval graft conditioning on rat livers. *Artif Organs*, 46(2), 239-245. <https://doi.org/10.1111/aor.14080>
- Walcher, F., Bauer, C., Paxian, M., Holanda, M., Larsen, R., & Marzi, I. (1996). The influence of resuscitation on hemodynamics and oxygen radical-induced reperfusion injury after arterialized liver transplantation in the rat. *J Surg Res*, 65(1), 9-14.  
<https://doi.org/10.1006/jsre.1996.0336>
- Wang, J. H., Ahn, I. S., Fischer, T. D., Byeon, J. I., Dunn, W. A., Jr., Behrns, K. E., Leeuwenburgh, C., & Kim, J. S. (2011). Autophagy suppresses age-dependent ischemia and reperfusion injury in livers of mice. *Gastroenterology*, 141(6), 2188-2199 e2186. <https://doi.org/10.1053/j.gastro.2011.08.005>
- Westerkamp, A. C., Mahboub, P., Meyer, S. L., Hottenrott, M., Ottens, P. J., Wiersema-Buist, J., Gouw, A. S., Lisman, T., Leuvenink, H. G., & Porte, R. J. (2015). End-ischemic machine perfusion reduces bile duct injury in donation after circulatory death rat donor livers independent of the machine perfusion temperature. *Liver Transpl*, 21(10), 1300-1311. <https://doi.org/10.1002/lt.24200>
- Wu, G., Tomei, L. D., Bathurst, I. C., Zhang, F., Hong, C. B., Issel, C. J., Columbano, A., Salley, R. K., & Chien, S. (1997). Antiapoptotic compound to enhance hypothermic liver preservation. *Transplantation*, 63(6), 803-809. <https://doi.org/10.1097/00007890-199703270-00003>
- Xin, J., Yang, T., Wu, X., Wu, Y., Liu, Y., Liu, X., Jiang, M., & Gao, W. (2023). Spatial transcriptomics analysis of zone-dependent hepatic ischemia-reperfusion injury murine model. *Commun Biol*, 6(1), 194. <https://doi.org/10.1038/s42003-023-04564-0>
- Xu, F., Hua, C., Tautenhahn, H. M., Dirsch, O., & Dahmen, U. (2020). The Role of Autophagy for the Regeneration of the Aging Liver. *Int J Mol Sci*, 21(10).  
<https://doi.org/10.3390/ijms21103606>
- Xue, S., He, W., Zeng, X., Tang, Z., Feng, S., Zhong, Z., Xiong, Y., Wang, Y., & Ye, Q. (2018). Hypothermic machine perfusion attenuates ischemia/reperfusion injury against rat livers donated after cardiac death by activating the Keap1/Nrf2/ARE signaling pathway. *Mol Med Rep*, 18(1), 815-826. <https://doi.org/10.3892/mmr.2018.9065>
- Yang, H., Wang, H., & Andersson, U. (2020). Targeting Inflammation Driven by HMGB1. *Front Immunol*, 11, 484. <https://doi.org/10.3389/fimmu.2020.00484>
- Yang, L., Cao, H., Sun, D., Lin, L., Zheng, W. P., Shen, Z. Y., & Song, H. L. (2020). Normothermic Machine Perfusion Combined with Bone Marrow Mesenchymal Stem Cells Improves the Oxidative Stress Response and Mitochondrial Function in Rat Donation After Circulatory Death Livers. *Stem Cells Dev*, 29(13), 835-852.  
<https://doi.org/10.1089/scd.2019.0301>
- Zeng, C., Hu, X., He, W., Wang, Y., Li, L., Xiong, Y., & Ye, Q. (2017). Hypothermic machine perfusion ameliorates inflammation during ischemiareperfusion injury via sirtuin1 mediated deacetylation of nuclear factorkappaB p65 in rat livers donated after circulatory death. *Mol Med Rep*, 16(6), 8649-8656.  
<https://doi.org/10.3892/mmr.2017.7738>
- Zeng, X., Li, M., Fan, X., Xue, S., Liang, W., Fang, Z., Zeng, C., Fan, L., Xiong, Y., Wang, Y., & Ye, Q. (2019). Hypothermic Oxygenated Machine Perfusion Alleviates Donation After Circulatory Death Liver Injury Through Regulating P-selectin-dependent and -independent Pathways in Mice. *Transplantation*, 103(5), 918-928.  
<https://doi.org/10.1097/TP.0000000000002621>

- Zeng, X., Wang, S., Li, S., Yang, Y., Fang, Z., Huang, H., Wang, Y., Fan, X., & Ye, Q. (2019). Hypothermic oxygenated machine perfusion alleviates liver injury in donation after circulatory death through activating autophagy in mice. *Artif Organs*, 43(12), E320-e332. <https://doi.org/10.1111/aor.13525>
- Zhou, W., Peng, S., Du, P., Zhou, P., Xue, C., & Ye, Q. (2022). Hypothermic oxygenated perfusion combined with TJ-M2010-5 alleviates hepatic ischemia-reperfusion injury in donation after circulatory death. *Int Immunopharmacol*, 105, 108541. <https://doi.org/10.1016/j.intimp.2022.108541>



## 9 APPENDIXES

### 9.1 Supplement materials

Details of the chemicals, reagents, and kits are presented in Table S1. Similarly, details of laboratory materials, equipment, and software are mentioned in Table S2 and Table S3. The medium of perfusion are showed in Table S4. The histological buffer and antibodies are mentioned in Table S5 and Table S6. As shown in Table S7-9, western blot buffer, gel recipe, and antibodies are presented. As shown in Table S10, the clinical chemistry result in LTx study.

**Table S1. List of materials and equipment**

Materials and equipment	Manufacturer
18 G steel cannula	Harvard Apparatus
22 G catheter	B.BRAUN, 628566
6-0 silk	Ethicon, 640696
7-0 prolene	Ethicon, 600430
8-0 prolene	Ethicon, 6000178
Autoclavable Moist Chamber	Hugo Sachs Elektronik, 73-4733
Automatic benchtop tissue processor	Leica, TP1020
Automatic biochemical analyzer	Roche, Cobas 8000
Blood gas analysis	Radiometer, ABL 90 Flex
Bubble Trap	Hugo-Sachs-Elektronik, V83163
Cytocam	Braedius Medical, Huizen
Fr 1 polyurethane cannula	VYGON
Fr 2 polyurethane cannula	VYGON
Heating Circulating Baths	Harvard Apparatus, 75-0310
HPE III Basic	Bareiss Prüfgerätebau GmbH
Membrane Oxygenator	Hugo Sachs Elektronik, T18728
Microsurgery Microscope	Leica, M60
Microtome device	Leica, RM2255
Mini-PROTEAN Tetra Cell Casting Module	BIO-RAD, 1658022EDU
Mini-PROTEAN Tetra Vertical Electrophoresis Cell for Precast Gels	BIO-RAD, 1658005EDU
Peristaltic Pump	Harvard-Apparatus, P-70
Positively charged slides	Epredia, J1800AMNZ
PVDF transfer membrane, 0.45 $\mu$ m	Thermo Fisher Scientific, 88518
Reusable Blood Pressure Transducers	AD Instruments, MLT-0380/D

Spectrometric device O2C	LEA Medizintechnik Giessen
Speed-e-Vac	Thermo Fisher Scientific, SPD111V-230
SpeedMill Plus	845-00007-2, Analytik Jena
Thermocycler	Biometra, 846-X-070-280
Thermomixer	Eppendorf, 5437
TissueLyser LT	Qiagen, 85600
Transwell inserts	Sarstedt, 83.3930.041
Water bath	LAUDA, H 16
Water Jacketed Reservoir 2L	Harvard Apparatus, 73-3441
Western blotting filter paper, extra thick	Thermo Fisher Scientific, 88620

**Table S2. List of chemicals, reagents, and kits**

Chemicals and reagents	Manufacturer
Acetylcholine chloride	Sigma, A6625
Ammonium persulfate (APS)	Sigma, A3678
Avidin/Biotin Blocking Kit	Abcam, ab64212
BCA protein assay kit	Thermo Fisher Scientific, 23225
BisTris	Roth, 9140.3
Commercially available ready-to-use protein block	Abcam, ab64226
Eosin	Sigma, HT110132
Eosin Y	Sigma, HT110332
Ethanol	Thermo Fisher Scientific, 16606002
Ethanol ( $\geq 99.5\%$ )	Roth, T868.1
Formaldehyde 4%	Otto Fischar, 27261
Glycine	Roth, HN07.2
Hematoxylin	Agilent, CS70030-2
Hematoxylin	Roth, T865.1
Heparin	B.BRAUN, 142263
Hydrochloric acid c(HCl)	Merck, 109063100
Immobilon western chemiluminescent HRP substrate	Millipore, WBKLS0500
Isoflurane	Cp-pharma, 1214
Isopropanol	Roth, 7343.1
Methanol	VWR, 20847.295
Mounting medium	Sigma, 03989
Page ruler prestained protein ladder	Thermo Fisher Scientific, 26619

PhosSTOP phosphatase inhibitor	Sigma, 4906837001
Positively charged slides	EpreDia, J1800AMNZ
Powdered milk	Roth, T145.2
Primary mouse monoclonal antibody	Abcam, ab22717
Rabbit polyclonal antibody	Abcam, ab18256
Resolving Gel Buffer for PAGE	BIO-RAD, 1610798
Ringer-lactate solution	Fresenius kabi, 14RL3320
Sodium chloride (NaCl)	Roth, P029.3
Sodium dodecyl sulphate (SDS)	Roth, CN30.2
Stacking Gel Buffer for PAGE	BIO-RAD, 161-0799
Streptavidin HRP	Abcam, ab64269
TEMED	Sigma, T9281
Tris	Roth, 5429
Tri-sodium citrate	Sigma, S-4641
Tween-20	Sigma, P9416
Veterinary Saline (500ml)	WDT, 18X1807
Xylol	Roth, 9713.3
$\beta$ -mercaptoethanol	Roth, 4227.1

**Table S3. List of software**

Software	Manufacturer
Image J	National Institutes of Health, Version 1.54h
GraphPad Prism 8.0	Dotmatics
LabChart	ADInstruments products
NDP.view2Plus image viewing	Hamamatsu Photonics, Version U12388-02
Origin	Electronic Arts
SPSS statistics 26.0	IBM
Histokat VirtualLiver	Fraunhofer MEVIS
Fusion FX7	Labtech International Ltd
Biorender	Biorender

**Table S4. Recipe of NMP medium used in animal experiments (750ml / rat)**

Reagent	Concentration	Manufacturer
Phenol red-free Williams E Medium	600ml	Thermofisher, A1217601
Fetal bovine serum	20%	PAN-Biotech, P30-3306

Penicillin- Streptomycin SOL	100 U/mL	Thermofisher, 15140122
L-glutamine	0,292 g/l	Sigma, G7513
Insulin	1U/L	LILLY, 1008623
Hydrocortisone	10 mg/L	Pfizer, 1005904
Heparin	1U/L	B.BRAUN, 142263

**Table S5. Buffers used in HE and IHC**

Reagents	Recipe
Sodium citrate buffer	2.94 g Tri-sodium citrate, 1 L dH <sub>2</sub> O, 0.5 mL Tween 20, PH=6
10× Tris-buffered saline (TBS)	24.228 g Tris, 87.66 g NaCl, 1L dH <sub>2</sub> O, pH 7.6
1× TBS / Tween (TBST)	100 ml 10× TBS, 1 mL Tween, dH <sub>2</sub> O

**Table S6. CYP and HMGB1 antibodies used for IHC-detection of expression and translocation**

Antibody	Dilution	Manufacturer
Anti-CYP1A2 antibody-monoclonal in mouse	1:3000	Abcam, ab22717
Rabbit Polyclonal HMGB1 antibody	1:2000	Abcam, ab18256
Goat Anti-Mouse IgG H&L (biotin)	1:2000	Abcam, ab6788
Goat Anti-rabbit IgG H&L (biotin)	1:5000	Abcam, ab6720

**Table S7. Buffers used in protein isolation and western blotting**

Reagents	Recipe
1× protein lysis buffer	RIPA buffer, SIGMA, R0278
4x Laemmli sample buffer	BIO-RAD, 1610747
5x running buffer	15.1 g Tris base, 94 g Glycine, 5 g SDS, 1 L dH <sub>2</sub> O, PH=8.3
1x loading buffer	2.5 % β-mercaptoethanol, 22.5 % 4x Laemmli sample buffer, 75 % lysis sample
10× Tris-buffered saline (TBS)	60.6 g Tris, 80.06 NaCl, 1L dH <sub>2</sub> O, pH 7.6
1× TBS / Tween (TBST)	100 ml 10× TBS, 1 mL Tween, dH <sub>2</sub> O
10x Transfer buffer	30.3 g Tris base, 144.1 g Glycine, 1 L dH <sub>2</sub> O
1x Transfer buffer	100 mL 10x Transfer buffer, 200 mL methanol, 700ml dH <sub>2</sub> O
5 % Block buffer	2.5 g powdered milk, 50mL 1x TBST

**Table S8. Recipe of stacking and separating gels.**

Component	Stacking gel (5%)	Separating gel (12%)
30 % Acrylamide	0.67 mL	4 mL
dH <sub>2</sub> O	2.98 mL	3.2 mL
1.5M Tris-HCL	-	2.6 mL
0.5M Tris-HCL	1.25 mL	-
10% SDS	50 µL	100 µL
10 % APS	50 µL	100 µL
TEMED	5 µL	10 µL

**Table S9. Antibodies used for Western blotting**

Antibody	Dilution	Manufacturer
Rabbit anti-light chain 3 (LC3)	1:1000	Abcam, ab48394
Rabbit anti-SQSTM1 (P62)	1:1000	Abcam, ab109012
Rabbit anti-glyceraldehyde-3-phosphate dehydrogenase (GAPDH)	1:15,000	Abcam, ab181602
Polyclonal goat antibody to rabbit IgG	1:10,000	Abcam, ab6721

**Table S10. Clinical chemistry before and after LTx**

Parameters	Before LTx	LTx 1h	LTx 24h
ALT (U/L)	34.7±14.1	1827.2±744.9*	662.8±407.5*#
Albumin (g/l)	42.3±1.9	27.3±1.4*	22.5±4.9*
Alkaline phosphatase (µmol/l)	1.49±0.42	2.4±0.6*	1.4±0.3
Amylase (µmol/l)	35.3±5.6	41.8±12.0	19.3±4.2*#
AST (U/L)	75.1±23.1	1684.1±791.6*	1497.4±583.9*
Direct bilirubin (µmol/l)	<3	<3	<3
Total bilirubin (µmol/l)	<3	<3	<3
Cholinesterase (µmol/l)	3.6±1.4	2.8±0.4	1.4±0.5
Cholesterol (mmol/l)	2.1±0.1	1.5±0.2*	1.8±0.2
C-reactive protein (mg/l)	<0.6	<0.6	<0.6
Γ-glutamyltransferase (µmol/l)	<0.05	0.06±0.02	0.12±0.05*#
Glucose (mmol/l)	13.8±1.5	15.1±4.8	7.3±2.2*#
Urea (mmol/l)	6.7±1.1	9.5±0.9	26.6±13.3
Creatinine (µmol/l)	34.2±2.7	86.7±18.5*	99±67.9
Lactate dehydrogenase (µmol/l)	191.8±47.9	4708.6±1909.2*	1891.8±694.8*#
Triglycerides (mmol/l)	1.15±0.3	0.49±0.4*	1.4±0.2#
Total protein (µmol/l)	61.5±1.1	38.9±3.5*	36.8±8.3*

\*: there is a significant difference compared to Before LTx ( $P < 0.05$ ); #: there is a significant difference compared to LTx 1h ( $P < 0.05$ ).

## 9.2 List of figures and tables

**Figure 1.** Global liver transplant activity in 2022 per million population

**Figure 2.** Mechanisms involved in liver IRI

**Figure 3.** Impact of donor properties on hepatic IRI

**Figure 4.** Schematic representation of SCS and NMP systems

**Figure 5.** Setup of the NMP system

**Figure 6.** Experimental design of NMP experiment

**Figure 7.** Experimental design for identification of optimal perfusion conditions representing the best balance between oxygen supply and waste removal

**Figure 8.** Experimental design for exploration of donor properties potentially affecting the outcome of NMP

**Figure 9.** Experimental design for investigating the relationship between age and autophagy

**Figure 10.** Experimental design for establishment of rat LTx model

**Figure 11.** Experimental design for investigation of early ischemia-reperfusion injury and liver microcirculation

**Figure 12.** Group distribution for investigating early IRI and liver microcirculation after reperfusion

**Figure 13.** The illustration of cellular features for modified SUZUKI score (X80)

**Figure 14.** Image analysis of whole slide scan with sections from liver lobes using Histokat pattern recognition algorithm

**Figure 15.** Image analysis of HMGB1 using Image J

**Figure 16.** Image illustrating the monitoring of liver microvascular perfusion via O2C in the liver

**Figure 17.** Cytocam IDF video microscope

**Figure 18.** Illustration of the three steps for establishing NMP: getting familiar with the steps of the procedure, improving flushing, improving perfusion

**Figure 19.** Sequence of images illustrating the improvement of flushing and perfusion

**Figure 20.** Impact of NMP condition on liver function (n=3/group)

**Figure 21.** Enzyme release and acid-base homeostasis in livers subjected to different perfusion conditions (n=3/group)

**Figure 22.** Impact of perfusion flow rate on zoned hepatic morphological damage and HMGB1 translocation (n=3/group)

**Figure 23.** Impact of medium change on zoned hepatic morphological damage (n=3/group)

**Figure 24.** Impact of medium change on zoned HMGB1 translocation (n=3/group)

- Figure 25.** Bile production and liver stiffness in respect to donor properties
- Figure 26.** Impact of donor properties on liver enzymes release and acid-base homeostasis
- Figure 27.** Impact of donor condition on morphological damage
- Figure 28.** Impact of donor condition on HMGB1 translocation
- Figure 29.** Impact of donor condition on CYP1A2 expression
- Figure 30.** Impact of donor properties on hepatic perfusion
- Figure 31.** Impact of age on autophagy markers
- Figure 32.** Impact of age on expression of autophagy markers in livers subjected to NMP
- Figure 33.** Illustration of the phases needed for establishing rat LTx model
- Figure 34.** Learning curve for establishing stable rat LTx
- Figure 35.** Illustration of six cases of LTx survival at 24h
- Figure 36.** Illustration of improvement of reperfusion quality for rat LTx model
- Figure 37.** Stepwise illustration of LTx procedures
- Figure 38.** Impact of reperfusion on hepatic hemodynamics
- Figure 39.** Impact of early perfusion injury on hepatic microcirculation
- Figure 40.** Impact of transplant on liver function
- Figure 41.** The blood count after early LTx
- Figure 42.** Morphological damage, HMGB1 translocation, and CYP1A2 expression early after LTx
- Figure 43.** The correlation between liver microcirculation and liver damage and blood count
- Figure 44.** Liver microarchitecture, oxygen gradient, and HE and HMGB1 staining different flow rate NMP, and transplantation livers
- 
- Table 1.** Criteria for the Modified Suzuki score
- Table 2.** The definition and characteristics of key parameters in CytoCam
- Table 3.** The overview for establishment of the rat LTx model
- Table 4.** Vessel anastomosis practice in cadaver
- Table 5.** SHVC, PV, and BD anastomosis practice in cadaver
- Table 6.** The time of needed of each surgical step including the anastomosis in Phase B1, Phase C1, Phase C2
- Table 7.** The time of each procedure and anastomosis in Phase C3 and Phase C4
- Table 8.** The time of each procedure of LTx for comparison study
- Table 9.** The category of DCD and the Maastricht classification
- Table 10.** The literature work-up of ways to induce DCD for liver machine perfusion model

**Table 11.** The physiological portal vein flow in rats



### 9.3 Permission to use previously published figures from other publications

09.04.24, 12:29

RightsLink Printable License

#### SPRINGER NATURE LICENSE TERMS AND CONDITIONS

Apr 09, 2024

---

This Agreement between Mr. Xinpei Chen ("You") and Springer Nature ("Springer Nature") consists of your license details and the terms and conditions provided by Springer Nature and Copyright Clearance Center.

License Number	5764720851339
License date	Apr 09, 2024
Licensed Content Publisher	Springer Nature
Licensed Content Publication	Nature Reviews Gastroenterology & Hepatology
Licensed Content Title	Machine perfusion of the liver: applications in transplantation and beyond
Licensed Content Author	Carlo D. L. Ceresa et al
Licensed Content Date	Jan 7, 2022
Type of Use	Thesis/Dissertation
Requestor type	non-commercial (non-profit)
Format	print and electronic
Portion	figures/tables/illustrations
Number of figures/tables/illustrations	1
Will you be translating?	no

Circulation/distribution	1 - 29
Author of this Springer Nature content	no
Title of new work	Ischemia-reperfusion injury in a rat model of normothermic oxygenated machine perfusion and liver transplantation
Institution name	Jena university
Expected presentation date	Apr 2024
Order reference number	xpc1993
Portions	Figure 1
Requestor Location	Mr. Xinpei Chen salvador allende platz 1  jena, 07747 Germany Attn: Mr. Xinpei Chen
Total	0.00 EUR

#### Terms and Conditions

##### **Springer Nature Customer Service Centre GmbH Terms and Conditions**

The following terms and conditions ("Terms and Conditions") together with the terms specified in your [RightsLink] constitute the License ("License") between you as Licensee and Springer Nature Customer Service Centre GmbH as Licensor. By clicking 'accept' and completing the transaction for your use of the material ("Licensed Material"), you confirm your acceptance of and obligation to be bound by these Terms and Conditions.

##### **1. Grant and Scope of License**

1. 1. The Licensor grants you a personal, non-exclusive, non-transferable, non-sublicensable, revocable, world-wide License to reproduce, distribute, communicate to the public, make available, broadcast, electronically transmit or create derivative works using the Licensed Material for the purpose(s) specified in your RightsLink Licence Details only. Licenses are granted for the specific use requested in the order and for no other use, subject to these Terms and Conditions. You acknowledge and agree that the rights granted to you under this License do not include the right to

modify, edit, translate, include in collective works, or create derivative works of the Licensed Material in whole or in part unless expressly stated in your RightsLink License Details. You may use the Licensed Material only as permitted under this Agreement and will not reproduce, distribute, display, perform, or otherwise use or exploit any Licensed Material in any way, in whole or in part, except as expressly permitted by this License.

1. 2. You may only use the Licensed Content in the manner and to the extent permitted by these Terms and Conditions, by your RightsLink License Details and by any applicable laws.

1. 3. A separate license may be required for any additional use of the Licensed Material, e.g. where a license has been purchased for print use only, separate permission must be obtained for electronic re-use. Similarly, a License is only valid in the language selected and does not apply for editions in other languages unless additional translation rights have been granted separately in the License.

1. 4. Any content within the Licensed Material that is owned by third parties is expressly excluded from the License.

1. 5. Rights for additional reuses such as custom editions, computer/mobile applications, film or TV reuses and/or any other derivative rights requests require additional permission and may be subject to an additional fee. Please apply to [journalpermissions@springernature.com](mailto:journalpermissions@springernature.com) or [bookpermissions@springernature.com](mailto:bookpermissions@springernature.com) for these rights.

## 2. Reservation of Rights

Licensor reserves all rights not expressly granted to you under this License. You acknowledge and agree that nothing in this License limits or restricts Licensor's rights in or use of the Licensed Material in any way. Neither this License, nor any act, omission, or statement by Licensor or you, conveys any ownership right to you in any Licensed Material, or to any element or portion thereof. As between Licensor and you, Licensor owns and retains all right, title, and interest in and to the Licensed Material subject to the license granted in Section 1.1. Your permission to use the Licensed Material is expressly conditioned on you not impairing Licensor's or the applicable copyright owner's rights in the Licensed Material in any way.

## 3. Restrictions on use

3. 1. Minor editing privileges are allowed for adaptations for stylistic purposes or formatting purposes provided such alterations do not alter the original meaning or intention of the Licensed Material and the new figure(s) are still accurate and representative of the Licensed Material. Any other changes including but not limited to, cropping, adapting, and/or omitting material that affect the meaning, intention or moral rights of the author(s) are strictly prohibited.

3. 2. You must not use any Licensed Material as part of any design or trademark.

3. 3. Licensed Material may be used in Open Access Publications (OAP), but any such reuse must include a clear acknowledgment of this permission visible at the same time as the figures/tables/illustration or abstract and which must indicate that the Licensed Material is not part of the governing OA license but has been reproduced with permission. This may be indicated according to any standard referencing system but must include at a minimum 'Book/Journal title, Author, Journal Name (if applicable), Volume (if applicable), Publisher, Year, reproduced with permission from SNCSC'.

#### 4. STM Permission Guidelines

4. 1. An alternative scope of license may apply to signatories of the STM Permissions Guidelines ("STM PG") as amended from time to time and made available at <https://www.stm-assoc.org/intellectual-property/permissions/permissions-guidelines/>.
4. 2. For content reuse requests that qualify for permission under the STM PG, and which may be updated from time to time, the STM PG supersede the terms and conditions contained in this License.
4. 3. If a License has been granted under the STM PG, but the STM PG no longer apply at the time of publication, further permission must be sought from the Rightsholder. Contact [journalpermissions@springernature.com](mailto:journalpermissions@springernature.com) or [bookpermissions@springernature.com](mailto:bookpermissions@springernature.com) for these rights.

#### 5. Duration of License

5. 1. Unless otherwise indicated on your License, a License is valid from the date of purchase ("License Date") until the end of the relevant period in the below table:

Reuse in a medical communications project	Reuse up to distribution or time period indicated in License
Reuse in a dissertation/thesis	Lifetime of thesis
Reuse in a journal/magazine	Lifetime of journal/magazine
Reuse in a book/textbook	Lifetime of edition
Reuse on a website	1 year unless otherwise specified in the License
Reuse in a presentation/slide kit/poster	Lifetime of presentation/slide kit/poster. Note: publication whether electronic or in print of presentation/slide kit/poster may require further permission.
Reuse in conference proceedings	Lifetime of conference proceedings
Reuse in an annual report	Lifetime of annual report
Reuse in training/CME materials	Reuse up to distribution or time period indicated in License
Reuse in newsmedia	Lifetime of newsmedia
Reuse in coursepack/classroom materials	Reuse up to distribution and/or time period indicated in license

#### 6. Acknowledgement

6. 1. The Licensor's permission must be acknowledged next to the Licensed Material in print. In electronic form, this acknowledgement must be visible at the same time as the figures/tables/illustrations or abstract and must be hyperlinked to the journal/book's homepage.
6. 2. Acknowledgement may be provided according to any standard referencing system and at a minimum should include "Author, Article/Book Title, Journal name/Book imprint, volume, page number, year, Springer Nature".

#### 7. Reuse in a dissertation or thesis

7. 1. Where 'reuse in a dissertation/thesis' has been selected, the following terms apply: Print rights of the Version of Record are provided for; electronic rights for use only on institutional repository as defined by the Sherpa guideline ([www.sherpa.ac.uk/romeo/](http://www.sherpa.ac.uk/romeo/)) and only up to what is required by the awarding institution.
7. 2. For theses published under an ISBN or ISSN, separate permission is required. Please contact [journalpermissions@springernature.com](mailto:journalpermissions@springernature.com) or [bookpermissions@springernature.com](mailto:bookpermissions@springernature.com) for these rights.
7. 3. Authors must properly cite the published manuscript in their thesis according to current citation standards and include the following acknowledgement: *'Reproduced with permission from Springer Nature'*.

## 8. License Fee

You must pay the fee set forth in the License Agreement (the "License Fees"). All amounts payable by you under this License are exclusive of any sales, use, withholding, value added or similar taxes, government fees or levies or other assessments. Collection and/or remittance of such taxes to the relevant tax authority shall be the responsibility of the party who has the legal obligation to do so.

## 9. Warranty

9. 1. The Licensor warrants that it has, to the best of its knowledge, the rights to license reuse of the Licensed Material. **You are solely responsible for ensuring that the material you wish to license is original to the Licensor and does not carry the copyright of another entity or third party (as credited in the published version).** If the credit line on any part of the Licensed Material indicates that it was reprinted or adapted with permission from another source, then you should seek additional permission from that source to reuse the material.

9. 2. EXCEPT FOR THE EXPRESS WARRANTY STATED HEREIN AND TO THE EXTENT PERMITTED BY APPLICABLE LAW, LICENSOR PROVIDES THE LICENSED MATERIAL "AS IS" AND MAKES NO OTHER REPRESENTATION OR WARRANTY. LICENSOR EXPRESSLY DISCLAIMS ANY LIABILITY FOR ANY CLAIM ARISING FROM OR OUT OF THE CONTENT, INCLUDING BUT NOT LIMITED TO ANY ERRORS, INACCURACIES, OMISSIONS, OR DEFECTS CONTAINED THEREIN, AND ANY IMPLIED OR EXPRESS WARRANTY AS TO MERCHANTABILITY OR FITNESS FOR A PARTICULAR PURPOSE. IN NO EVENT SHALL LICENSOR BE LIABLE TO YOU OR ANY OTHER PARTY OR ANY OTHER PERSON OR FOR ANY SPECIAL, CONSEQUENTIAL, INCIDENTAL, INDIRECT, PUNITIVE, OR EXEMPLARY DAMAGES, HOWEVER CAUSED, ARISING OUT OF OR IN CONNECTION WITH THE DOWNLOADING, VIEWING OR USE OF THE LICENSED MATERIAL REGARDLESS OF THE FORM OF ACTION, WHETHER FOR BREACH OF CONTRACT, BREACH OF WARRANTY, TORT, NEGLIGENCE, INFRINGEMENT OR OTHERWISE (INCLUDING, WITHOUT LIMITATION, DAMAGES BASED ON LOSS OF PROFITS, DATA, FILES, USE, BUSINESS OPPORTUNITY OR CLAIMS OF THIRD PARTIES), AND WHETHER OR NOT THE PARTY HAS BEEN ADVISED OF THE POSSIBILITY OF SUCH DAMAGES. THIS LIMITATION APPLIES NOTWITHSTANDING ANY FAILURE OF ESSENTIAL PURPOSE OF ANY LIMITED REMEDY PROVIDED HEREIN.

## 10. Termination and Cancellation

10. 1. The License and all rights granted hereunder will continue until the end of the applicable period shown in Clause 5.1 above. Thereafter, this license will be terminated and all rights granted hereunder will cease.

10. 2. Licensor reserves the right to terminate the License in the event that payment is not received in full or if you breach the terms of this License.

## 11. General

11. 1. The License and the rights and obligations of the parties hereto shall be construed, interpreted and determined in accordance with the laws of the Federal Republic of Germany without reference to the stipulations of the CISG (United Nations Convention on Contracts for the International Sale of Goods) or to Germany's choice-of-law principle.

11. 2. The parties acknowledge and agree that any controversies and disputes arising out of this License shall be decided exclusively by the courts of or having jurisdiction for Heidelberg, Germany, as far as legally permissible.

11. 3. This License is solely for Licensor's and Licensee's benefit. It is not for the benefit of any other person or entity.

**Questions?** For questions on Copyright Clearance Center accounts or website issues please contact [springernaturesupport@copyright.com](mailto:springernaturesupport@copyright.com) or +1-855-239-3415 (toll free in the US) or +1-978-646-2777. For questions on Springer Nature licensing please visit <https://www.springernature.com/gp/partners/rights-permissions-third-party-distribution>

### Other Conditions:

Version 1.4 - Dec 2022

**Questions?** [customer@copyright.com](mailto:customer@copyright.com).

---



[Sign In/Register](#)



### Metabolic zonation of the liver: The oxygen gradient revisited

**Author:** Thomas Kietzmann  
**Publication:** Redox Biology  
**Publisher:** Elsevier  
**Date:** April 2017

*© 2017 The Author. Published by Elsevier B.V.*

#### Creative Commons Attribution-NonCommercial-No Derivatives License (CC BY NC ND)

This article is published under the terms of the [Creative Commons Attribution-NonCommercial-No Derivatives License \(CC BY NC ND\)](#). For non-commercial purposes you may copy and distribute the article, use portions or extracts from the article in other works, and text or data mine the article, provided you do not alter or modify the article without permission from Elsevier. You may also create adaptations of the article for your own personal use only, but not distribute these to others. You must give appropriate credit to the original work, together with a link to the formal publication through the relevant DOI, and a link to the Creative Commons user license above. If changes are permitted, you must indicate if any changes are made but not in any way that suggests the licensor endorses you or your use of the work.

Permission is not required for this non-commercial use. For commercial use please continue to request permission via RightsLink.

[BACK](#)

[CLOSE WINDOW](#)

## GEORG THIEME VERLAG KG ORDER DETAILS

Apr 29, 2024

---

Order Number	501902665
Order date	Apr 29, 2024
Licensed Content Publisher	Georg Thieme Verlag KG
Licensed Content Publication	Seminars in Liver Disease
Licensed Content Title	The Role of Liver Zonation in Physiology, Regeneration, and Disease
Licensed Content Author	Regeant Panday, Chase P. Monckton, Salman R. Khetani
Licensed Content Date	Feb 4, 2022
Licensed Content Volume	42
Licensed Content Issue	01
Type of Use	Dissertation/Thesis
Requestor type	non-commercial (non-profit)
Format	print and electronic
Portion	figures/tables/images
Number of figures/tables/images	1
Will you be translating?	no
Distribution quantity	1
Title of new work	Ischemia-reperfusion injury in a rat model of normothermic oxygenated machine perfusion and liver transplantation
Institution name	Jena university
Expected presentation date	Apr 2024
Order reference number	XPC1818
Portions	Figure 1 Mr. Xinpei Chen salvador allende platz 1
Requestor Location	jena, 07747 Germany Attn: Mr. Xinpei Chen
Publisher Tax ID	13-5650435
Total	Not Available

---



## 9.4 Curriculum vitae

### Personal Information

Name: Xinpei Chen

Gender: Male

Nationality: Chinese

Birth Date: 05.06.1993

Email: Xinpei.chen@outlook.com

Mobile Phone: +8618308335186

Address: Salvador-Allende-Platz 1, Jena Germany



### Education

2012.09-2017.07 Southwest Medical University Bachelor's degree

2017.09-2020.06 Southwest Medical University Master's degree

2021.12-Present Jena University MD student

### Publications

#### First author

1. **Chen X**, Luo D, Mei B, Du J, Liu X, Xie H, Liu L, Su S, Mai G. Immunogenicity of COVID-19 vaccines in solid organ transplant recipients: a systematic review and meta-analysis. *Clin Microbiol Infect.* 2023 Apr;29(4):441-456. doi: 10.1016/j.cmi.2022.12.004.
2. Luo D#, **Chen X#**, Du J, Mei B, Wang A, Kuang F, Fang C, Gan Y, Peng F, Yang X, Dahmen U, Li B, Song S. Immunogenicity of COVID-19 vaccines in chronic liver disease patients and liver transplant recipients: A systematic review and meta-analysis. *Liver Int.* 2023 Jan;43(1):34-48. doi: 10.1111/liv.15403.
3. Luo D#, **Chen X#**, Dai Y, Kuang F, Kang M, Li B, Su S. Cholecystectomy and risk of liver disease: a systematic review and meta-analysis of 27 million individuals. *Int J Surg.* 2023 May 1;109(5):1420-1429. doi: 10.1097/JS9.0000000000000332.

# Equal contribution

#### Co-author

1. H. M. Tautenhahn, T. Ricken, U. Dahmen, L. Mandl, L. Bütow, S. Gerhäuser, L. Lambers, **X. Chen**, E. Lehmann, O. Dirsch, and M. König, SimLivA—Modeling ischemia-reperfusion injury in the liver: A first step towards a clinical decision support tool, *GAMM-Mitteilungen.* (2024), e202370003. <https://doi.org/10.1002/gamm.202370003>
2. Luo D, Mei B, Wang P, Li X, **Chen X**, Wei G, Kuang F, Li B, Su S. Prevalence and risk factors for persistent symptoms after COVID-19: a systematic review and meta-analysis. *Clin Microbiol Infect.* 2024 Mar;30(3):328-335. doi: 10.1016/j.cmi.2023.10.016.

## **Conferences**

1. JSAM Ageing Retreat-Poster Xinpei Chen and Uta Dahmen. Modulation of autophagy to reduce the age-related augmented ischemia reperfusion injury in a rat model of normothermic oxygenated machine perfusion (NOMP) and liver transplantation. Jena, Germany. 06.10.2022.

## 9.5 Acknowledgements

I would like to express my sincerest gratitude to my dear supervisor **Prof. Dr. med. Uta Dahmen**, the head of Experimental Transplantation Surgery, Department of General, Visceral and Vascular Surgery, Friedrich-Schiller-University Jena Hospital. I am very grateful for her constructive comments throughout the research project and the writing process. Her unique educational perspective and innovative guidance were important for the completion of the research project. Her patient and professional guidance have helped me to further develop my research skills and scientific thinking. She not only comforted me when I was sick but also enthusiastically helped me contact physicians. I would like to express my sincere gratitude to her again for her kind and selfless help.

I would like to grateful **Prof. Dr. med. Utz Settmacher**, Director of the Department of General, Visceral and Vascular Surgery, Friedrich-Schiller-University Jena Hospital, for giving me the precious opportunity to work on liver research in his department.

I would like to express my gratitude to **PD. Dr. med. Olaf Dirsch**, Director of Institute of Pathology, BG Klinikum Unfallkrankenhaus Berlin. I am very grateful for his expert support in histopathology. His insightful comments to morphology have greatly improved the quality of the thesis.

I would like to thank my dear colleague and friend **Mohamed Albadry** for establishing staining protocols, performing tissue staining, analysis of staining and critical interpretation of results. His valuable support of animal surgery together with sound instructions of the monitoring system facilitated and improved the conduction of the experiments. With great appreciation I remember our endless scientific discussion and his enthusiastic help and encouragement in advice of the research and life.

I would like to thank my colleague **Haotian Chen** for his introduction into machine perfusion and analysis of the HE staining.

I would like to express to my colleague **Dr. Fengming Xu** for his help in revising the manuscript, and thank **Qingqing Dai** for his help in instruction of western blot.

Sincerely thanks to **Vanessa Buch, Caroll Willbrecht, and Ana Lucia Paz** for their crucial help with tissue staining.

I would like to deeply thank **Dr. Weiwei Wei, Carina Bachmann, Inka Reiner, Dr. Stefan Pentzold, Steffi Krauter, Mingjin Li, Mehul Bafna, and Mandy Peter**, my dear friends and colleagues, for their kind help and advice in life and research.

I would like to thank company **Vygon** for donation of bile duct cannulas and thank **Department of Clinical Chemistry and Laboratory Medicine** for the clinical chemistry measurements.

This project was supported by funding from the Foundation "Else Kröner-Fresenius-Stiftung" within the Else Kröner Graduate School for Medical Students "Jena School for Ageing Medicine (JSAM)". I am sincerely grateful to Else Kröner-Fresenius-Stiftung funding agency and JSAM coordination team especially **Prof. Dr. med. Otto W. Witte** and **Prof. Dr. med. Regine Heller** for providing me the opportunity to carry out my research work and supporting me unstintingly over the years.

Here we acknowledge the use of BioRender, to designed and create figures and the use of Grammarly to revise and edit the text.

Lastly, I am deeply thankful to my family for their boundless support, patience, and understanding throughout this challenging period.

## 9.6 Ehrenwörtliche Erklärung

Hiermit erkläre ich, dass

mir die geltende Promotionsordnung der Medizinischen Fakultät der Friedrich-Schiller-Universität bekannt ist,

ich die Dissertation selbst angefertigt habe, keine Textabschnitte eines Dritten oder eigener Prüfungsarbeiten ohne Kennzeichnung übernommen und alle von mir benutzten Hilfsmittel, persönlichen Mitteilungen und Quellen in meiner Arbeit angegeben habe, mich folgende Personen bei der Auswahl und Auswertung des Materials sowie bei der Herstellung des Manuskripts unterstützt haben:

Prof. Dr. med. Uta Dahmen

die Hilfe einer kommerziellen Promotionsvermittlung nicht in Anspruch genommen wurde und dass Dritte weder unmittelbar noch mittelbar geldwerte Leistungen von mir für Arbeiten erhalten haben, die im Zusammenhang mit dem Inhalt der vorgelegten Dissertation stehen.

Die Arbeit wurde bisher weder im In- noch Ausland in gleicher oder ähnlicher Form einer anderen Prüfungsbehörde vorgelegt.

Ich versichere, daß ich nach bestem Wissen die reine Wahrheit gesagt und nichts verschwiegen habe.

Ort, Datum

Unterschrift des Verfassers